Evapotranspiration from a Cypress and Pine Forest Subjected to Natural Fires in Volusia County, Florida, 1998-99

U.S. GEOLOGICAL SURVEY
Water-Resources Investigations Report 01-4245

Prepared in cooperation with
St. Johns River Water Management District
County of Volusia

USGS
science for a changing world

Evapotranspiration from a Cypress and Pine Forest Subjected to Natural Fires, Volusia County, Florida, 1998-99

By D. M. Sumner

U.S. GEOLOGICAL SURVEY

Water-Resources Investigations Report 01–4245

Prepared in cooperation with the

St. Johns River Water Management District
County of Volusia

Tallahassee, Florida
2001

U.S. DEPARTMENT OF THE INTERIOR
GALE A. NORTON, Secretary

U.S. GEOLOGICAL SURVEY
Charles G. Groat, Director

For additional information write to:

District Chief
U.S. Geological Survey, WRD
Suite 3015
227 North Bronough Street
Tallahassee, FL 32301

Copies of this report can be purchased from:

U.S. Geological Survey
Branch of Information Services
Box 25286
Denver, CO 80225-0286
888-ASK-USGS

Additional information about water resources in Florida is available on the World Wide Web at
http://fl.water.usgs.gov

CONTENTS

Abstract 1
Introduction 1
Acknowledgements 2
Purpose and Scope 2
Description of the Study Area 2
Methods for Measurement and Simulation of Evapotranspiration 8
Measurement of Evapotranspiration 9
Eddy-Correlation Method 9
Source Area of Measurements 10
Instrumentation 12
Calculation of Turbulent Fluxes 13
Consistency of Measurements with Energy Budget 15
Simulation of Evapotranspiration 17
Evapotranspiration Models 17
Partitioning of Measured Evapotranspiration 18
Measurement of Environmental Variables 20
Results of Evapotranspiration Measurement and Simulation 23
Calibration of Evapotranspiration Model 31
Application of Evapotranspiration Model 35
Water Budget 43
Summary and Conclusions 47
References 49
Appendix I 53

FIGURES

1-3. Maps showing:
1. Location of Tiger Bay watershed 3
2. Distribution of vegetation in vicinity of evapotranspiration station 5
3. Infrared photograph (July 7, 1998) of vicinity of evapotranspiration station showing areas burned during fires of June 1998 6
4. Illustration showing photographic times series of vegetation in vicinity of evapotranspiration station 7
5. Photograph showing krypton hygrometer and sonic anemometer mounted at top of tower at evapotranspiration station 8
6. Photograph showing evapotranspiration station being serviced by hydrologic technician 9
7. Graph showing radial extent of source areas of turbulent flux and net radiation measurements 11
8. Graph showing wind direction frequency pattern at location of evapotranspiration station 19
9. Map showing location of rain gages in vicinity of Tiger Bay watershed 22
10-37. Graphs showing:
10. Diurnal pattern of rejected flux measurements 23
11. Relation between measured 30-minute averages of photosynthetically active radiation (PAR) and latent heat flux (λE) 24
12. Relation between measured 30-minute averages of photosynthetically active radiation (PAR) and sensible heat flux (H) 24
13. Measured and photosynthetically active radiation (PAR)-estimated values of (a) latent heat flux and (b) sensible heat flux during 10-day period in late February 1998 25
14. Average diurnal pattern of energy fluxes and photosynthetically active radiation (PAR) 26
15. Relation between daily values of measured net radiation and photosynthetically active radiation (PAR) 27

16. Average daily net radiation for burned and unburned areas 27
17. Average daily photosynthetically active radiation (PAR) 28
18. Temporal distribution of daily relative energy-budget closure 29
19. Relation between daily energy-budget closure and average daily friction velocity 29
20. Average daily latent heat flux measured by the eddy correlation method and the energy-budget variant 30
21. Average daily sensible heat flux measured by the eddy correlation method and the energy-budget variant 30
22. Daily values of fraction of burned fraction of turbulent flux measurement 31
23. Relation between soil moisture content and water level 32
24. Temporal variability of normalized difference vegetation index (NVDI) 32
25. Temporal variability in relative error of evapotranspiration model 34
26. Comparison of simulated and measured values of daily latent heat flux 35
27. Water-table depth and cumulative rainfall 36
28. Average daily air temperature 36
29. Average daily latent heat flux and evapotranspiration 37
30. Average daily potential latent heat flux and potential evapotranspiration 37
31. Average daily sensible heat flux 39
32. Average daily Bowen ratio 39
33. Shallow, volumetric soil moisture at evapotranspiration station 40
34. Temporal variability of daily values of relative evapotranspiration 40
35. Relation between relative evapotranspiration and depth to water table 41
36. Relation between relative evapotranspiration and photosynthetically active radiation (PAR) 41
37. The Priestley-Taylor variable $\Delta/(\Delta+\gamma)$ as a function of temperature 42
38. Illustration showing water budget for Tiger Bay watershed during calendar years 1998 - 1999 44
39. Graph showing runoff from Tiger Bay watershed 45

TABLES

1. Study instrumentation 10
2. Relative fraction of burned vegetation sensed by eddy correlation instrumentation 12
3. Summary of parameters and error statistics for daily evapotranspiration models 33
4. Sensitivity of evapotranspiration models to environmental variables 43
5. Water budget of Tiger Bay watershed 43
6. Potential evapotranspiration and relative rates of annual water-budget terms for Tiger Bay watershed 46
7. Average rate of change in water-table depth at monitor wells 47
8. Comparison of estimates of specific yield based on evapotranspiration estimated with the energy-budget variant and with the standard eddy correlation method 47

CONVERSION FACTORS, VERTICAL DATUM, ABBREVIATIONS, AND SYMBOLS

Multiply	By	To obtain
	Length	
millimeter (mm)	0.03937	inch
centimeter (cm)	0.3937	inch
meter (m)	3.281	foot
kilometer (km)	0.6215	mile
	Area	
hectare	2.471	acre
	Flux	
millimeter per day (mm/d)	0.03937	inch per day
millimeter per year (mm/yr)	0.03937	inch per year
watt per square meter (W/m^2)	0.0342 at 0 ^oC	millimeter per day
watt per square meter (W/m^2)	0.0354 at 25 ^oC	millimeter per day
watt per square meter (W/m^2)	0.0359 at 50 ^oC	millimeter per day
	Flow	
cubic meter per second (m^3/s)	35.31	cubic foot per second
	Energy	
joule (J)	0.2388	calorie
	Energy flux density	
watt per square meter (W/m^2)	0.001433	calorie per square centimeter per minute
	Pressure	
pascal (Pa)	0.0002953	inch of mercury
	0.0001450	pound per square inch
	0.01	millibar
	Photosynthetically active radiation	
micromole per square meter per second ($\mu moles/(m^2 \cdot s)$)	6.02×10^{17}	photon per square meter per second

Sea level: In this report sea level refers to the National Geodetic Vertical Datum of 1929--a geodetic datum derived from a general adjustment of the first-order level nets of the United States and Canada, formerly called Sea Level Datum of 1929.

Horizontal coordinate information is referenced to the North American Datum of 1983 (NAD83).

Altitude, as used in this report, refers to distance above or below sea level.

Temperature is given in degrees Celsius (^oC), which can be converted to degrees Fahrenheit (^oF) by the following equation:

$$^oF = 1.8(^oC) + 32;$$

and can be converted to degrees Kelvin (^oK) by the following equation:

$$^oK = ^oC + 273.15.$$

Additional abbreviations

AVHRR	Advanced Very High Resolution Radiometer
CSI	Campbell Scientific, Inc.
CV	coefficient of variation
EROS	Earth Resources Observation Systems
MODFLOW	U.S. Geological Survey Modular Finite-Difference Ground-Water Flow Model
NOAA	National Oceanic and Atmospheric Administration
NDVI	normalized-difference vegetation index
PAR	photosynthetically active radiation
REBS	Radiation and Energy Balance Systems, Inc.
RMY	R. M. Young, Inc.
SEE	standard error of estimate
TDR	time domain reflectometry
TE	Texas Electronics, Inc.
USGS	U.S. Geological Survey

List of Symbols

Roman

B	Bowen ratio, equal to the ratio of sensible and latent heat fluxes
c	Vapor density (g/m^3) or virtual temperature (in ^oC)
C_{1j}-C_{3j}	Empirical parameters within evapotranspiration model for surface cover j
C_a	Absolute water-budget closure, in mm/yr
C_p	Specific heat capacity of air, in J/(g·°C)
C_r	Relative water-budget closure, in percent
d	Momentum displacement height of vegetation, in m
e	Vapor pressure, in kPa
e_s	Saturation vapor pressure, in kPa
E	Evapotranspiration rate, in $g/(m^2 \cdot s)$
ET	Evapotranspiration rate, in mm/yr
f_i	PAR-weighted fraction of the day that wind direction is from burn zone i
F	Factor used in krypton hygrometer correction that accounts for molecular weights of air and atmospheric abundance of oxygen, equal to 0.229 g·°C/J
g_i	Fractional contribution of burned area within burn zone i to the measured latent heat flux when wind direction is from burn zone i
G	Soil heat flux at land surface, in W/m^2
h	Canopy height, in m
h_{wt}	Water-table depth below a reference level placed at the highest water level observed at the evapotranspiration station (uplands environment) during the study period, in m
H	Sensible heat flux, in W/m^2
H_{cor}	Sensible heat flux as estimated by the energy-budget variant of the eddy correlation method, in W/m^2
i	An index for the burn zones (I to IV)
j	An index denoting the surface cover; j=1 (unburned areas); j=2 (burned areas during post-fire/pre-logging period; j=3 (burned areas during initial post-logging period); and j=4 (burned areas during final post-logging period)
k	An index for the 48 measurements of 30-minute averages within a given day
K_o	Extinction coefficient of hygrometer for oxygen, in $m^3/g \cdot cm$)
K_w	Extinction coefficient of hygrometer for water, in $m^3/g \cdot cm$)
L	Leakage to the Upper Floridan aquifer, in mm/yr
NIR	Reflectance of near-infrared radiation, dimensionless
NDVI	Normalized-difference vegetation index, dimensionless

P	Precipitation, in mm/yr
P_a	Atmospheric pressure, in Pa
PAR	Photosynthetically active radiation, in µmoles/(m^2·s)
PET	Potential evapotranspiration, in mm/yr or W/m^2
q	Specific humidity, in g water/g moist air
r_h	Aerodynamic resistance, in seconds per meter
R	Runoff, in mm/yr
R_d	Gas constant for dry air, equal to 0.28704 J/^{o}C/g
R_n	Net radiation, in W/m^2
R_{nb}	Net radiation for burned areas, in W/m^2
R_{nu}	Net radiation for unburned areas, in W/m^2
S	change in storage of energy in the biomass and air, in W/m^2
S_y	Specific yield, in mm^3 water/ mm water-level change/mm^2
T_a	Air temperature, in ^{o}C
T_s	Sonic temperature, in ^{o}C
u	Lateral wind speed along coordinate x-direction, in m/s
u^*	Friction velocity, in m/s
v	Lateral wind speed along coordinate y-direction, in m/s
Vis	Reflectance of visible radiation, dimensionless
w	Wind speed along coordinate z-direction, in m/s
w_b	Fraction of the measured latent heat flux originating from burned areas, dimensionless
x	One of two orthogonal coordinate directions within a plane parallel to canopy surface
y	One of two orthogonal coordinate directions within a plane parallel to canopy surface
z	Coordinate direction perpendicular to canopy surface
z_s	Height of sensors above land surface, in m
z_m	Roughness length of canopy for momentum, in m

Greek

α	Priestley-Taylor coefficient, dimensionless
$\delta_i(\Psi_k)$	A binary function equal to 1 if Ψ_k is within burn zone i and otherwise equals 0
Δ	Slope of the saturation vapor pressure curve, in kPa/^{o}C
Δh_{avg}	Average rate of change in water-table depth, in mm/yr

ΔS	Rate of change in watershed storage computed as a residual of the water budget, in mm/yr
η	Angle of rotation about the z-axis to align u into the x-direction on the x-y plane, in radians
γ	Psychrometric constant, in kPa/^{o}C
λ	Latent heat of vaporization, in J/g
λE	Latent heat flux, in W/m^2
λE_b	Latent heat flux from burned areas, in W/m^2
λE_{bk}	Latent heat flux from burned surface covers for time step k, in W/m^2
λE_{bm}	Daily latent heat flux derived from burned surface covers and measured by the flux sensors, in W/m^2
λE_{cor}	Latent heat flux as estimated by the energy-budget variant of the eddy correlation method, in W/m^2
λE_u	Latent heat flux from unburned areas, in W/m^2
θ	Angle of rotation in the y-direction to align *w* along the z-direction, in radians
ρ	Air density, in g/m^3
ρ_v	Vapor density, in g/m^3
Ψ_k	Wind direction for a given time period within a given day

Evapotranspiration from a Cypress and Pine Forest Subjected to Natural Fires in Volusia County, Florida, 1998-99

By D. M. Sumner

ABSTRACT

Daily values of evapotranspiration from a watershed in Volusia County, Florida, were estimated for a 2-year period (January 1998 through December 1999) by using an energy-budget variant of the eddy correlation method and a Priestley-Taylor model. The watershed consisted primarily of pine flatwood uplands interspersed within cypress wetlands. A drought-induced fire in spring 1998 burned about 40 percent of the watershed, most of which was subsequently logged. The model reproduced the 449 measured values of evapotranspiration reasonably well ($r^2 = 0.90$) over a wide range of seasonal and surface-cover conditions. Annual evapotranspiration from the watershed was estimated to be 916 millimeters (36 inches) for 1998 and 1,070 millimeters (42 inches) for 1999. Evapotranspiration declined from near potential rates in the wet conditions of January 1998 to less than 50 percent of potential evapotranspiration after the fire and at the peak of the drought in June 1998. After the drought ended in early July 1998 and water levels returned to near land-surface, evapotranspiration increased sharply; however, the evapotranspiration rate was only about 60 percent of the potential rate in the burned areas, compared to about 90 percent of the potential rate in the unburned areas. This discrepancy can be explained as a result of fire damage to vegetation. Beginning in spring 1999, evapotranspiration from burned areas increased sharply relative to unburned areas, sometimes exceeding unburned evapotranspiration by almost 100 percent. Possible explanations for the dramatic increase in evapotranspiration from burned areas could include phenological changes associated with maturation or seasonality of plants that emerged after the fire or successional changes in composition of plant community within burned areas.

Variations in daily evapotranspiration are primarily the result of variations in surface cover, net radiation, photosynthetically active radiation, air temperature, and water-table depth. A water budget for the watershed supports the validity of the daily measurements and estimates of evapotranspiration. A water budget constructed using independent estimates of average rates of rainfall, runoff, and deep leakage, as well as evapotranspiration, was consistent within 3.8 percent. An alternative water budget constructed using evapotranspiration estimated by the standard eddy correlation method was consistent only within 9.1 percent. This result indicates that the standard eddy correlation method is not as accurate as the energy-budget variant.

INTRODUCTION

The importance of evapotranspiration in the hydrologic cycle has long been recognized; in central Florida, evapotranspiration is second only to precipitation in magnitude. Of the approximately 1,320 millimeters (mm) of mean annual rainfall in central Florida, 680 to 1,220 mm have been estimated to return to the atmosphere as evapotranspiration (Tibbals, 1990; Sumner, 1996). Despite the importance of evapotranspiration in the hydrologic cycle, the magnitude,

seasonal and diurnal distributions, and relation to environmental variables of evapotranspiration remain relatively unknown. Uncertainty in evapotranspiration from non-agricultural vegetation is particularly apparent. The mixed cypress wetland and pine flatwood forest cover examined in the present investigation is common in central Florida, as are the fires that burned much of the forest during the study. Accurate estimates of evapotranspiration from commonly occurring land covers are fundamental to the quantitative understanding necessary for prudent management of Florida's water resources.

The eddy correlation method has been used successfully to directly measure evapotranspiration in Florida (Bidlake and others (1993); Knowles (1996); and Sumner (1996)). This micrometeorological method offers several advantages to alternative water-budget approaches (lysimeter or regional water budget) by providing more areal integration and less site disruption than lysimeters, by eliminating the need to estimate other terms of a water budget (precipitation, deep percolation, runoff, and storage), and by allowing relatively fine temporal resolution (less than 1 hour).

Evapotranspiration can be estimated by using evapotranspiration models. These models also provide insight into the relative importance of individual environmental variables in the evapotranspiration process. The Priestley-Taylor model (Priestley and Taylor, 1972) for evaporation from a wet surface (potential evapotranspiration), modified to allow for non-potential conditions (Flint and Childs, 1991), has successfully simulated evapotranspiration in the Florida environment (Knowles, 1996; Sumner, 1996; and German, 2000).

The U.S. Geological Survey (USGS), in cooperation with the St. Johns River Water Management District and the County of Volusia, began a 4-year study in 1996 to estimate the temporal pattern of evapotranspiration in the Tiger Bay watershed, Volusia County, Fla., a forested watershed, and to develop a quantitative description of the effect of environmental variability on evapotranspiration from forested areas in Florida. This analysis can provide guidance in the estimation of evapotranspiration and the description of the relation between the environment and evapotranspiration in other areas with similar environmental characteristics. During the study period, the watershed experienced a severe drought and natural fires, which provided the opportunity to study the effects of such extreme events on the evapotranspiration process.

Acknowledgements

The author gratefully extends his appreciation to Catherine Lowenstein and her staff at the Tiger Bay State Forest for providing assistance during this study. The contributions of Timothy Curran and Jerome Kelly of the USGS, Altamonte Springs, Fla., in construction and maintenance of the evapotranspiration station are gratefully acknowledged.

Purpose and Scope

This report presents daily estimates of evapotranspiration during a 2-year period from a forested watershed (Tiger Bay, Volusia County, Fla.), which was subjected to natural fires, and provides evaluations of the causal relations between the environment and evapotranspiration. Measurements were made on a nearly continuous basis from January 1998 through December 1999 at an evapotranspiration station just outside the watershed, using eddy correlation and meteorological instrumentation. An evapotranspiration model based on the Priestley-Taylor equation was used to estimate evapotranspiration for burned and unburned areas and to quantify the relation between evapotranspiration and the environment. A water budget of the watershed was constructed to assess the validity of the eddy correlation-measured evapotranspiration totals for the 2-year period.

Description of the Study Area

The study area is the approximately 7,500-hectare Tiger Bay watershed within Volusia County, Fla. (fig. 1). The watershed was almost completely forested in January 1998, but was subjected to extensive burning and logging during the study period. The watershed characteristics are typical of many areas within the lower coastal plain of the southeastern United States - nearly flat, slowly draining land with a vegetative cover consisting primarily of pine flatwood uplands interspersed within cypress wetlands. The northern part of the watershed mostly is within the 9,500-hectare Tiger Bay State Forest; the southern part of the watershed primarily is privately owned land used for timber production. The watershed is within the relatively flat Talbott Terrace physiographic area (Rutledge, 1985, fig. 1). More than 90 percent of the watershed is at an altitude of 11 to 13 meters (m).

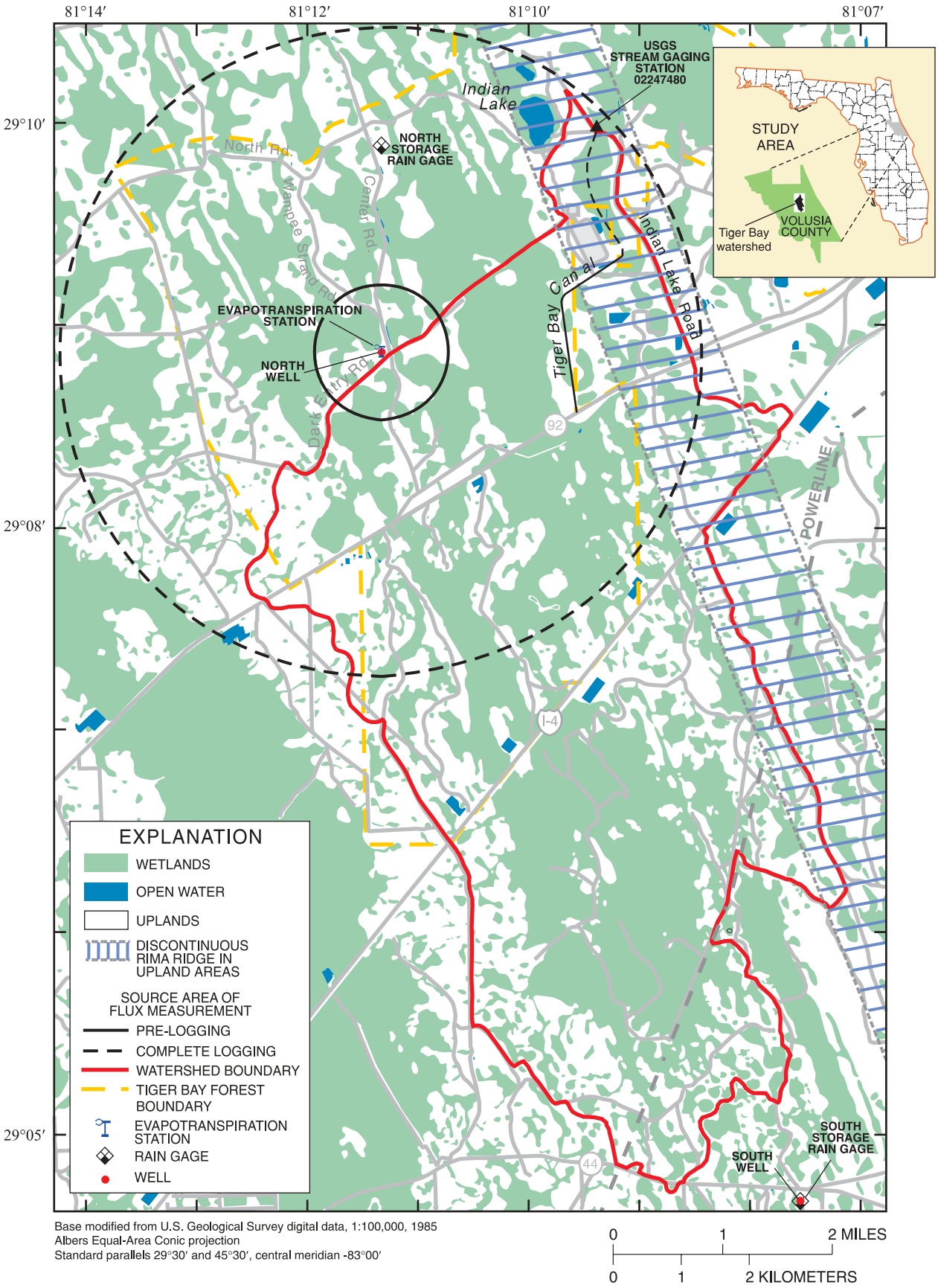

Figure 1. Location of Tiger Bay watershed.

Small variations in local topography result in areal variations in hydroperiod. A low-lying wetland can be inundated much of the year, whereas an adjacent upland, less than a few tens of centimeters (cm) elevated above the wetland, may only occasionally or never exhibit standing water. Most of the surface runoff from the watershed is through inter-connected wetlands (Riekerk and Korhnak, 2000).

More than 95 percent of the watershed is forested. Two tree species dominate the forest cover in the watershed: slash pine (evergreen) and pond cypress (deciduous; leaves drop in November-December with regrowth in March-April). The distribution of vegetation in the vicinity of the evapotranspiration station is shown in figure 2.

Vegetation in the watershed reflects the variation in hydroperiod (Simonds and others, 1980). Wetlands are dominated by pond cypress (*Taxodium ascendens*), with lesser amounts of other wetland tree species including blackgum (*Nyssa biflora*), loblolly bay (*Gordonia lasianthus*), and red maple (*Acer rubrum*). The understory of wetlands consists of a wide variety of plants including leather fern (*Acrostichum danaeifolium*), marsh fern (*Thelypteris palustris*), cinnamon fern (*Osmunda cinnamomea*), swamp lily (*Crinum americanum*), maidencane (*Panicum hemitomon*), red root (*Lachnanthes caroliniana*), hooded pitcher plant (*Sarracenia minor*), St. John's Wort (*Hypericum fasciculatum*), yellow colic root (*Aletris lutea*), pipewort (*Eriocaulon decangulare*), and white-topped sedge (*Rhynchospora colorata*). Water level varies from about 0.3 m above land surface to as much as 1 m below land surface in low-lying areas, although these areas are inundated more than 50 percent of the time (Simonds and others, 1980).

Uplands generally are either slash pine tree (*Pinus elliottii*) plantations or naturally seeded pine flatwoods (primarily slash pine with some longleaf pine (*Pinus palustris*)). These areas have an understory including saw palmetto (*Serenoa repens*), gallberry (*Ilex glabra*), wax myrtle (*Myrica cerifera*), red root (*Lachnanthes caroliniana*), and broomsedge (*Andropogon virginicus*). Understory vegetation in the pine plantations is control-burned about every 3 years. Water level varies from about 0.1 m above land surface to as much as 2 m below land surface in uplands; however, water levels are always greater than 2 m below land surface in the small part of the uplands within the Rima Ridge (fig. 1). The Rima Ridge consists of discontinuous remnants of terrace deposits parallel to the present-day coastline (Rutledge, 1985, fig. 1). Vegetation on the ridge areas includes sand live oak (*Quercus geminata*) and sand pine (*Pinus clausa*). Most of the limited urbanization within the Tiger Bay watershed is on the Rima Ridge.

Brush fires burned extensively throughout peninsular Florida during spring 1998 as a result of a severe drought. A high-pressure system remained stationary over the State, blocking the normal pattern of convective thunderstorms (The Orlando Sentinel, 1998). During the 3-month period, April-June, National Oceanic and Atmospheric Administration (NOAA) stations at Daytona Beach and DeLand recorded about 10 and 30 percent of long-term, average precipitation, respectively. Brush fires, ignited by lightning strikes, began in Volusia County on June 19, 1998, and continued until rainfall resumed in late June and early July, burning about 55,000 hectares (one-fifth of the County) and about 40 percent of the watershed (fig. 3). Although areas of both wetlands and uplands were burned during the June-July fires, a comparison of figures 1 and 3 reveals that upland areas were burned more extensively than wetland areas. Re-growth of understory vegetation occurred rapidly after the fires ceased and the rains began. Emergent growth of red root (*Lachnanthes caroliniana*) in burned areas was particularly evident. Some trees were killed by the fire, whereas other burned trees were merely damaged and exhibited leaf regrowth soon after the fire (fig. 4). Large-scale harvesting of insect-infested, fire-damaged trees (both living and dead trees) occurred during the months following the fires. Of the approximately 4,800 hectares that burned within the 9,500-hectare Tiger Bay State Forest, about 3,200 hectares were logged (Catherine Lowenstein, Tiger Bay State Forest, oral commun., 2000). Fires moved from west-to-east through the area of the evapotranspiration station on June 25, 1998. Damaged trees in the vicinity of the evapotranspiration station were logged during November-December 1998.

The two dominant soil groups of the watershed also reflect the areal variation in hydroperiod and vegetation (Baldwin and others, 1980). Wetlands tend to be underlain by organic soils (hyperthermic family of Terric Medisaprists) of the Samsula-Terra Ceia-Tomoka group, that are very poorly drained. The uplands tend to be underlain by poorly drained soils (sandy, siliceous, hyperthermic family of Ultic Haplaquods) of the Pomona-Wauchula group that have a dark, organic-stained subsoil underlain by loamy material.

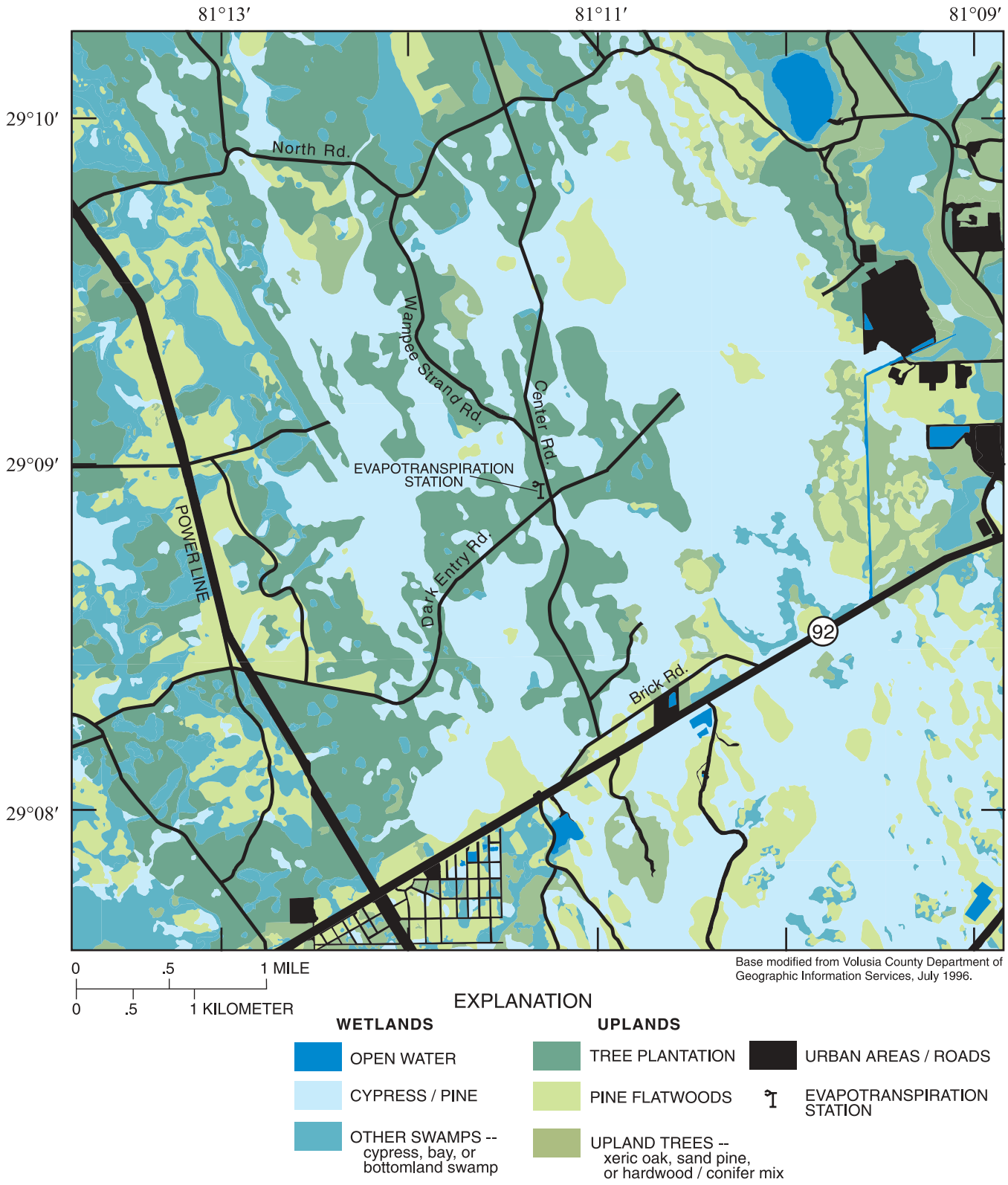

Figure 2. Distribution of vegetation in vicinity of evapotranspiration station.

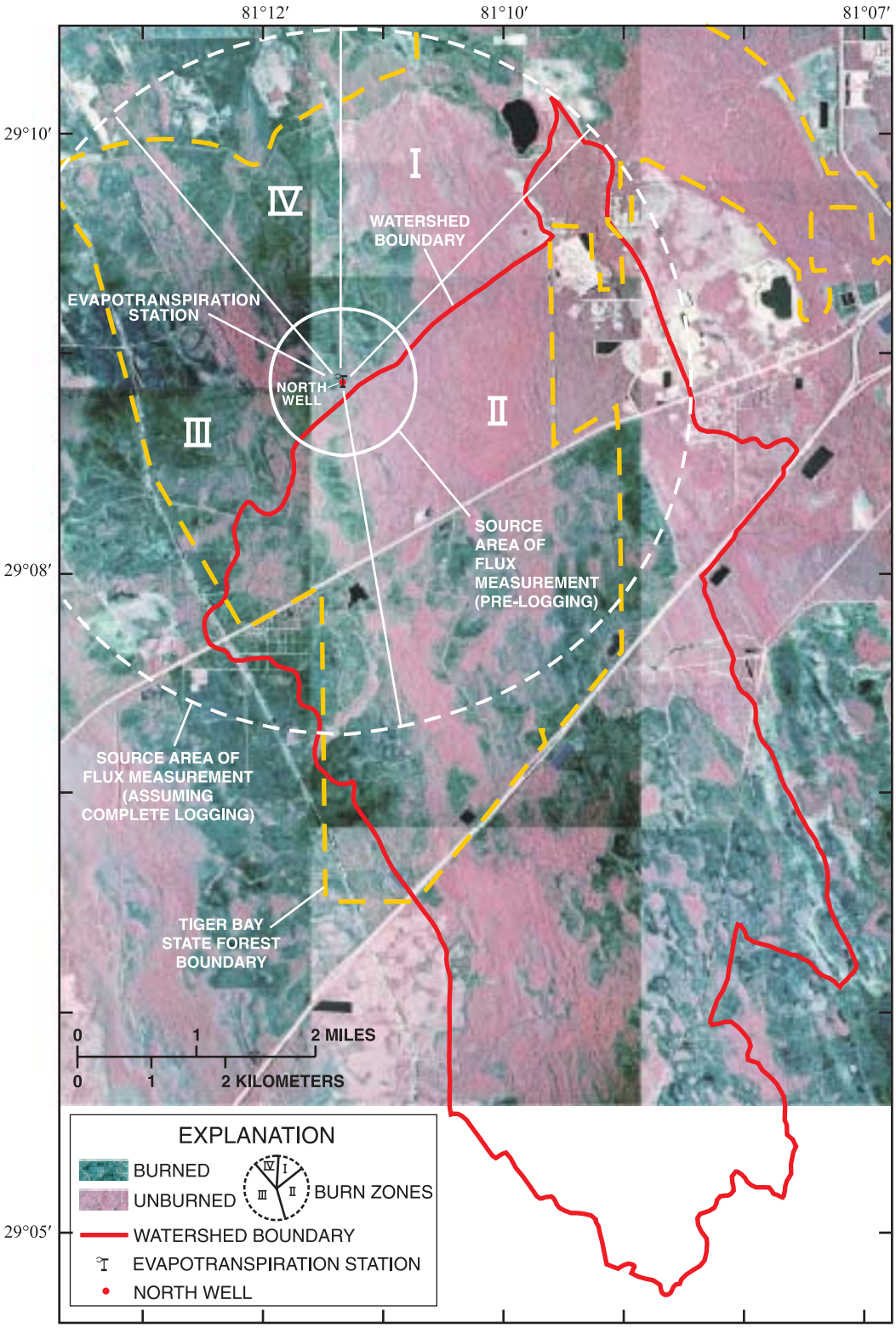

Notes: This image is a composite of aerial photographs produced by Aerial Cartographics of America, Inc. under contract with Tiger Bay State Forest. The photographs were taken from an altitude of about 12,000 feet using a 6-inch focal length camera and Kodak Aerochrome II infrared film 2443.

Unburned areas generally were not logged and logging of the burned areas was partial (about two-thirds). Therefore, the "complete logging" source area depicted in this figure is of a larger radius than that of the true post-logging source data.

Figure 3. Infrared photograph (July 7, 1998) of vicinity of evapotranspiration station showing areas burned during fires of June 1998.

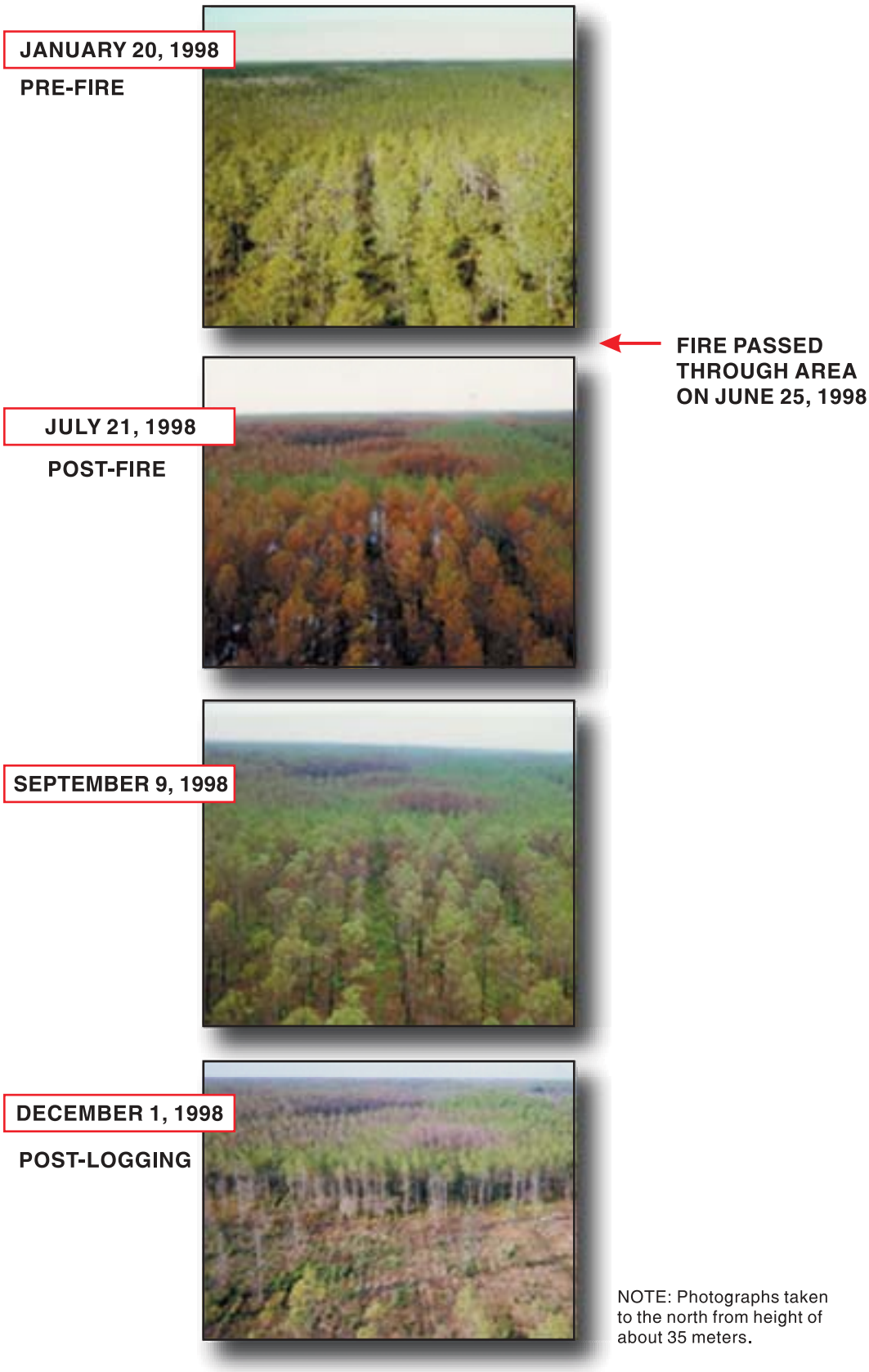

Figure 4. Photographic times series of vegetation in vicinity of evapotranspiration station.

The climate of central Florida is humid subtropical and is characterized by a warm, wet season (June-September) and a mild, relatively dry season (October-May). During the dry season, precipitation commonly is associated with frontal systems. Rainfall averages about 1,350 mm/yr in Volusia County (Rutledge, 1985). More than 50 percent of the annual rainfall generally occurs during the wet season when diurnal thunderstorm activity is common. Mean air temperature in the study area is about 21 ^{o}C, ranging from occasional winter temperatures below 0 ^{o}C to summer temperatures approaching 35 ^{o}C. Diurnal temperature variations average about 12 ^{o}C.

Rainfall to the watershed leaves the basin as runoff, evapotranspiration, or deep leakage from the surficial aquifer system to the underlying Upper Floridan aquifer (Kimrey, 1990; Phelps, 1990). Intermittent runoff gaged at Tiger Bay canal along the northern edge of the watershed (fig. 1) averaged 0.47 cubic meters per second (m^3/s) or about 200 millimeters per year (mm/yr) from 1978 to 1999 (USGS, 1999a). Evapotranspiration has been estimated to average about 990 mm/yr over Volusia County (Rutledge, 1985) and about 890 mm/yr in the Tiger Bay watershed (Camp, Dresser and McKee, Inc., 1996). Previous researchers have documented relatively small differences in the annual evapotranspiration rates from the two primary land covers. Bidlake and others (1993) estimated annual cypress evapotranspiration (970 mm) to be only 8.5 percent less than that from pine flatwoods (1,060 mm), based on studies conducted in Sarasota and Pasco Counties, Fla. Liu (1996) estimated average annual evapotranspiration from both covers to be 1,080 mm, based on a study conducted in Alachua County, Fla.

The hydraulic head in the surficial aquifer system within the watershed generally is above that of the underlying Upper Floridan aquifer. Consequently, water leaks downward from the surficial aquifer system, through the intermediate confining unit, to the Upper Floridan aquifer. Deep leakage was estimated (based on ground-water flow simulations) to have been about 56 mm/yr prior to ground-water development, but in 1995, the rate was estimated to have doubled to 112 mm/yr, as a result of lowering the hydraulic head in the Upper Floridan aquifer by pumping (Stan Williams, St. Johns River Water Management District, oral commun., 2000).

METHODS FOR MEASUREMENT AND SIMULATION OF EVAPOTRANSPIRATION

Evapotranspiration was measured at a site just outside the study area (fig. 1) using the eddy correlation method in a manner similar to that described by Sumner (1996). The site chosen for the evapotranspiration station was within an 18.3-m-tall, 30-year-old pine plantation (fig. 2). Eddy correlation instrumentation was mounted on a 36.5-m-tall Rohn 45G communications-type tower at the site (figs. 5 and 6), and data were

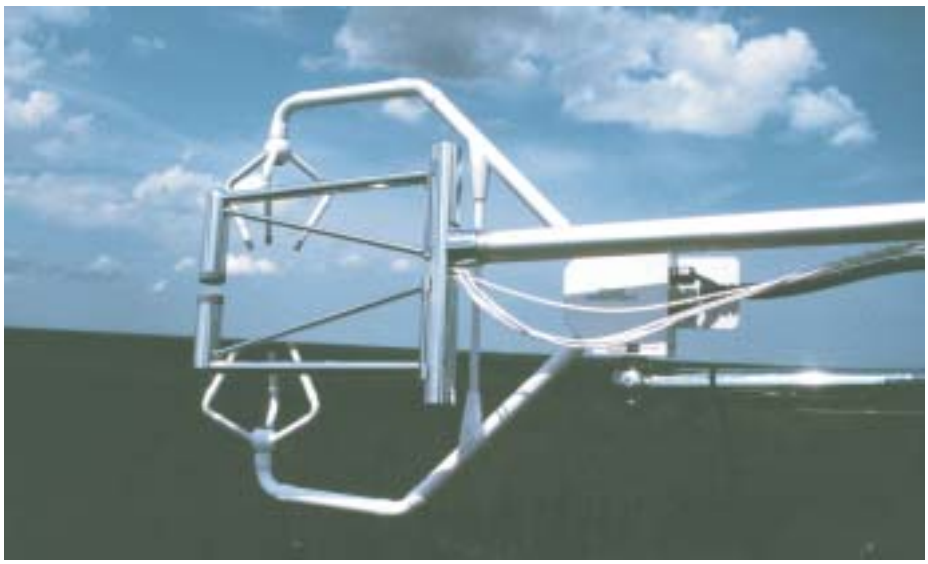

Figure 5. Krypton hygrometer (foreground) and sonic anemometer (background) mounted at top of tower at evapotranspiration station.

Figure 6. Evapotranspiration station being serviced by hydrologic technician.

collected for a 2-year period from January 1, 1998, to December 31, 1999. Other meteorological instrumentation also was deployed on or around the tower to collect data for evapotranspiration modeling and to provide ancillary data for the eddy correlation analysis. Instrumentation used in the study is described in table 1. Measured daily values of evapotranspiration were used to calibrate evapotranspiration models (modified Priestley-Taylor). Evapotranspiration was estimated for burned and unburned areas using the calibrated evapotranspiration models. A water budget for the watershed over the study period was constructed based on measured or estimated values of precipitation, evapotranspiration, runoff, leakage, and storage.

Measurement of Evapotranspiration

Eddy-Correlation Method

The eddy correlation method (Dyer, 1961; Tanner and Greene, 1989) was used to measure two components of the energy budget of the plant canopy: latent and sensible heat fluxes. Latent heat flux (λE) is the energy removed from the canopy in the liquid-to-vapor phase change of water, and is the product of the heat of vaporization of water (λ) and the evapotranspiration rate (E). Sensible heat (H) is the heat energy removed from the canopy as a result of a temperature gradient between the canopy and the air. Both latent and sensible heat fluxes are transported by turbulent eddies in the air. Turbulence is generated by a combination of frictional and convective forces. The energy available to generate turbulent fluxes of vapor and heat is equal to the net radiation (Rn) minus the sum of the heat flux into the soil surface (G) and the change in storage (S) of energy in the biomass and air. The energy involved in fixation of carbon dioxide usually is negligible (Brutsaert, 1982, p. 144). Net radiation is the difference between incoming radiation (shortwave solar radiation and longwave atmospheric radiation) and outgoing radiation (reflected shortwave and longwave radiation; and emitted longwave canopy radiation). Energy is transported to and from the base of the canopy by conduction through the soil. Assuming that net horizontal advection of energy is negligible, the energy-budget equation, for a control volume extending from land surface to a height z_s at which the turbulent fluxes are measured, has the following form:

$$R_n - G - S = H + \lambda E, \qquad (1)$$

where

the left side of equation 1 represents the available energy and the right side represents the turbulent flux of energy;

R_n is net radiation to or from plant canopy, in watts per square meter;

G is soil heat flux at land surface, in watts per square meter;

S is change in storage of energy in the biomass and air, in watts per square meter;

H is sensible heat flux at height z_s above land surface, in watts per square meter;

λE is latent heat flux at height z_s above land surface, in watts per square meter; and

the sign convention is such that R_n and G are positive downwards; H and λE are positive upwards.

Table 1. Study instrumentation

[CSI, Campbell Scientific, Inc.; REBS, Radiation and Energy Balance Systems, Inc.; RMY, R. M. Young, Inc.; TE, Texas Electronics, Inc.; negative height is depth below land surface]

Type of measurement	Instrument	Height(s) above land surface (meters)
Evapotranspiration	CSI eddy correlation system including Model CSAT3 three-dimensional sonic anemometer and Model KH20 krypton hygrometer	36.5
Air temperature/relative humidity	CSI Model HMP35C temperature and relative humidity probe	1.5, 9.1, 18.3, and 35
Net radiation	REBS Model Q-7.1 net radiometer	35
Wind speed/direction	RMY Model 05305-5 Wind Monitor-AQ	35
Photosynthetically active radiation (PAR)	LI-COR, Inc. Model LI190SB quantum sensor	35
Soil moisture	CSI Model CS615 water content reflectometer	0 to -.3
Precipitation	TE Model 525 tipping bucket rain gage and NovaLynx Model 260-2520 forester's (storage) rain gages (2)	18.3 (tipping bucket) and 1 (storage)
Water level in well	Druck, Inc. Model PDCR950 pressure transducer	-2
Datalogging	CSI Model 10X and Model 21X dataloggers; 12 volt deep-cycle batteries (2); 20 watt solar panels (2)	0 to 1

The eddy correlation method is a conceptually simple, one-dimensional approach for measuring the turbulent fluxes of vapor and heat above a surface. For the case of vapor transport above a flat, level landscape, the time-averaged product of measured values of vertical wind speed (w) and vapor density (ρv) is the estimated vapor flux (evapotranspiration rate) during the averaging period, assuming that the net lateral advection of vapor is negligible. Because of the insufficient accuracy of instrumentation available for measurement of actual values of wind speed and vapor density, this procedure generally is performed by monitoring the fluctuations of wind speed and vapor density about their means, rather than monitoring their actual values. This formulation is represented by the following equations:

$$E = \overline{w\rho_v} = \overline{(\bar{w} + w')(\bar{\rho_v} + \rho_v')} \ , \qquad (2)$$

$$= (\overline{\bar{w}\bar{\rho_v}} + \overline{\bar{w}\rho_v'} + \overline{w'\bar{\rho_v}} + \overline{w'\rho_v'}) \text{, and} \qquad (3)$$

$$\overline{w'\rho_v'} = covariance(w, \rho_v) \ , \qquad (4)$$

where

E is evapotranspiration rate, in grams per square meter per second;

w is vertical wind speed, in meters per second;

ρ_v is vapor density, in grams per cubic meter; and overbars and primes indicate means over the averaging period and deviations from means, respectively.

The first term of the right side of equation 3 is approximately zero because mass-balance considerations dictate that mean vertical wind speed perpendicular to the surface is zero; this conclusion is based on an assumption of constant air density (correction for temperature-induced air-density fluctuations is discussed later in this report). The second and third terms are zero based on the definition that the mean fluctuation of a variable is zero. Therefore, it is apparent from equation 4 that vertical wind speed and vapor density must be correlated in order for the value of vapor flux to be non-zero. The turbulent eddies that transport water vapor (and sensible heat) produce fluctuations in both the direction and magnitude of vertical wind speed. The ascending eddies must on average be more moist than the descending eddies for evapotranspiration to occur, that is, upward air movement must be positively correlated with vapor density and downward air movement must be negatively correlated with vapor density.

Source Area of Measurements

The source area for a turbulent flux measurement defines the area (upwind of measurement location) contributing to the measurement. The source area can consist of a single vegetative cover if that cover is adequately extensive. This condition is met if the given cover extends sufficiently upwind such that the atmospheric boundary layer has equilibrated with the cover from ground surface to at least the height of the instrumentation. If this condition is not met, the flux measurement is a composite of fluxes from two or more covers within the source area.

The source area is defined in this report as the area contributing to 90 percent of the sensor measurement. Schuepp and others (1990) provide an estimate of the source area, and the relative contributions within the source area, based on an analytical solution of a one-dimensional (upwind) diffusion equation for a uniform surface cover. In this approach, source area varies with instrument height (z_s), zero displacement height (d), roughness length for momentum (z_m), and atmospheric stability. The instrument height in this study was 36.5 m. Campbell and Norman (1998, p. 71) proposed empirical relations based on canopy height (h) for zero displacement height (d~.65h) and roughness length for momentum (z_m~.10h). Uniform canopy heights of 18.3 m (pre-logging) and 0.3 m (assuming complete logging) were assumed in this analysis. The source area estimates were made assuming mildly unstable conditions; the Obukhov stability length (Businger and Yaglom, 1971) was set equal to -10 m. The source area increases as the height of the instrument above the vegetative canopy increases and as the roughness length for momentum decreases; therefore, the extensive logging that occurred following the fires enlarged the source area. The source area for the turbulent flux measurements (fig. 7) was estimated to be within an upwind distance of about 1,000 m (pre-logging) or 4,800 m (assuming complete logging). As stated earlier, unburned areas generally were not logged and logging of the burned areas was partial (about two-thirds). Therefore, the "complete logging" source area depicted in figure 7 is of a larger radius than that of the true post-logging source area.

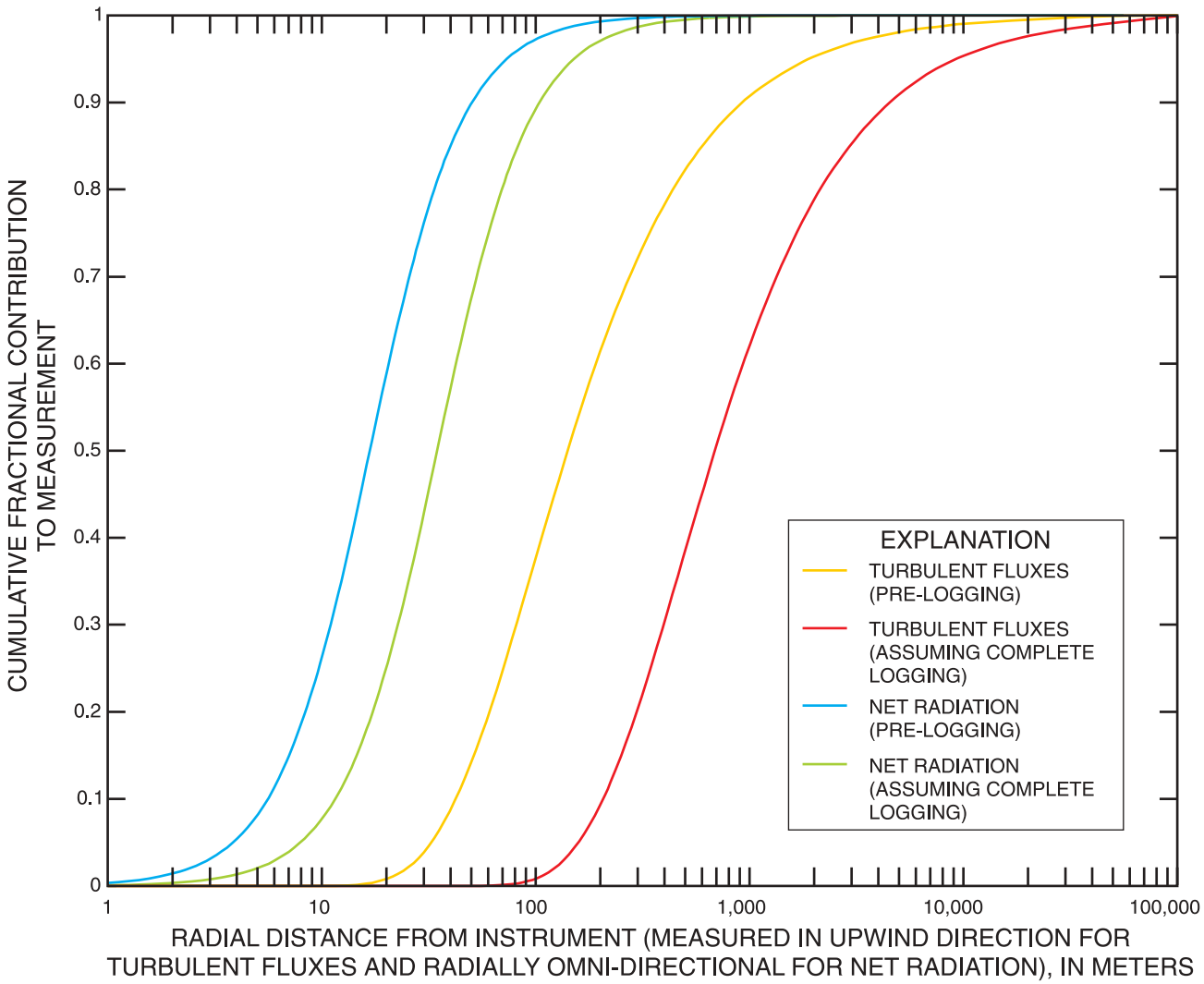

Figure 7. Radial extent of source areas of turbulent flux and net radiation measurements.

The site of the evapotranspiration station was chosen such that the source area of the turbulent flux measurements would be representative of the relative mix of wetlands and uplands in the pre-fire watershed (fig. 1). Before the fire and associated logging, the source area of the turbulent flux measurement (fig. 1) consisted of: 43.7 percent upland, 56.1 percent wetland, and 0.2 percent lake. These relative fractions of wetland and upland were very close to those of the entire Tiger Bay watershed (43.8 percent upland, 55.5 percent wetland, and 0.7 percent lake) before the fires. Also, areas of wetland and upland within the pre-fire source area were interspersed, indicating that turbulent flux measurements approximated a representative value of the composite mix of wetlands and uplands, regardless of the wind direction.

Fires within the watershed during spring 1998 changed the primary components of source area heterogeneity from wetland/upland to burned/unburned (fig. 3) and complicated interpretation of the turbulent flux measurements. Burned and unburned areas were not well-interspersed, resulting in measurements that reflected varying fractions of burned and unburned areas, depending on the wind direction. Following the fires, turbulent fluxes representative of burned areas were measured, both pre- and post-logging, when the wind was from the northwest (zone IV in fig. 3). Turbulent fluxes representative of unburned areas were measured when the wind was from the east (zone II) throughout the study period. The absence of near-station burning in zone II, and therefore a lack of subsequent near-station logging in this zone, resulted in a consistently small (radius of 1,000 m), and unburned, source area throughout the study period when the wind was from zone II. Turbulent fluxes representative of burned areas were measured following the fires and prior to logging when the wind was from the northeast (zone I). With the expansion of the source area associated with logging, however, the post-logging turbulent flux measurements were representative of a composite of burned and unburned areas when the wind was from zone I. Examination of the estimated (Schuepp and others, 1990) cumulative fractional contribution to the turbulent flux measurement as a function of upwind distance from the measurement (fig. 7) provided information to approximate the relative degree of burned/unburned area compositing. Based on this approach, an estimate was made that post-logging turbulent flux measurements made when the wind was from zone I reflected a surface cover that was 75 percent burned and 25 percent unburned. Burned and unburned areas within zone III were relatively well interspersed and in approximately equal relative amounts following the fires. Therefore, post-fire turbulent fluxes measured when the wind was from zone III were assumed to reflect a surface cover that was 50 percent burned and 50 percent unburned. Estimates of the relative contribution (as a function of wind direction and status of the surface cover) of burned vegetation to the measured turbulent flux signal are summarized in table 2. These estimates were used to develop weighting coefficients indicative of the fraction of the turbulent flux measurement for a given day that reflected burned vegetation, which is further discussed later in this report.

Table 2. Relative fraction of burned vegetation sensed by eddy correlation instrumentation

[The sector is in degrees measured clockwise from north (fig. 3); g_i is the fractional contribution of burned area within burn zone i to the measured latent heat flux when wind direction is from burn zone i]

Burn zone i	Sector	g_i		
		Pre-fire	Post-fire/ pre-logging	Post-logging
I	0 to 45	0.0	1.0	0.75
II	45 to 170	.0	0	0
III	170 to 320	.0	0.5	.5
IV	320 to 360	.0	1	1

Instrumentation

Instrumentation capable of high-frequency resolution must be used in an application of the eddy correlation method because of the relatively high frequency of the turbulent eddies that transport water vapor. Instrumentation included a three-axis sonic anemometer and a krypton hygrometer to measure or infer variations in wind speed and vapor density, respectively (fig. 5). The sonic anemometer relies on three pairs of sonic transducers to detect wind-induced changes in the transit time of emitted sound waves and to infer fluctuations in wind speed in three orthogonal directions. The measurement path length between transducer pairs is 10.0 cm (vertical) and 5.8 cm (horizontal); the

transducer path angle from the horizontal is 60 degrees. In contrast to some sonic anemometers used previously (Sumner, 1996), the transducers of this improved anemometer are not permanently destroyed by exposure to moisture, and thus are suitable for long-term deployment. Operation of the anemometer used in this study ceases when moisture on the transducers disrupts the sonic signal, but recommences upon drying of the transducers.

The hygrometer relies on the attenuation of ultraviolet radiation, emitted from a source tube, by water vapor in the air along the 1-cm path to the detector tube. The instrument pathline was laterally displaced 10 cm from the midpoint of the sonic-transducer pathlines. Hygrometer voltage output is proportional to the attenuated radiation signal, and fluctuations in this signal can be related to fluctuations in vapor density by Beer's Law (Weeks and others, 1987). Similar to the anemometer, the hygrometer ceases data collection when moisture obscures the windows on the source or detector tubes. Also, the tube windows become "scaled" with exposure to the atmosphere, resulting in a loss of signal strength. The hygrometer is designed such that vapor density fluctuations are accurately measured in spite of variable signal strength; however, if signal strength declines to near-zero values, the fluctuations cannot be discerned. Periodic cleaning of the windows (performed monthly in this study) with a cotton swab and distilled water restores signal strength. Eddy correlation instrument-sampling frequency was 8 Hertz with 30-minute averaging periods. The eddy correlation instrumentation was placed about 18.2 m above the tree canopy (fig. 6). Data were processed and stored in a datalogger near ground-level.

To be representative of the surface cover, flux measurements must be made in the inertial sublayer, where vertical flux is constant with height and lateral variations in vertical flux are negligible (Monteith and Unsworth, 1990, p. 234). Measurements made in the underlying roughness sublayer can reflect individual roughness elements (for example, individual trees or gaps between trees), rather than the composite surface cover. Garrat (1980) defines the lower boundary of the inertial sublayer to be at a height such that the difference of this height and the zero displacement height (d) is much greater than the roughness length for momentum (z_m). Employing Campbell and Norman's (1998, p. 71) empirical relations and assuming that "much greater than" implies greater by a factor of ten (10), leads to an instrument height (z_s) requirement of $z_s > 1.65h$. A factor of about 2 was used in this study as a conservative measure. As a conservative measure, the instrument height (36.5 m) used in this study was about twice canopy height.

Calculation of Turbulent Fluxes

Latent heat flux was estimated based on a modified form of equation 4:

$$\lambda E = \lambda\left(\overline{w'\rho'_v} + \frac{\rho_v H}{\rho C_p (T_a + 273.15)} + \frac{F K_o H}{K_w (T_a + 273.15)}\right), \quad (5)$$

where

λE is latent heat flux, in watts per square meter;

λ is latent heat of vaporization of water, estimated as a function of temperature (Stull, 1988), in joules per gram;

ρ is air density, estimated as a function of air temperature, total air pressure, and vapor pressure (Monteith and Unsworth, 1990), in grams per cubic meter;

H is sensible heat flux, in watts per square meter;

C_p is specific heat capacity of air, estimated as a function of temperature and relative humidity (Stull, 1988), in joules per gram per degree Celsius;

T_a is air temperature, in degrees Celsius;

F is a factor that accounts for molecular weights of air and atmospheric abundance of oxygen, equal to 0.229 gram-degree Celsius per joule;

K_o is extinction coefficient of hygrometer for oxygen, estimated as 0.0045 cubic meters per gram per centimeter (Tanner and others, 1993);

K_w is extinction coefficient of hygrometer for water, equal to the manufacturer-calibrated value, in cubic meters per gram per centimeter; and overbars and primes indicate means over the averaging period and deviations from the means, respectively.

The second and third terms of the right side of equation 5 account for temperature-induced fluctuations in air density (Webb and others, 1980) and for the sensitivity of the hygrometer to oxygen (Tanner and Greene, 1989), respectively.

Similarly to vapor transport, sensible heat can be estimated by:

$$H = \rho C_p \overline{w'T_a'} \; . \qquad (6)$$

The sonic anemometer is capable of measuring "sonic" temperature based on the dependence of the speed of sound on this variable (Kaimal and Businger, 1963; Kaimal and Gaynor, 1991). Schotanus and others (1983) related the sonic sensible heat based on measurement of sonic temperature fluctuations to the true sensible heat given in equation 6. Those researchers included a correction, for the effect of wind blowing normal to the sonic acoustic path, that has been incorporated directly into the anemometer measurement by the manufacturer (E. Swiatek, Campbell Scientific, Inc., written commun., 1998), leading to a simplified form of the Schotanus and others (1983) formulation given by:

$$\overline{w'T_a'} = \overline{w'T_s'} - 0.51(\overline{T_a + 273.15})\overline{w'q'} \, , \qquad (7)$$

where

T_s is the sonic temperature, in degrees Celsius; and

q is specific humidity, in grams of water vapor per grams of moist air.

Based on the relation between specific humidity and vapor density (ρ_v) (Fleagle and Businger, 1980):

$$q \approx \frac{\rho_v R_d (T_a + 273.15)}{P_a} \, , \qquad (8)$$

where

ρ_v is vapor density, in grams per cubic meter,

equation 7 can be expressed in terms of fluctuations in the hygrometer-measured water vapor density rather than fluctuations in specific humidity as:

$$\overline{w'T_a'} = \overline{w'T_s'} - \frac{0.51 R_d \overline{(T_a + 273.15)}^2 \, \overline{w'\rho_v'}}{P_a} \, , \qquad (9)$$

where

R_d is the gas constant for dry air (0.28704 joules per degree Celsius per gram); and

P_a is atmospheric pressure, in pascals (assumed to remain constant at 100,700 pascals at top of tower at about 48 meters above sea level).

Estimation of turbulent fluxes (eqs. 5 and 6) relies on an accurate measurement of velocity fluctuations perpendicular to the lateral airstream. The study area is relatively flat and level, indicating that the airstream is approximately perpendicular to gravity and the sonic anemometer was oriented with respect to gravity with a bubble level. Measurement of wind speed in three orthogonal directions with the sonic anemometer allows for a more refined orientation of the collected data with the natural coordinate system through mathematical coordinate rotations. The magnitude of the coordinate rotations are determined by the components of the wind vector in each 30-minute averaging period. The wind vector is composed of three time-averaged components (u, v, w) in the three coordinate directions (x, y, z). Using a bubble level, direction z initially was approximately oriented with respect to gravity, and the other two directions were arbitrary. Tanner and Thurtell (1969) and Baldocchi and others (1988) outline a procedure in which measurements made in the initial coordinate system are transformed into values consistent with the natural coordinate system. First, the coordinate system is rotated by an angle η about the z-axis to align u into the x-direction on the x-y plane. Next, rotation by an angle θ is performed about the y-direction to align w along the z-direction. These rotations force $\overline{v}$ and $\overline{w}$ equal to zero, and, therefore, $\overline{u}$ is pointed directly into the airstream. A third rotation is sometimes used in complex situations (such as a curving airstream around a mountain) to force $\overline{v'w'}$ equal to zero, although Baldocchi and others (1988) indicate that two rotations generally are adequate. The angle θ approximates the angle at which the original sensor orientation was "mis-leveled" with respect to a direction perpendicular to the lateral airstream. The coordinate rotation-transformed covariances needed to compute turbulent fluxes are given by:

$$(\overline{w'c'})_r = \overline{w'c'}\cos\theta - \overline{u'c'}\sin\theta\cos\eta - \overline{v'c'}\sin\theta\sin\eta, \qquad (10)$$

where

$(\overline{w'c'})_r$ is the rotated covariance;

c' is the fluctuation in either vapor density (ρ_v) or virtual temperature (T_s); and

$\overline{w'c'}$, $\overline{u'c'}$, and $\overline{v'c'}$ are covariances measured in the original coordinate system;

$$\cos\theta = \sqrt{\frac{(u^2 + v^2)}{(u^2 + v^2 + w^2)}}, \quad (11)$$

$$\sin\theta = \frac{w}{\sqrt{(u^2 + v^2 + w^2)}}, \quad (12)$$

$$\cos\eta = \frac{u}{\sqrt{(u^2 + v^2)}}, \text{ and} \quad (13)$$

$$\sin\eta = \frac{v}{\sqrt{(u^2 + v^2)}}. \quad (14)$$

The presence of the tower and the anemometer produced spurious turbulence which possibly impacted measured velocity fluctuations, particularly when the wind was from the tower-side of the sensor. Turbulent flux data for which the inferred mis-leveling angle θ was greater than 10 degrees were excluded based on the assumption that spurious turbulence was the cause of the excessive amount of coordinate rotation.

Consistency of Measurements with Energy Budget

Previous investigators (Moore, 1976; Lee and Black, 1993; Bidlake and others, 1993; Goulden and others, 1996; Sumner, 1996; Twine and others, 2000; and German, 2000) have described a recurring problem with the eddy correlation method: a common discrepancy of the measured latent and sensible heat fluxes with the energy-budget equation (eq. 1). The usual case is that measured turbulent fluxes ($H + \lambda E$) are less than the measured available energy ($R_n - S$). Bidlake and others (1993) accounted for only 49 and 80 percent of the measured available energy with measured turbulent fluxes ($H + \lambda E$) at cypress swamp and pine flatwood sites, respectively. Turbulent fluxes measured above a coniferous forest by Lee and Black (1993) accounted for only 83 percent of available energy. Several researchers (Moore, 1976; Goulden and others, 1996; German, 2000) have shown that the eddy correlation method performs best in windy conditions (relatively high friction velocity, u*). Friction velocity is directly proportional to wind speed, but also incorporates the frictional effects of the plant canopy and land surface on the wind and the effects of atmospheric stability (Campbell and Norman, 1998, eq. 7.24). Friction velocity can be computed with three-dimensional sonic anemometer measurements of velocity fluctuations as (Stull, 1988, eq. 2.10b):

$$u^* = \sqrt{\sqrt{\overline{u'w'}^2 + \overline{v'w'}^2}}. \quad (15)$$

Goulden and others (1996) concluded that eddy correlation-measured values of carbon flux from a forest were underestimated when u^* was less than 0.17 m/s. German (2000) noted that at u^* greater than 0.3 m/s, little discrepancy existed between measured available energy and measured turbulent fluxes.

Possible explanations for the observed discrepancy between the measured turbulent fluxes and the measured available energy include: a sensor frequency response that is insufficient to capture high-frequency eddies; an averaging period insufficient to capture low-frequency eddies, resulting in a non-zero mean wind speed perpendicular to the airstream; drift in the absolute values of anemometer and hygrometer measurements resulting in statistical non-stationarity within the averaging period; lateral advection of energy; and overestimation of available energy. Lateral advection of energy is not a likely explanation because most of the studies reporting underestimation of turbulent fluxes were conducted at sites with adequately extensive surface covers. Measurement of the soil heat flux and storage terms of the available energy can be problematic, given the difficulty in making representative measurements of these terms; however, the turbulent flux underestimation occurs even with a daily composite of fluxes (in which case these terms generally are negligible).

Likewise, overestimation of net radiation seems unlikely, given the relative simplicity and laboratory calibration of net radiometers. For these reasons, it was assumed in this study that the available energy was accurately measured and that any error in energy-budget closure was associated with errors in measurement of turbulent fluxes.

Moore (1976) also noticed an underestimation of turbulent fluxes and suggested that this underestimation would likely apply equally to each of the turbulent fluxes (sensible and latent heat flux), leading to the conclusion that the ratio of the fluxes can be measured adequately. This assumption seems reasonable, given that the same turbulent eddies transport both sensible and latent heat, and therefore, any eddies that are missed by the instrumentation because of anemometer response or averaging period would have a proportionally equal effect on both turbulent fluxes. German (2000) provided empirical support for this assumption at a sawgrass site in south Florida where simultaneous measurement of the ratio of fluxes was based on two approaches: the eddy correlation method (using instrumentation identical to that used in the present study) and the measurement of temperature and vapor pressure differentials between vertically separated sensors (Bowen, 1926). These independent approaches for estimating the ratio of turbulent fluxes were in reasonable agreement during the daylight hours when evapotranspiration predominated. Assuming that the ratio of turbulent fluxes is adequately measured by the eddy correlation method, the energy budget equation (eq. 1), along with turbulent fluxes (H and λE) measured using the standard eddy correlation technique, can be used to produce corrected (H_{cor} and λE_{cor}) turbulent fluxes in an energy-budget variant of the eddy correlation method:

$$R_n - G - S = H_{cor} + \lambda E_{cor} = \lambda E_{cor}(1 + B), \quad (16)$$

where the Bowen ratio (B) is given by:

$$B = \frac{H}{\lambda E} . \quad (17)$$

Rearranging eq. 16:

$$\lambda E_{cor} = \frac{R_n - G - S}{1 + B} , \text{ and} \quad (18)$$

$$H_{cor} = R_n - G - S - \lambda E_{cor} . \quad (19)$$

Instrumentation was installed at the evapotranspiration station to provide estimates of soil heat flux (G) and changes in stored energy (S) in the biomass and air. Soil heat flux at a depth of 8 cm was measured at two representative locations using soil heat-flux plates. An estimate of the soil heat flux at land surface was computed based on the estimated change in stored energy in the soil above the heat flux plates. The changes in stored energy in the soil above the heat flux plates were estimated based on thermocouple-measured changes in soil temperature and estimates of soil heat capacity. The estimates of soil heat capacity were based on mineralogy, soil bulk density, and soil moisture content. Soil moisture content was measured using time-domain reflectometry (TDR) probes placed within the upper 8 cm of soil. Thermocouples were installed at multiple locations within the trunks of representative trees to allow for estimation of changes in storage of energy within the biomass. Estimates of biomass density (based on tree surveys) and biomass heat capacity (available from previous studies) also are required for calculation of changes in biomass stored energy. Changes in storage of energy in the air generally are small in comparison with soil heat flux and biomass heat storage, but were estimated based on measurement of the temperature and relative humidity profile below the turbulent flux sensors. With the exception of the temperature and relative humidity sensors, all of the instrumentation intended to provide data to estimate soil heat flux and changes in stored energy was destroyed by earth-moving equipment used to construct a fire break around the evapotranspiration station a few hours before a fire passed through the area of the station.

Energy generally enters the soil surface and is stored in the biomass and air during the day and released at night. Evaluation of equations 18 and 19 was facilitated by using daily composites of terms in these equations and assuming that soil heat flux and changes in energy storage in the biomass and air were negligible over a diurnal cycle. This approach allowed for neglect of those terms of the energy budget that were not measured as a result of fire-damaged instrumentation.

During periods of rapid temperature changes (for example, cold front passage), however, the net soil heat flux and the net change in energy stored in the biomass and air over a diurnal cycle may not be negligible.

As mentioned previously, problems such as scaling of hygrometer windows, moisture on anemometer or hygrometer, or excessive coordinate rotation can result in missing 30-minute turbulent flux data. These data must be estimated prior to construction of daily composites of turbulent fluxes. In the present study, regression analysis of measured turbulent flux data and photosynthetically active radiation (PAR) was used to estimate unmeasured values of turbulent fluxes. These regression-estimated values of turbulent fluxes are not as reliable as measured values; therefore, the fraction of daily-composited turbulent flux data derived from regression estimates was limited to 25 percent (up to 6 hours per day). The procedure outlined above for culling, estimating, and compositing 30-minute turbulent flux data still resulted in missing values for some days.

Simulation of Evapotranspiration

An evapotranspiration model was developed for estimating daily values of evapotranspiration representative of both burned and unburned areas. Post-fire measurements of evapotranspiration generally reflected a composite of evapotranspiration from burned and unburned vegetation. A model was developed that reflected the mixture of source area characteristics and allowed calculation of the evapotranspiration from each source area.

Evapotranspiration Models

The eddy correlation instrumentation can have extended periods of inoperation, as discussed previously. However, more robust meteorological and hydrologic instrumentation (sensors for measurement of net radiation, air temperature, relative humidity, PAR, wind speed, soil moisture, and water-table depth) can provide nearly uninterrupted data collection. Evapotranspiration models, calibrated to measured turbulent flux data and based on continuous meteorological and hydrologic data, can provide continuous estimates of evapotranspiration. Evapotranspiration models also can provide insight into the cause-and-effect relation between the environment and evapotranspiration.

Physics-based evapotranspiration models generally rely on the work of Penman (1948), who developed an equation for evaporation from wet surfaces based on energy budget and aerodynamic principles. That equation has been applied to estimate evapotranspiration from well-watered, dense agricultural crops (reference or potential evapotranspiration). In Penman's equation, the transport of latent and sensible heat fluxes from a "big leaf " to the sensor height is subject to an aerodynamic resistance. The big leaf assumption implies that the plant canopy can be conceptualized as a single source of both latent and sensible heat at a given height and temperature. Inherent in the Penman approach is the assumption of a net one-dimensional, vertical transport of vapor and heat from the canopy. The Penman equation is given by:

$$\lambda E = \frac{\Delta(R_n - G - S) + \frac{\rho C_p (e_s - e)}{r_h}}{\Delta + \gamma}, \qquad (20)$$

where

λE is latent heat flux, in watts per square meter;
Δ is slope of the saturation vapor-pressure curve, in kilopascals per degree Celsius;
G is soil heat flux at land surface, in watts per square meter;
S is change in storage of energy in the biomass and air, in watts per square meter;
C_p is specific heat capacity of the air, in joules per gram per degree Celsius;
e_s is saturation vapor pressure, in kilopascals;
e is vapor pressure, in kilopascals;
r_h is aerodynamic resistance, in seconds per meter; and
γ is the psychrometric "constant", equal to approximately 0.067 kilopascals per degree Celsius, but varying slightly with atmospheric pressure and temperature.

The first term is known as the energy term; the second term is known as the aerodynamic term.

Priestley and Taylor (1972) proposed a simplification of the Penman equation for the case of saturated atmosphere ($e = e_s$), for which the aerodynamic term is zero:

$$\lambda E = \frac{\Delta(R_n - S)}{\Delta + \gamma}. \qquad (21)$$

However, Priestley and Taylor (1972) noted that empirical evidence suggests that evaporation from extensive wet surfaces is greater than this amount, presumably because the atmosphere generally does not attain saturation. Therefore, the Priestley-Taylor coefficient, α, was introduced as an empirical correction to the theoretical expression (eq. 21):

$$\lambda E = \alpha \frac{\Delta (R_n - S)}{\Delta + \gamma}. \qquad (22)$$

This formulation assumes that the energy and aerodynamic terms of the Penman equation are proportional to each other. The value of α has been estimated to be 1.26, which indicates that under potential evapotranspiration conditions, the aerodynamic term of the Penman equation is about 21 percent of the total latent heat flux. Eichinger and others (1996) have shown that the empirical value of α has a theoretical basis; a nearly constant value of α is expected under the existing range of Earth-atmospheric conditions.

Previous studies (Flint and Childs, 1991; Stannard, 1993; Sumner, 1996) have applied a modified form of the Priestley-Taylor equation. The approach in these studies relaxes the Penman assumption of a free-water surface or a dense, well-watered canopy by allowing α to be less than 1.26 and to vary as a function of environmental factors. The Penman-Monteith equation (Monteith, 1965) is a more theoretically rigorous generalization of the Penman equation that also accounts for a relaxation of the these Penman assumptions. However, Stannard (1993) noted that the modified Priestley-Taylor approach to simulation of observed evapotranspiration rates was superior to the Penman-Monteith approach for a sparsely vegetated site in the semi-arid rangeland of Colorado. Similarly, Sumner (1996) noted that the modified Priestley-Taylor approach performed better than did that of Penman-Monteith for a site of herbaceous, successional vegetation in central Florida. Therefore, the modified Priestley-Taylor approach was chosen for the present investigation.

Partitioning of Measured Evapotranspiration

An evapotranspiration model (daily resolution) was developed to partition the measured evapotranspiration into two components characteristic of the primary types of surface cover (burned and unburned) of the watershed during the study period. As mentioned previously, upland areas were more likely to have been burned during the June-July 1998 fires than wetland areas. Therefore, to some extent, the model results also reflect the variation between upland and wetland evapotranspiration. The model was of the following form:

$$\lambda E = (1 - w_b)\lambda E_u + w_b \lambda E_b, \qquad (23)$$

where

λE is measured latent heat flux at station, in watts per square meter;

w_b is the fraction of the measured latent heat flux originating from burned areas, dimensionless;

λE_u is latent heat flux from unburned areas, in watts per square meter; and

λE_b is latent heat flux from burned areas, in watts per square meter.

The weighting coefficient (w_b) for a given day must incorporate the spatial distribution of surface cover types near the point of flux measurement (fig. 3 and table 2), the changing (upwind) source area for the measurement associated with changes in wind direction, and the diurnal changes in evapotranspiration. If the relative fraction of burned surface cover in the upwind source area remained constant for a given day (that is, the wind direction remained from a given zone of a relatively uniform mixture of surface cover types), w_b would be simply the fraction of burned surface cover within the zone. Also, if evapotranspiration from each surface cover type remained constant during a given day, w_b would be simply the time-weighted average of the fraction of burned surface cover within the upwind source areas. However, intra-day changes in source area composition, associated with changes in wind direction, and the strong diurnal cycle in evapotranspiration had to be considered during computation of day-by-day values of w_b. For example, suppose that the wind were from the west during the night and from the east during the day. In this situation, the measured daily evapotranspiration would be much more representative of the surface cover to the east because daytime evapotranspiration generally is much higher than nighttime evapotranspiration. Strong diurnal biases in wind direction (fig. 8) exist in the study area, which can lead to situations such as that described. Therefore, weighting coefficients must reflect these diurnal patterns in evapotranspiration.

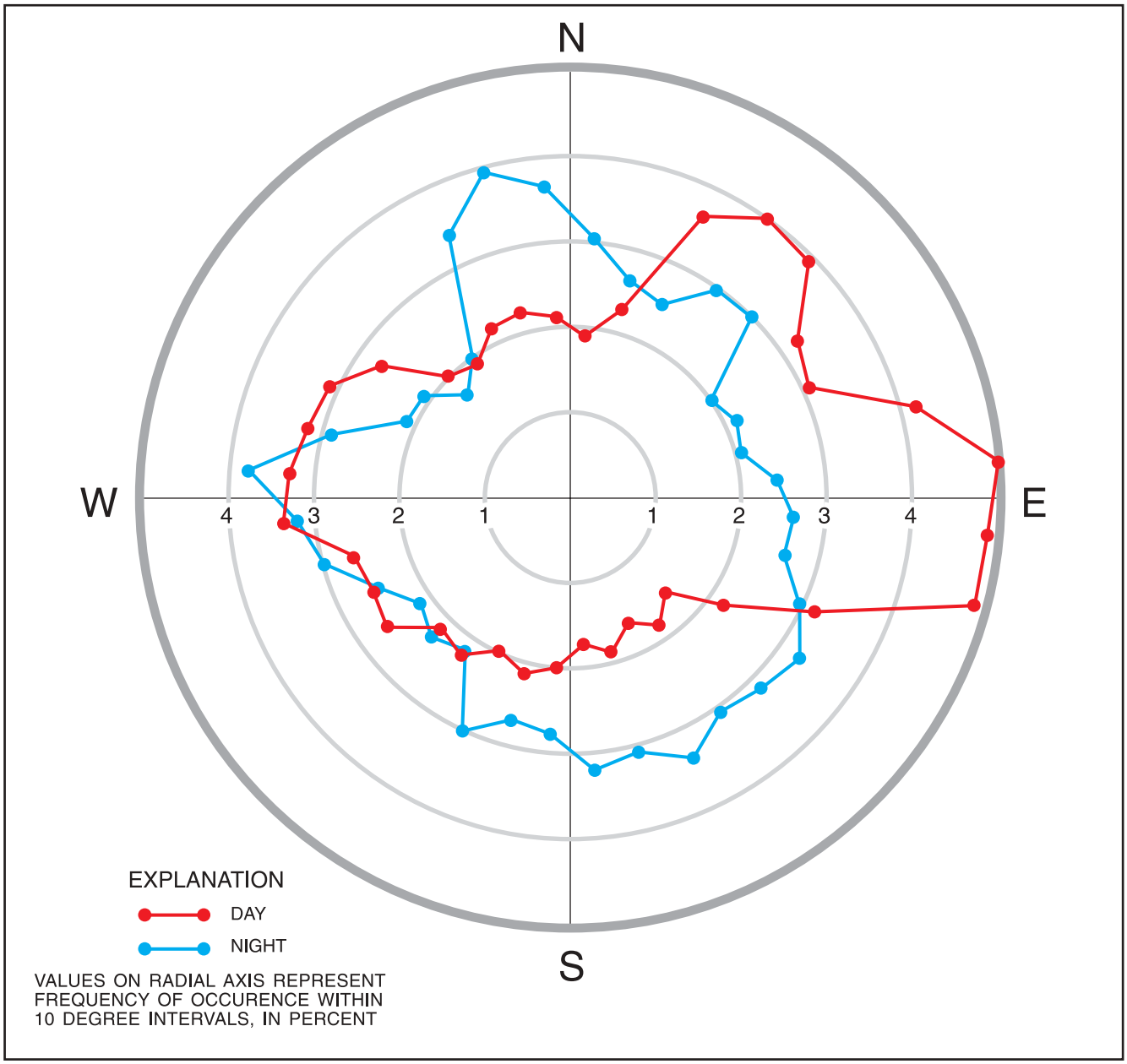

Figure 8. Wind direction frequency pattern at location of evapotranspiration station.

The diurnal pattern of evapotranspiration during a given day generally is strongly correlated with the diurnal pattern of incoming radiation, as can be inferred from the Priestley-Taylor equation (eq. 22) or seen empirically (Sumner, 1996). PAR was used as a surrogate for the factors that produce intra-day variations in evapotranspiration for both surface cover types. Nighttime PAR is equal to zero, implying that only daytime winds from a given zone are assumed to contribute to the measured latent heat flux for a given day. Other factors (such as variations in air temperature) that contribute to the diurnal pattern of evapotranspiration were considered minor, compared to the effect of PAR, and were not considered in the determination of weights for use in eq. 23. The computation for the day-by-day values of w_b is derived in Appendix I and given by:

$$w_b = \sum_{i=I}^{IV} g_i f_i, \qquad (24)$$

where

g_i is the fractional contribution of burned area within burn zone i to the measured latent heat flux when wind direction is from burn zone i (table 2);

i is an index for the burn zones (fig. 3); and

f_i is the PAR-weighted fraction of the day that wind direction is from burn zone i and is computed as:

$$f_i = \frac{\sum_{k=1}^{48} PAR_k \delta_i(\Psi_k)}{\sum_{k=1}^{48} PAR_k}, \quad (25)$$

where

k is an index for the 48 measurements of 30-minute averages within a given day;

PAR_k is the measured PAR for time period k within a given day;

$\delta_i(\Psi_k)$ is a binary function equal to 1 if Ψ_k is within burn zone i and otherwise equals 0; and

Ψ_k is the wind direction for time period k within a given day.

In the evapotranspiration model (eq. 23), both λE_u and λE_b are simulated by the modified Priestley-Taylor equation (eq. 22) with individual Priestley-Taylor α functions. The α function for λE_u was assumed to remain unchanged throughout the 2-year study period; however, the α function for λE_b was divided into multiple time periods to reflect the radical change in surface cover of the burned areas following the fire, logging, and regrowth of vegetation. The measurements of average, daily evapotranspiration provided a standard with which to calibrate the Priestley-Taylor evapotranspiration model. Calibration of the Priestley-Taylor model involved quantification of the functional relations between the Priestley-Taylor α and environmental variables. This quantification was achieved through identification of the form of the functional relation (trial-and-error approach) and estimation of the parameters of that relation (regression analysis) that produced optimal correspondence between measured and simulated values of latent heat flux.

The form of the calibrated model (eq. 23) allowed for evapotranspiration to be estimated for any mix of burned and unburned areas through appropriate specification of w_b. Daily values of evapotranspiration for burned and unburned areas were estimated with w_b equal to 1 and 0, respectively. Evapotranspiration from the watershed was estimated with w_b equal to 0 and 0.4 (burned fraction of watershed) prior to and following the fires, respectively; potential evapotranspiration from the watershed was estimated with similar weighting, but with a Priestley-Taylor α equal to a constant value of 1.26.

Measurement of Environmental Variables

Meteorological, hydrologic, and vegetative data were collected in the study area for several reasons: (1) as ancillary data required by the energy-budget variant of the eddy correlation method, (2) as independent variables within the evapotranspiration model, and (3) to construct a water budget for the Tiger Bay watershed. Meteorological variables monitored included net radiation, air temperature, relative humidity, wind speed, and PAR. These data were recorded by dataloggers at 15-second intervals, using instrumentation summarized in table 1, and the resulting 30-minute means were stored.

Two net radiometers, each deployed at a height of 35 m, provided redundant measurements of net radiation at the evapotranspiration station. Measured values of net radiation were corrected for wind-speed effects as suggested by the instrument manual for the Radiation and Energy Balance Systems, Inc., Model Q-7.1 net radiometer. In late 1999, missing net radiation data necessitated an estimate of net radiation based on a regression of PAR and net radiation. PAR consists of that part of incoming solar radiation that is used in plant photosynthesis and is highly correlated with incoming solar radiation. Based on data collected during 1993-1994 in Orange County, Fla., solar radiation (in watts per square meter) can be approximated (standard error of estimate = 11 watts per square meter) as 0.49 times PAR (in micromoles per second per square meter).

The source area of the net radiation measurement was estimated by using the approach of Reifsnyder (1967) and Stannard (1994). The measurement of net radiation had a much smaller source area than the turbulent flux measurement (fig. 7). About 90 percent of the source area for the net radiometers was within a radial distance of 55 m (pre-logging) or 110 m (post-logging). Therefore, the source area for the net radiometer in the near-vicinity of the evapotranspiration station was one of the following: (1) pine plantation (pre-logging), (2) burned pine plantation (post-fire, but

pre-logging), or (3) clear-cut, with understory regrowth (post-logging). Other covers also existed within the watershed, primarily wetlands and unburned pine lands. Lacking net radiation measurements over more than one cover, the assumption was made that net radiation measured at the unburned pine plantation was representative of all unburned surface covers. The period of record prior to the fire (the initial 175 days of 1998) was used to develop a regression-based predictor of net radiation as a function of PAR. This relation was used to estimate net radiation in unburned areas following the burning of the area around the evapotranspiration station. The net radiation measured at the evapotranspiration station following burning was assumed to be representative of all burned areas. Logging of the burned area near the evapotranspiration station occurred during a period of extensive logging throughout the watershed. Some error is introduced to the estimation of net radiation over burned areas because the logging was not simultaneous for all burned areas and because the logging over burned areas was not complete (as mentioned previously, two-thirds of the burned forest within Tiger Bay State Forest was logged). Estimates of daily net radiation for burned and unburned areas were composited into a value consistent with the turbulent flux measurements (eqs. 18 and 19) using the weighting coefficient (w_b) previously defined (eq. 24):

$$R_n = (1 - w_b)R_{nu} + w_b R_{nb}, \qquad (26)$$

where

R_n is composited net radiation, in watts per square meter;

R_{nu} is net radiation for unburned areas, in watts per square meter; and

R_{nb} is net radiation for burned areas, in watts per square meter.

A regression between post-logging, daily values of net radiation and PAR was used to estimate net radiation from burned and logged surfaces during the later part of 1999 after net radiometer domes were damaged, perhaps by birds.

Vegetation within the study area was mapped previously by Volusia County Department of Geographic Information Systems (1996a and 1996b) and Simonds and others (1980). Post-fire, infrared, aerial photographs were used to identify the areal distribution of burned vegetation in the watershed. Temporal variations in vegetation were documented with monthly photographs taken from the tower at the evapotranspiration station and with normalized difference vegetation index (NDVI) data. NDVI data were provided by the USGS Earth Resources Observation Systems (EROS) Data Center through analysis of the Advanced Very High Resolution Radiometer (AVHRR) data (Eidenshink, 1992; USGS, 1998b and 1999b) from operational National Oceanic and Atmospheric Administration (NOAA) polar-orbiting satellites. NDVI is defined as:

$$NDVI = \frac{NIR - Vis}{NIR + Vis}, \qquad (27)$$

where

NIR is near-infrared reflectance measured in AVHRR band 2 (725 - 1100 nanometers); and

Vis is visible reflectance measured in AVHRR band 1 (580 - 680 nanometers).

NDVI is highly correlated with the density of living, leafy vegetation. The physical basis for this correlation is the sharp contrast in the absorptivities of visible and near-infrared radiation by leaves, which absorb approximately 85 percent of incident visible radiation, but only 15 percent of near-infrared radiation (Campbell and Norman, 1998). Other ground covers (dead plant material, soil, and water) do not exhibit this extreme spectral differential in absorption. The AVHRR-computed NDVI data are provided at 2-week and 1-kilometer (km) by 1-km resolution. For the present study, NDVI data, within a 3-km by 3-km square and approximately centered on the location of the evapotranspiration station, were composited to quantify temporal trends in the density of living, leafy vegetation in the vicinity of the turbulent flux measurements during the study period.

Air temperature and relative humidity were monitored at the evapotranspiration station at heights of 1.5, 9.1, 18.3, and 35 m. The slope of the saturation vapor pressure curve (a function of air temperature) and vapor pressure deficit were computed in the manner of Lowe (1977) using the average of air temperature and relative humidity values measured at these four heights. A propeller-type anemometer to monitor wind speed and direction and a upward-facing quantum sensor to measure incoming PAR were deployed at a height of 35 m at the evapotranspiration station.

Hydrologic variables that were monitored included precipitation, water-table depth, stream discharge, and soil moisture. Precipitation records were obtained from a tipping bucket rain gage mounted at a height of about 18.3 m at the evapotranspiration station and from two storage rain gages installed in forest clearings and monitored weekly (fig. 9). Spatial variability in annual rainfall can be substantial within Volusia County, based on the long-term NOAA stations at DeLand and Daytona Beach (fig. 9). The Daytona Beach area, on average, receives about 15 percent less annual rainfall than does the DeLand area (National Oceanic and Atmospheric Administration, 1998 and 1999). The uncertainty associated with the rainfall distribution between these two stations precluded the use of both stations for estimation of rainfall to the Tiger Bay watershed during the study period. Rather, the rainfall totals from the two storage rain gages located near the watershed were averaged to provide estimates of rainfall to the watershed. Tipping bucket rain gages can underestimate rainfall, particularly during high-intensity events; therefore, the tipping bucket gage monitored at the evapotranspiration station was used primarily to provide a high-resolution description of the temporal rainfall pattern, and the storage rain gages were used primarily to estimate cumulative rainfall.

Water-table depth was monitored at two surficial-aquifer system wells at opposite ends of the watershed. Water-level measurements were obtained at 30-minute intervals using a pressure transducer in the north well (USGS site identification number 290813081111801),

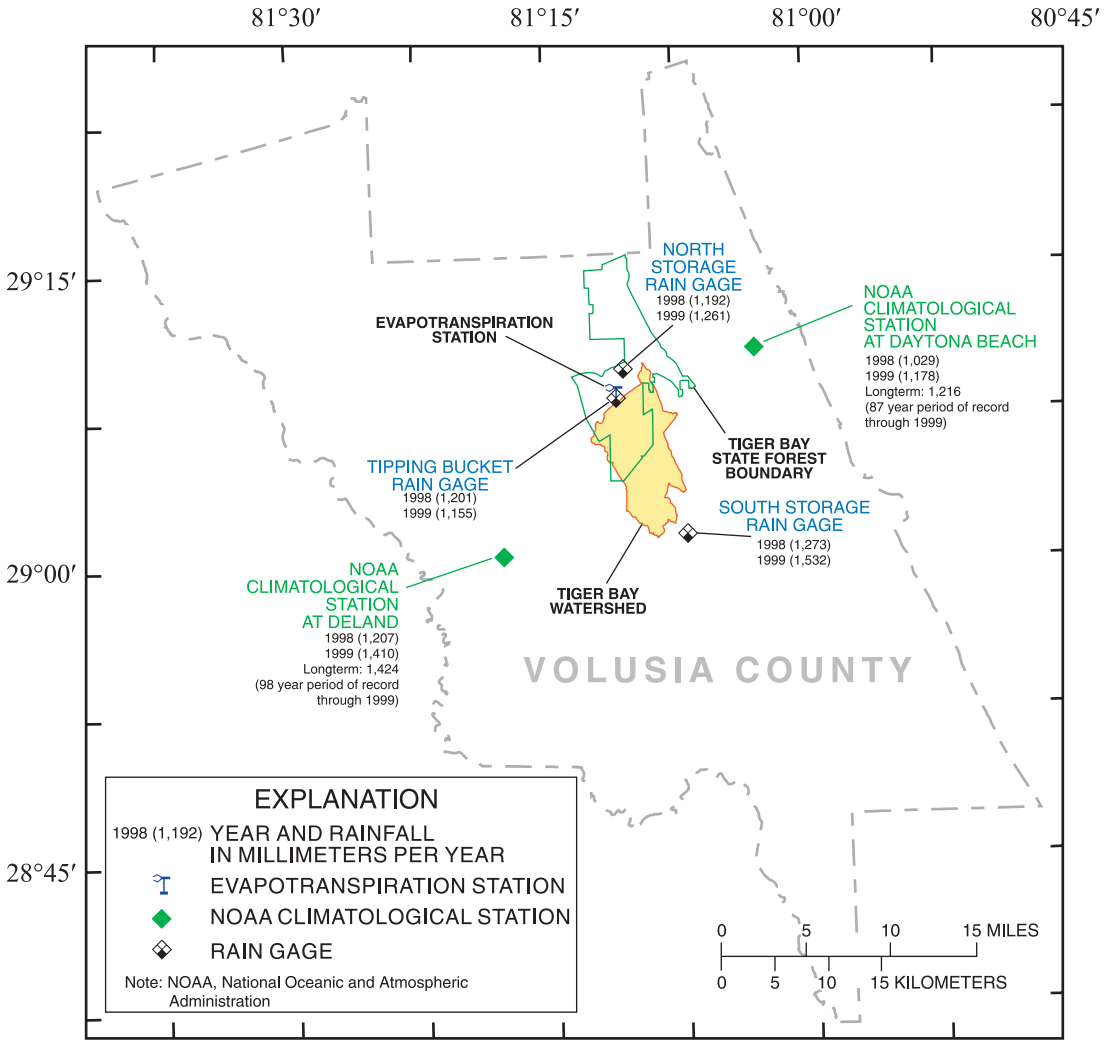

Figure 9. Location of rain gages in vicinity of Tiger Bay watershed.

located at the evapotranspiration station. The south well (USGS site identification number 290119081074001), at the location of the south storage rain gage (fig. 1), was measured weekly using an electric tape. Although the two wells monitored were located at opposite ends of the watershed (fig. 1), both wells were within similar upland settings. Although the water-table depth in wetland areas would be expected to be less than that measured in upland wells, water levels are expected to change at the same rate in the low relief environment of this watershed. Therefore, changes in the measured upland water-table depths can be regarded as indicators of changes in the representative water-table depth of the watershed.

Daily values of stream discharge for the only surface-water outflow from the Tiger Bay watershed, Tiger Bay canal near Daytona Beach (fig. 1; USGS station number 02247480), were obtained from the USGS database (U.S. Geological Survey, 1998a, 1999a, and 2000). Soil moisture at two representative locations at the evapotranspiration station was monitored using time-domain reflectometry (TDR) probes installed to provide an averaged volumetric soil moisture content within the upper 30 cm of the soil. Soil moisture measurements were made and recorded on the datalogger every 30 minutes. The TDR probes were damaged by a fire in late June 1998, but were replaced in early August 1998. The soil moisture measurements made at the evapotranspiration station probably are indicative of only the uplands; wetlands commonly are inundated at times when shallow upland soils are not.

RESULTS OF EVAPOTRANSPIRATION MEASUREMENT AND SIMULATION

Most (73 percent) of the 30-minute resolution eddy correlation measurements made during the 2-year study period were acceptable and could be used to develop an evapotranspiration model to estimate missing data and to discern the effects of environmental variables on evapotranspiration. Unacceptable measurements resulted from failure of the krypton hygrometer or sonic anemometer, or because of excessive (more than 10 degrees) coordinate rotation in the post-processing "leveling" of the anemometer data. Unacceptable data were most extensive in the evening and early-morning hours (fig. 10) because dew formation on the sensors during these times of day was common. This diurnal pattern of missing data was fortunate because turbulent fluxes are expected to be relatively small during the evening and early morning, when solar radiation is low. Missing data were estimated based on linear regression between the turbulent fluxes and PAR (figs. 11 and 12). Because PAR is zero at night, this approach assigned constant values of latent and sensible heat flux to missing nighttime data. The assumed constant value of nighttime latent heat flux assigned to missing data was 9.04 watts per square meter (fig. 11). This value generally was small relative to daytime values of latent heat flux, and therefore, not significantly inconsistent with the assumption of negligible nighttime latent heat flux inherent in the development of weighting coefficients (eqs. 23-25). Examples of measured and PAR-estimated turbulent fluxes are shown for a period in late February 1998 in figure 13.

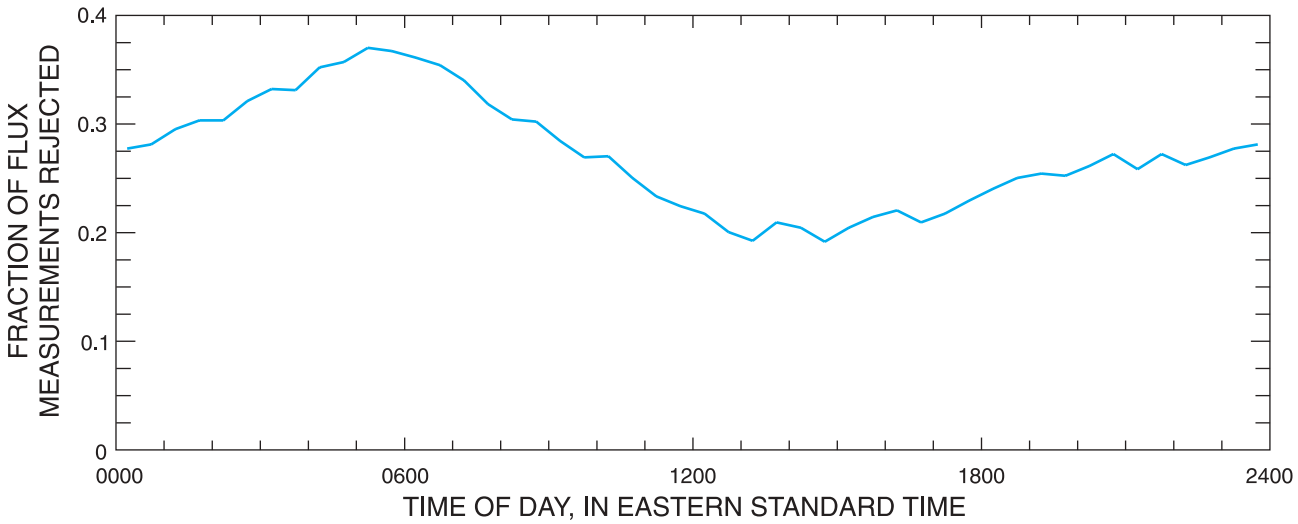

Figure 10. Diurnal pattern of rejected flux measurements.

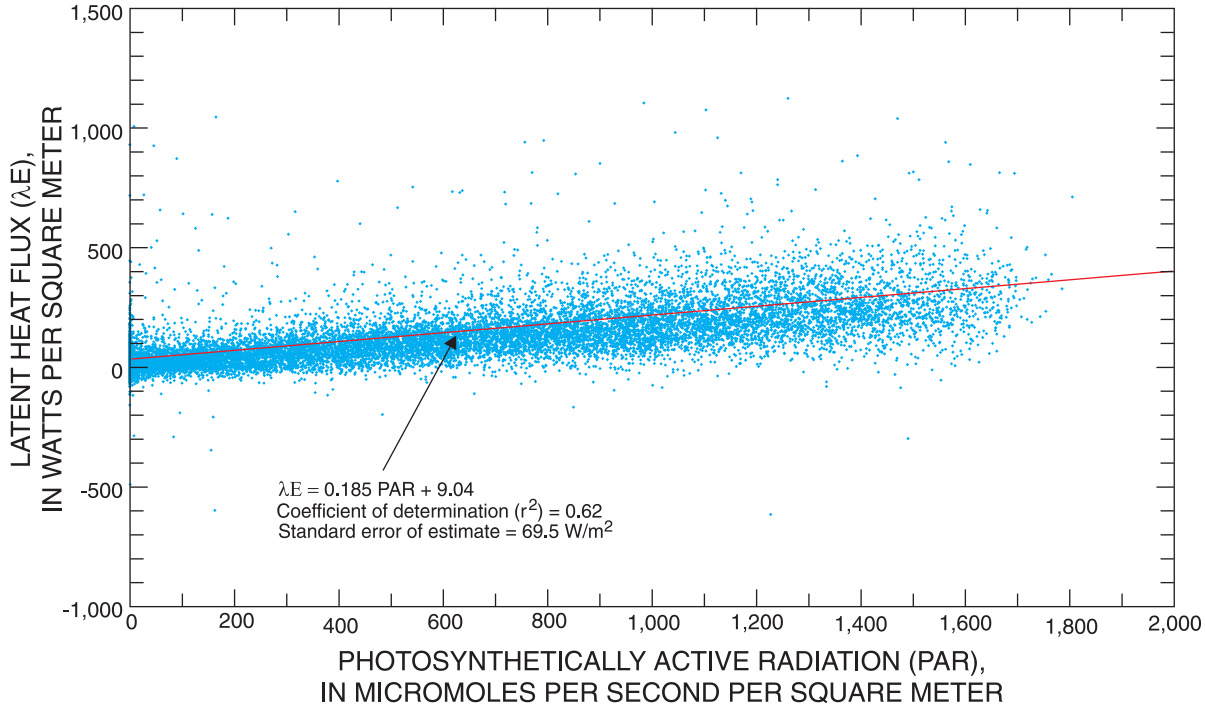

Figure 11. Relation between measured 30-minute averages of photosynthetically active radiation (PAR) and latent heat flux (λE).

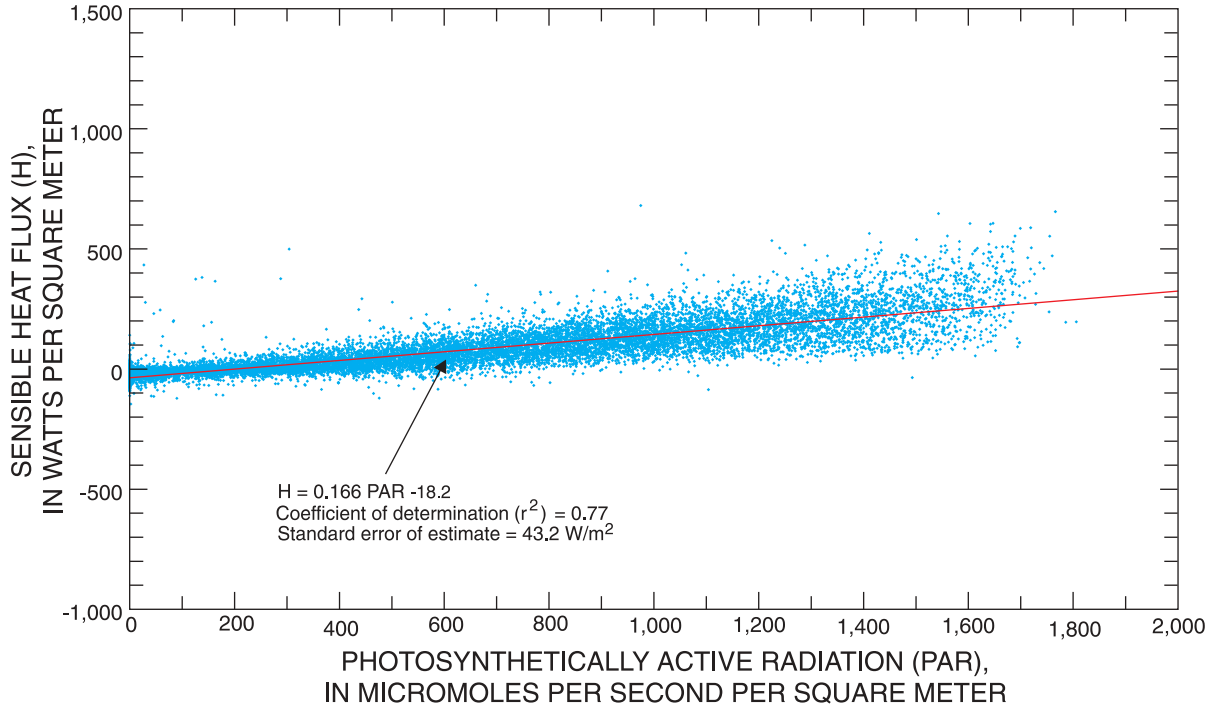

Figure 12. Relation between measured 30-minute averages of photosynthetically active radiation (PAR) and sensible heat flux (H).

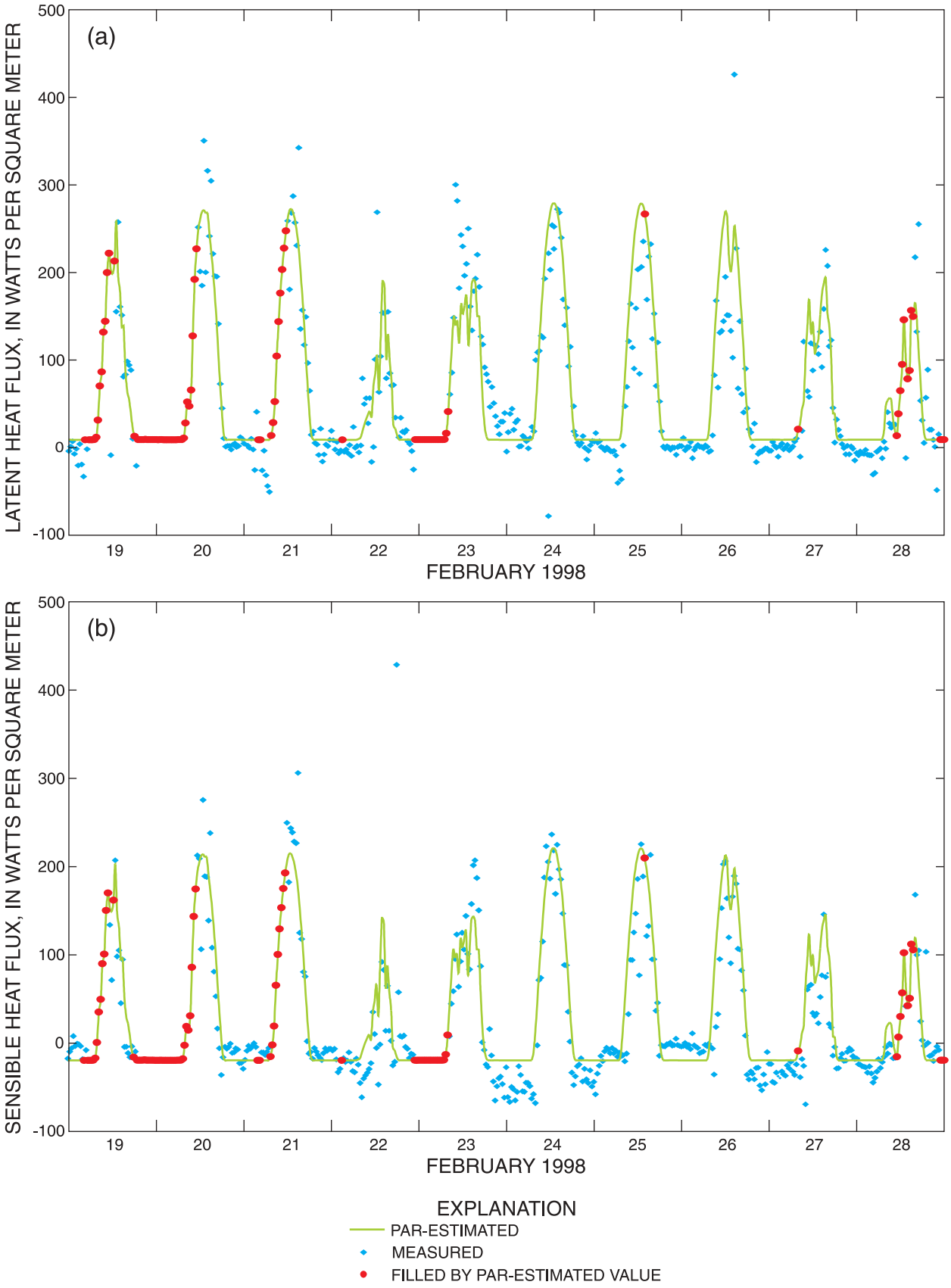

Figure 13. Measured and photosynthetically active radiation (PAR)-estimated values of (a) latent heat flux and (b) sensible heat flux during 10-day period in late February 1998.

Turbulent flux data exhibited pronounced diurnal patterns. The average diurnal pattern of turbulent fluxes and PAR (fig. 14) indicates that the vast majority of evapotranspiration occurs in daytime, driven by incoming solar radiation. During average daytime conditions, both latent and sensible heat flux are upward, with most of the available energy partitioned to latent heat flux. At night, the land or canopy surface cools below air temperature, producing a reversal in the direction of sensible heat flux (fig. 14). Although the average, nighttime latent heat flux is upward (fig. 14), dew formation (downward latent heat flux) commonly occurs.

The relation between net radiation and PAR varied as a result of the fire, logging, and regrowth. Regressions between daily values of net radiation and PAR are shown in figure 15 for three periods: pre-fire, post-fire/pre-logging, and post-logging. The measured and estimated values of daily net radiation for burned and unburned areas are shown in figure 16. Measured values of PAR, a quantity highly correlated with incoming solar radiation, are shown in figure 17.

The strong seasonality of net radiation evident in figure 16 was a consequence of the yearly solar cycle, which produces a sinusoidal input of solar radiation to the upper atmosphere. Deviations from the sinusoidal pattern (such as during September-October 1999) were largely the result of cloudy conditions that produced periods of low PAR. The cloudy and rainy period immediately after the fire resulted in relatively low values of PAR and low estimated values of net radiation in unburned areas. The measured (burned) net radiation, however, was relatively high, indicating that the surface reflectance of burned areas decreased markedly after the fire blackened much of the landscape. The measured net radiation for burned areas was about 20 percent higher than the estimated net radiation for unburned areas in the 6 months following the June 1998 fire. With the regrowth of vegetation, reflectance gradually increased to near pre-fire values in the post-logging period, and the differences between values of net radiation for burned and unburned areas were less distinct.

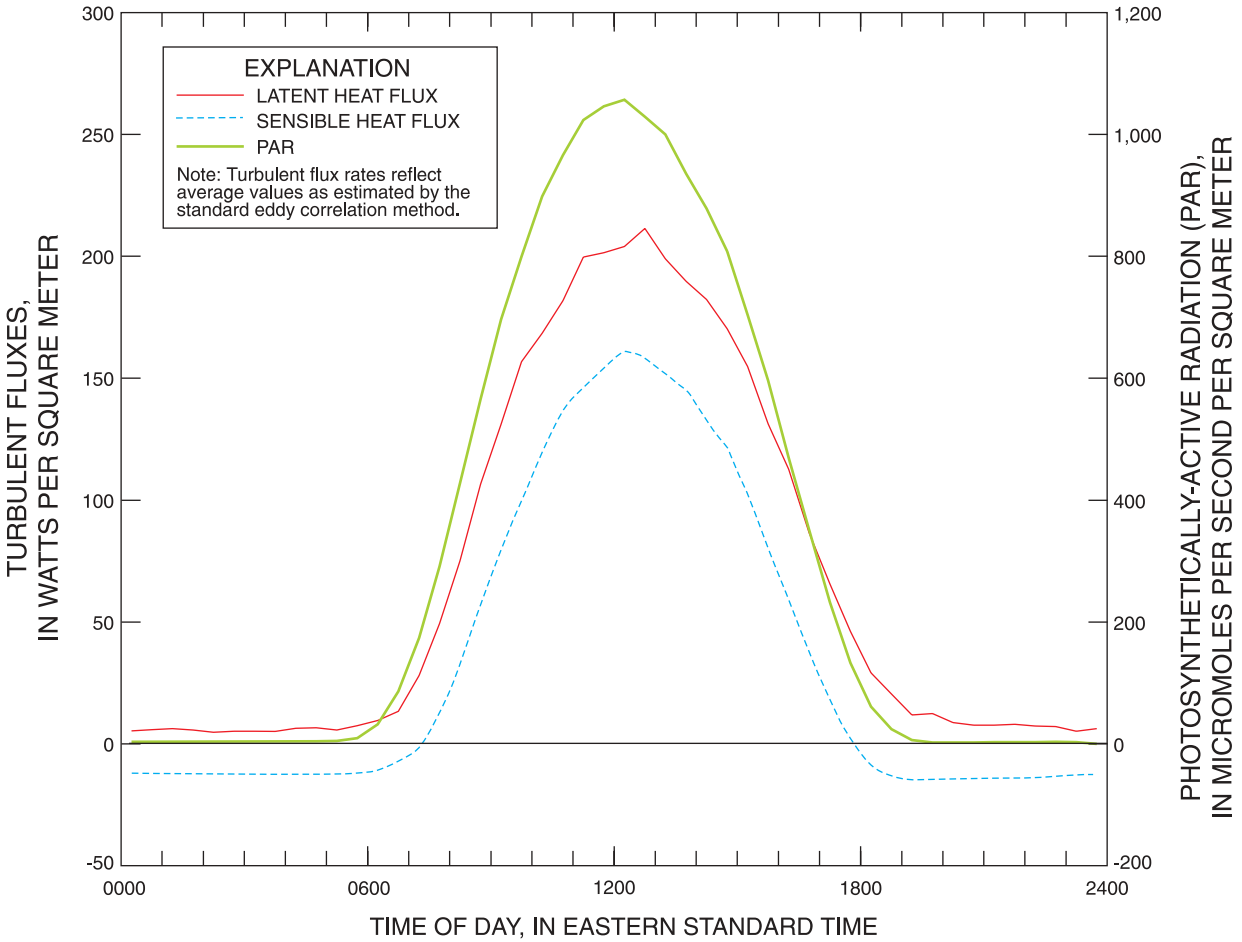

Figure 14. Average diurnal pattern of energy fluxes and photosynthetically active radiation (PAR).

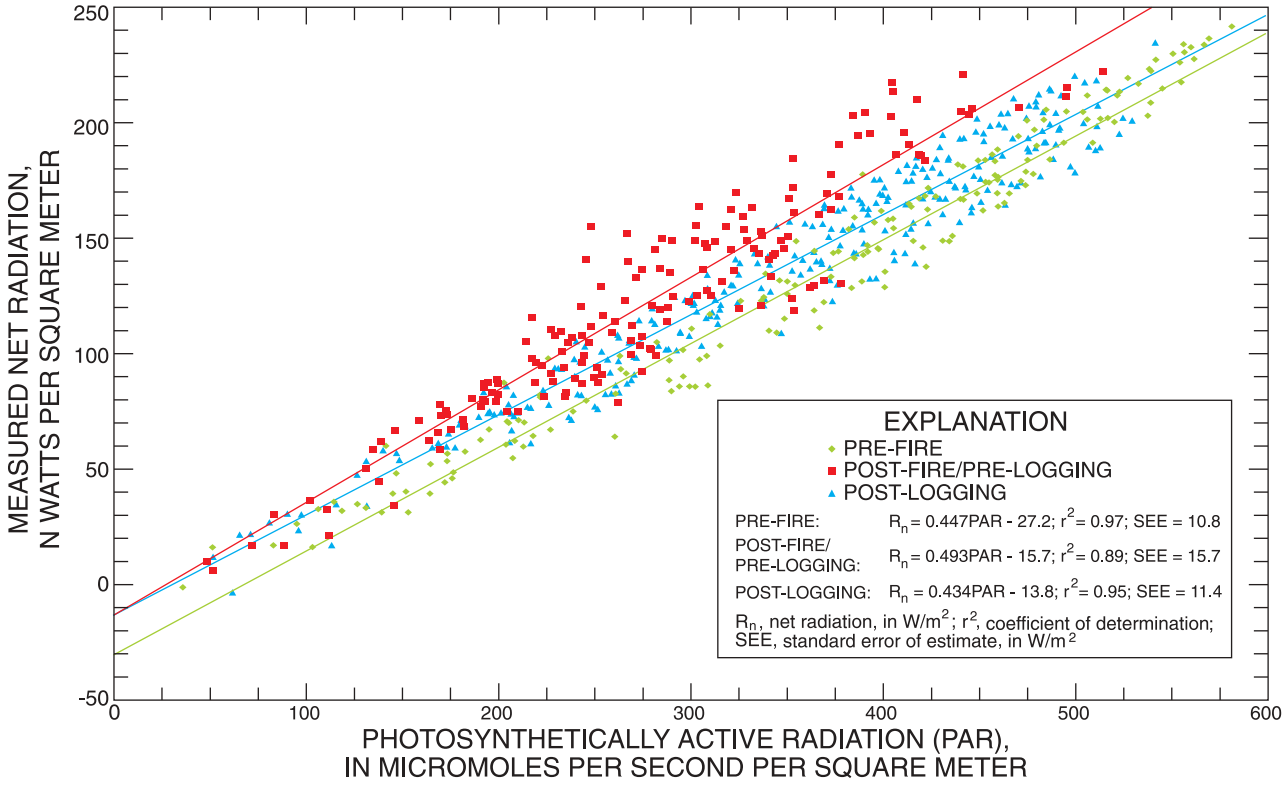

Figure 15. Relation between daily values of measured net radiation and photosynthetically active radiation (PAR).

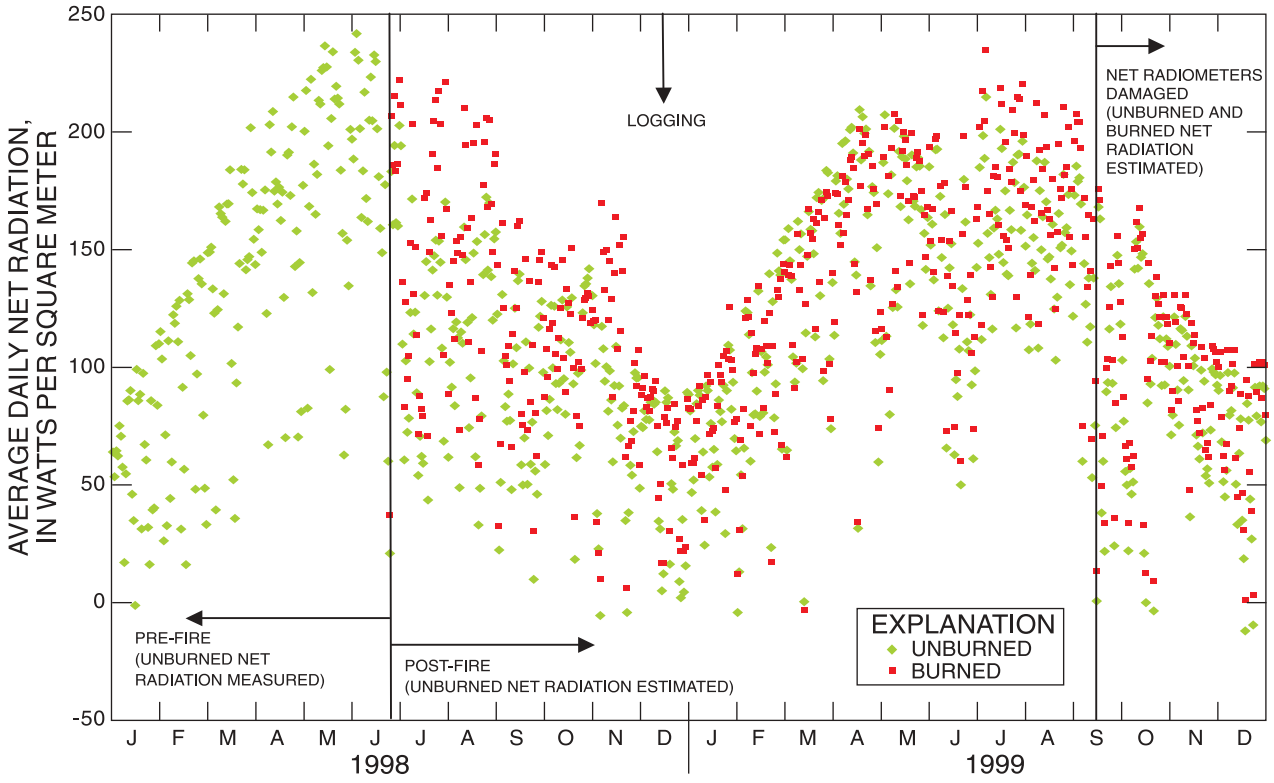

Figure 16. Average daily net radiation for burned and unburned areas.

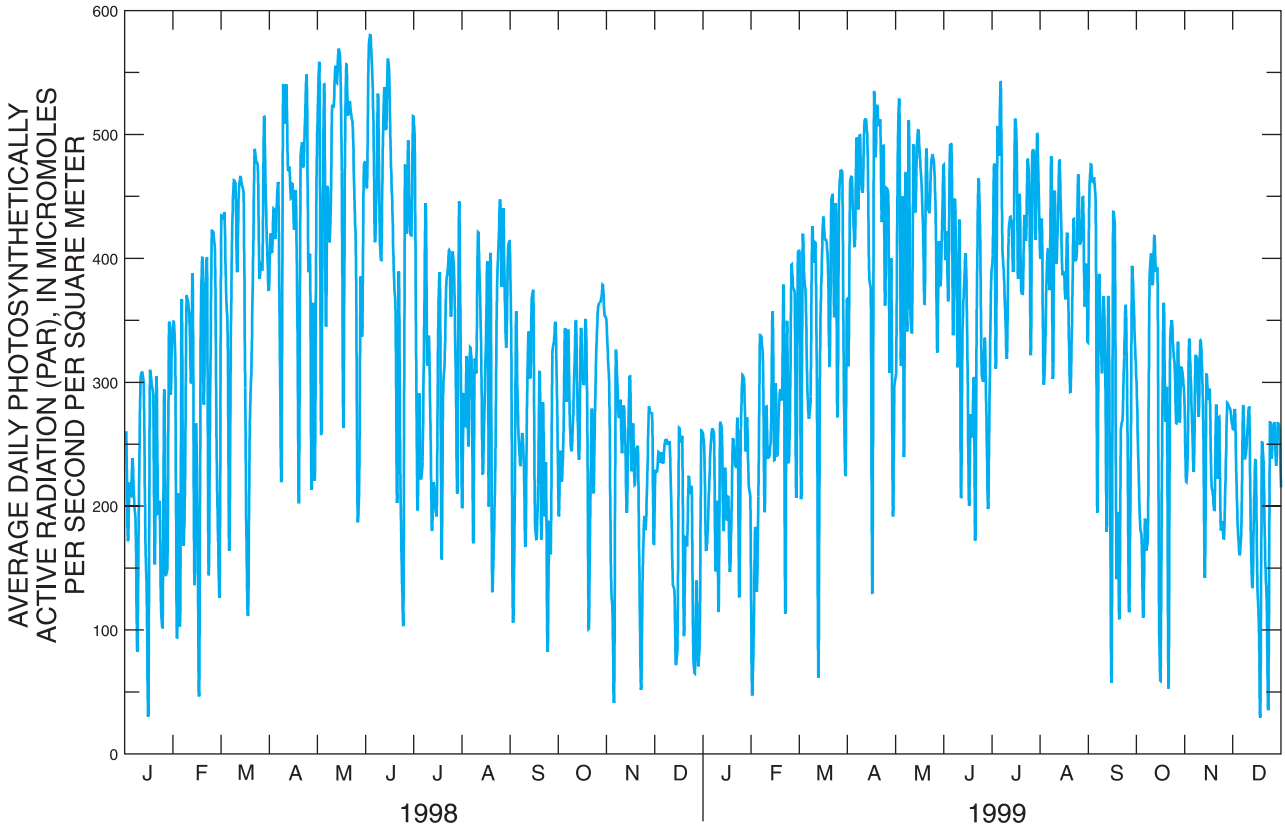

Figure 17. Average daily photosynthetically active radiation (PAR).

As described previously, daily composites of measured turbulent fluxes were constructed with the restriction that no more than 6 hours of data for a given day could be missing and subject to estimation using the gross PAR-based relations (figs. 11 and 12). This restriction limited the number of acceptable daily values of measured turbulent fluxes to 449 during the 2-year (730 days) study period. Only a small amount of the total turbulent flux (5.6 and 5.1 percent for latent and sensible heat flux, respectively) comprising the acceptable daily values was estimated by the PAR-based relation. As expected from previous studies, the available energy tended to be greater (measured turbulent fluxes accounted for only about 84.7 percent of estimated available energy) than the turbulent fluxes derived from the standard eddy correlation method (fig. 18), and the energy-budget closure tended to improve with increasing friction velocity (fig. 19). The measured turbulent fluxes generally accounted for estimated available energy at friction velocity values greater than about 0.6 m/s. The acceptable daily values of turbulent fluxes, computed by both the standard eddy correlation method (eqs. 5 and 6) and the energy-budget variant of the eddy correlation method (eqs. 18 and 19), are presented in figures 20 and 21. These values represent the fluxes measured at the evapotranspiration station, and therefore, represent varying proportions of burned and unburned source areas. The relative proportions varied widely following the fire (fig. 22), with values ranging from those that were almost completely representative of unburned areas ($w_b = 0$) to those that were about 80 percent representative of burned areas ($w_b = 0.8$). As a consequence of the previously mentioned discrepancy between available energy and measured turbulent fluxes, the standard eddy correlation method produced turbulent flux values that were, on average, only 84.7 percent of those produced by the energy-budget variant.

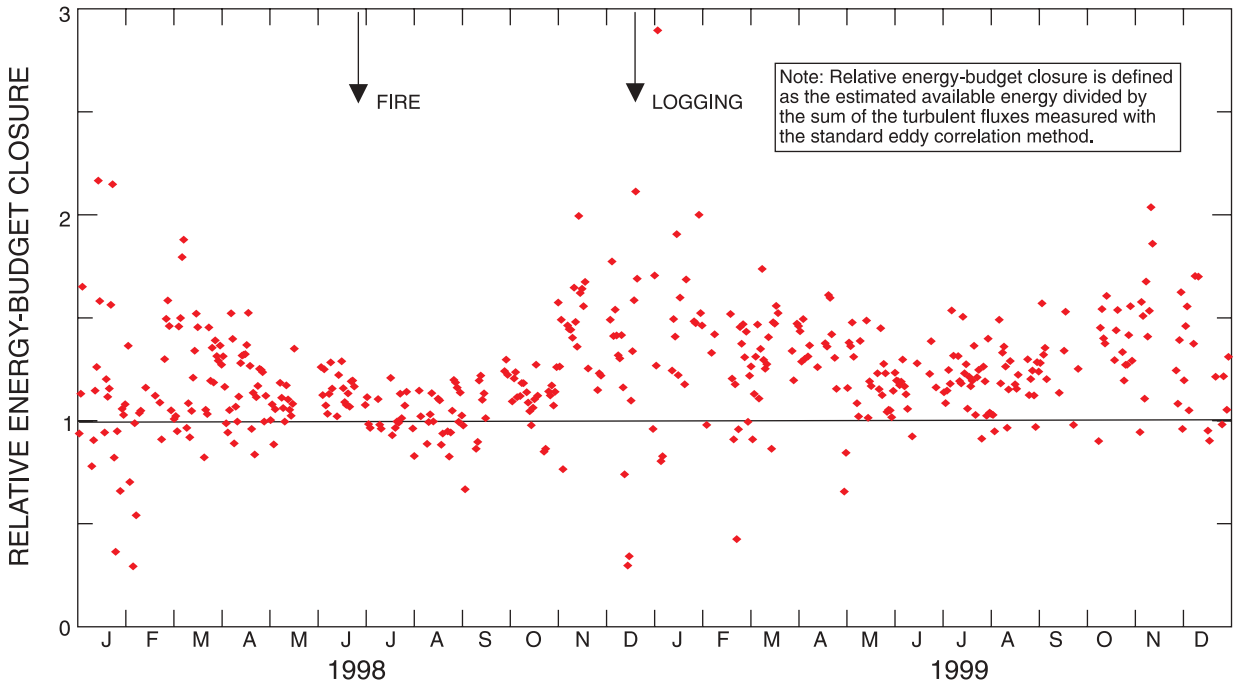

Figure 18. Temporal distribution of daily relative energy-budget closure.

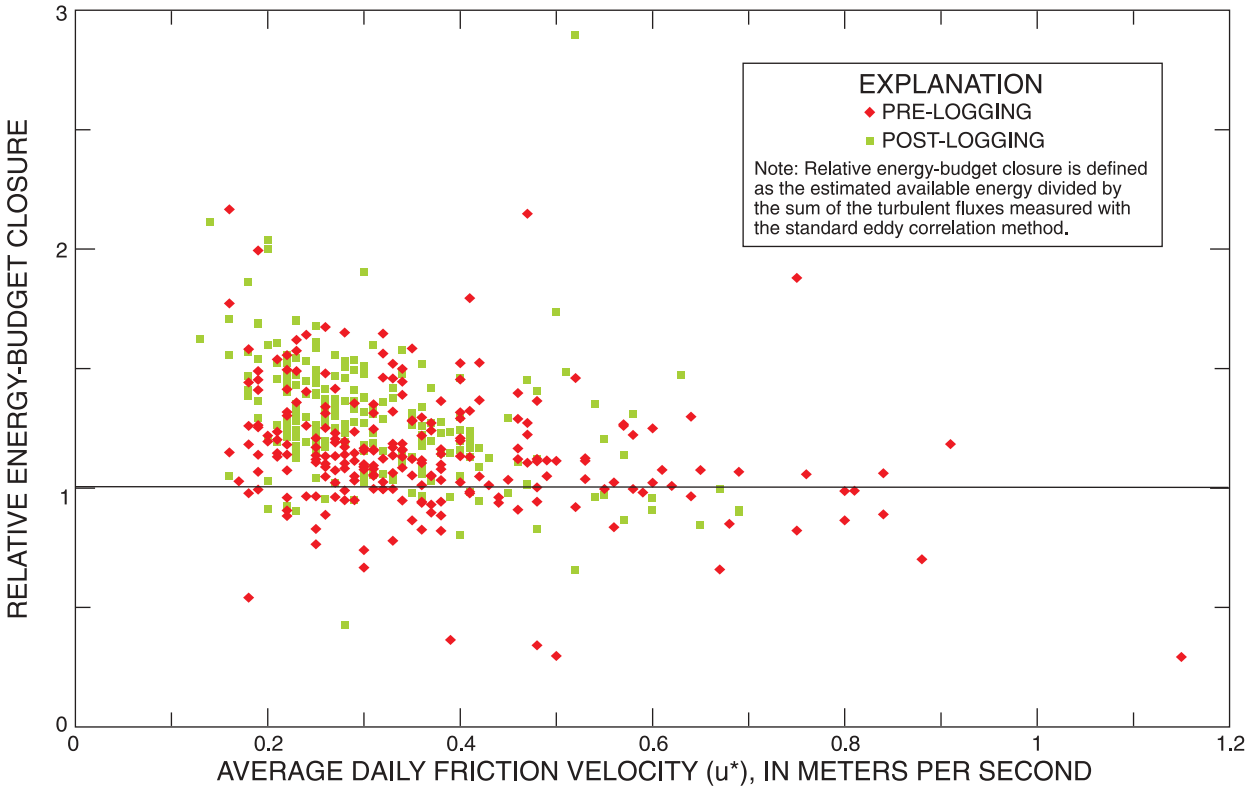

Figure 19. Relation between daily energy-budget closure and average daily friction velocity.

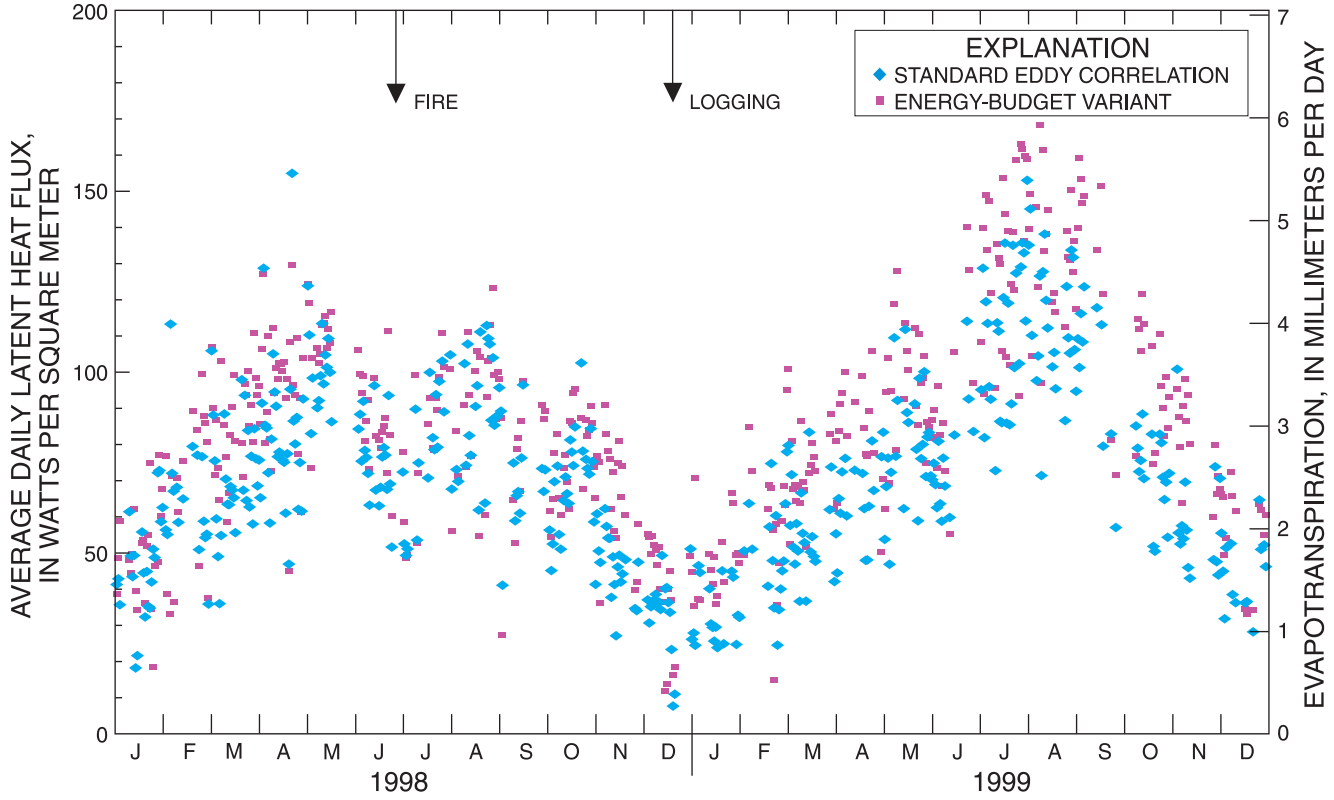

Figure 20. Average daily latent heat flux measured by the eddy correlation method and the energy-budget variant.

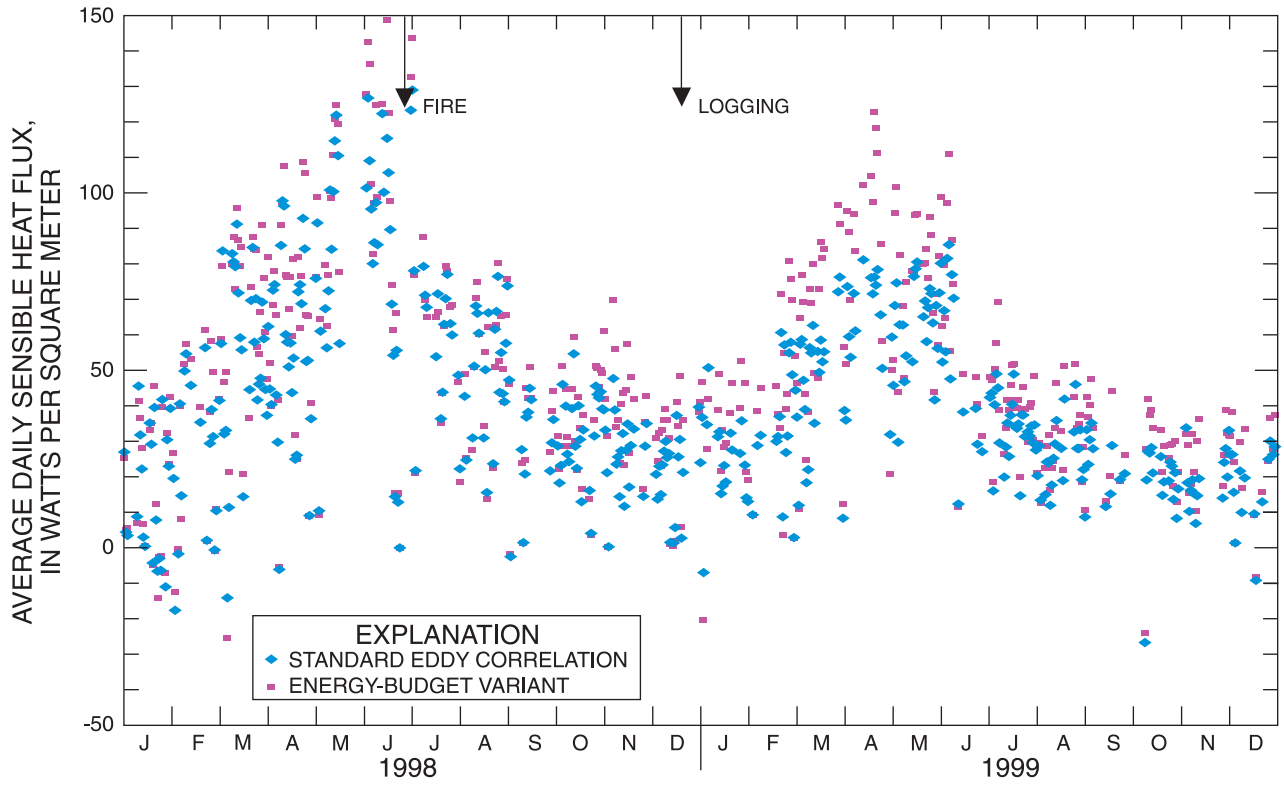

Figure 21. Average daily sensible heat flux measured by the eddy correlation method and the energy-budget variant.

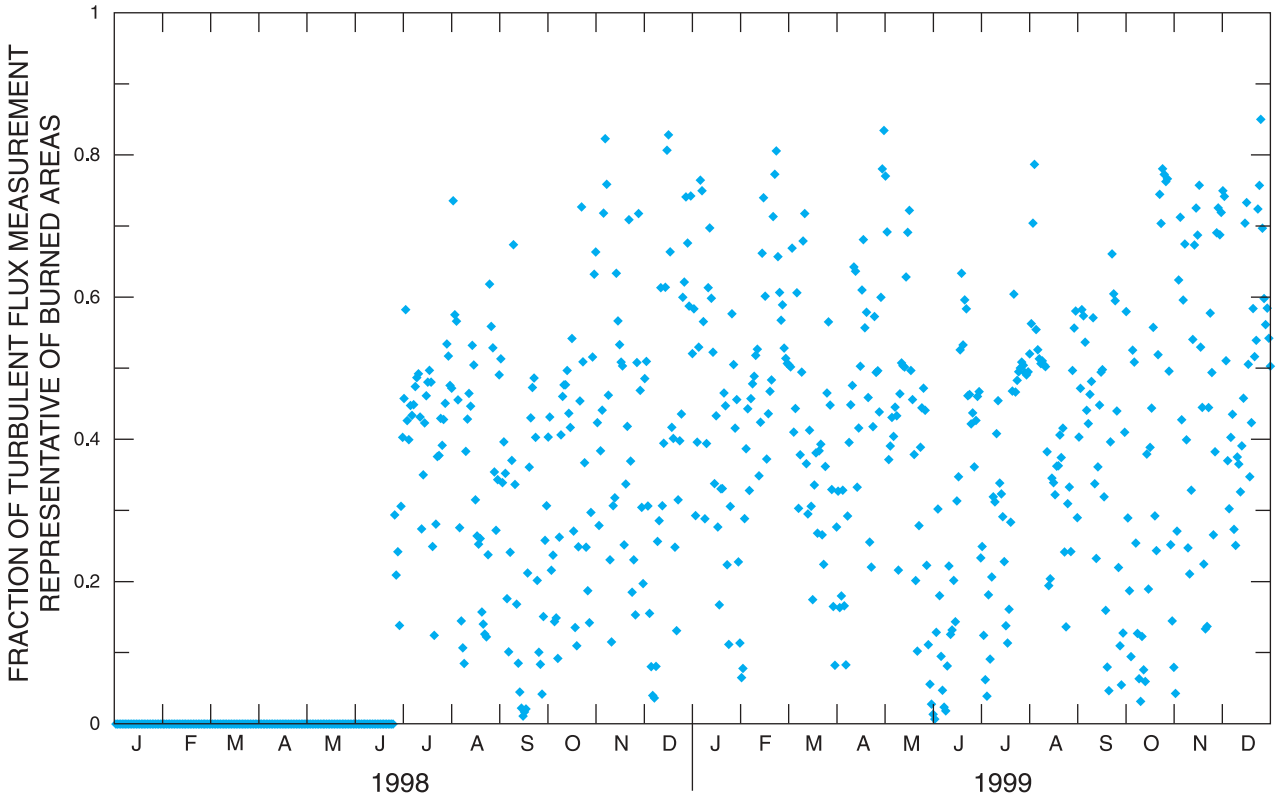

Figure 22. Daily values of fraction of burned fraction of turbulent flux measurement.

Calibration of Evapotranspiration Model

Calibration of the evapotranspiration model was essentially a process of determining the best functional form of the modified Priestley-Taylor coefficient α. The environmental variables considered as possible predictors of Priestley-Taylor α (eq. 22) included: water-table depth, soil moisture, PAR, air temperature, vapor-pressure deficit, daily rainfall, NDVI, and wind speed. Of these variables, only water-table depth, soil moisture, and PAR were identified as significant determinants of Priestley-Taylor α. Soil moisture was highly correlated with water-table depth (fig. 23), and therefore, one of these variables can be excluded from the α function to avoid redundancy. To enhance the transfer value of this study, water-table depth was retained as a variable in the α function, and soil moisture was eliminated, because water-level data are more commonly available than soil moisture data. In other environmental settings, such as areas with a relatively deep water table or coarse-textured soils, the water table may be hydraulically de-coupled from the shallow soil moisture much of the time, and a different functional representation of α than was used in this study would be appropriate.

Priestley-Taylor α was initially simulated with a three-part model incorporating the three different surface covers: (1) unburned areas; (2) post-fire/pre-logging, burned areas (June 25 to December 16, 1998); and (3) post-logging, burned areas (December 17, 1998, to December 31, 1999). The time divisions for the burned areas grossly approximated the observed variation in NDVI over the study period (fig. 24). The effects of the fire and transient regrowth of vegetation (fig. 4) on NDVI were evident (fig. 24). In the almost 6 months prior to the fire (January 1-June 24, 1998), NDVI maintained a relatively constant value of about 0.5. NDVI sharply declined at the time of the fire, but recovered within 4 months to a value of about 0.4, which was maintained throughout the remainder of the study. As a simplification, the effect of the transient aspect of vegetative regrowth within the 4-month recovery period was not incorporated into the model for α. Instead, the function of α for this recovery period, as for all time periods, was a function solely of water-table depth and PAR.

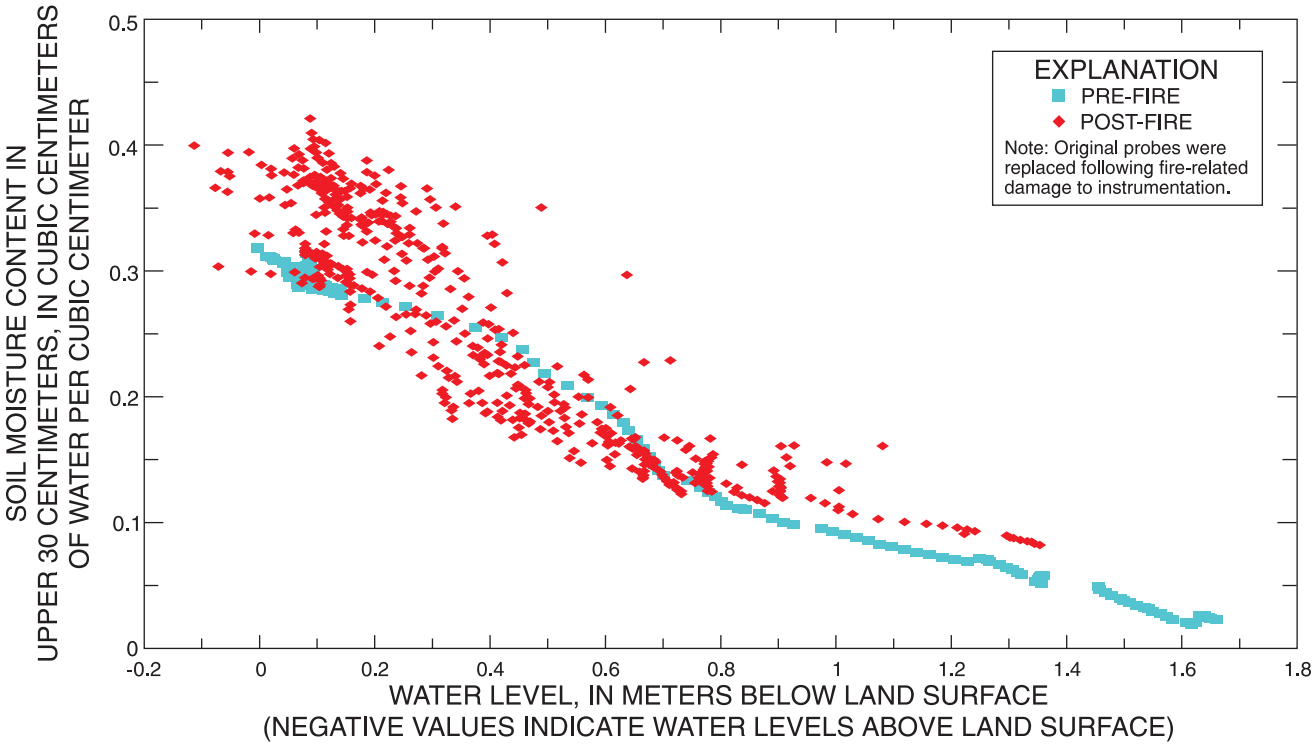

Figure 23. Relation between soil moisture content and water level.

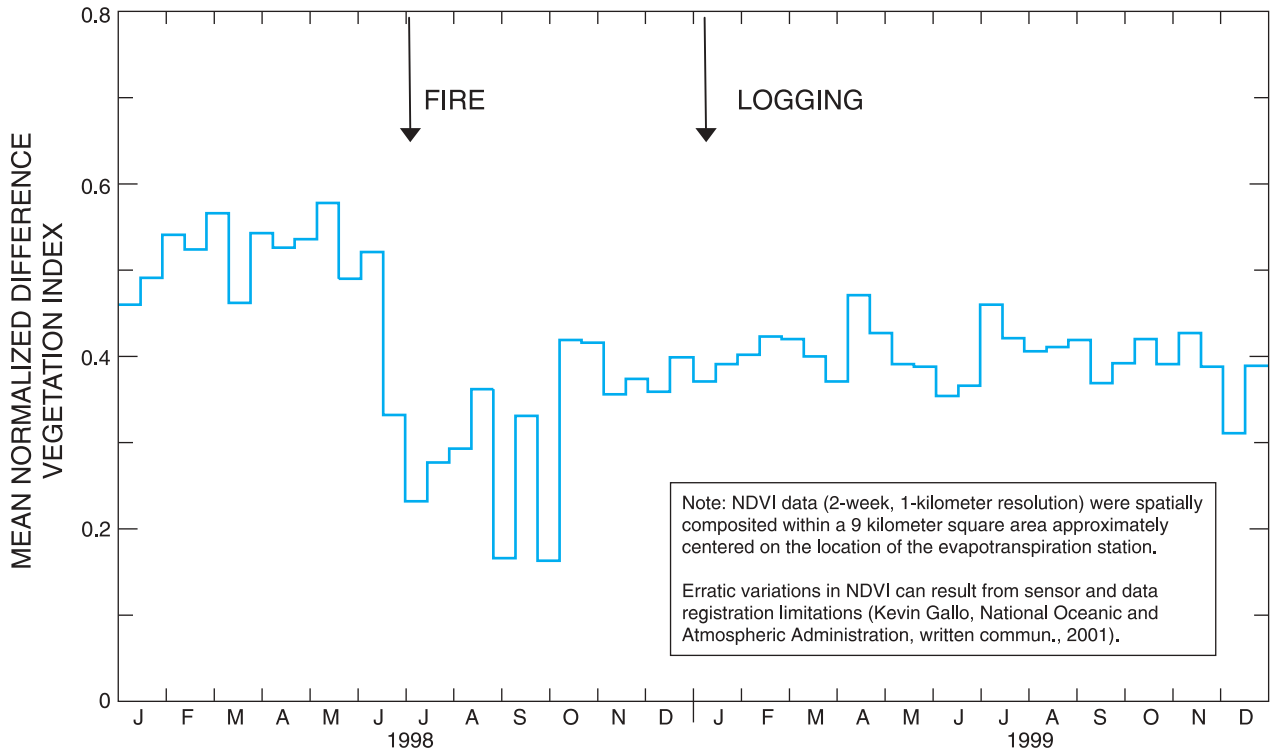

Figure 24. Temporal variability of normalized difference vegetation index (NVDI).

Table 3. Summary of parameters and error statistics for daily evapotranspiration models

[Parameters C_{1j}, C_{2j}, and C_{3j} are defined by the equation: $\alpha_j = (C_{1j}h_{wt} + C_{2j}PAR + C_{3j})$ where: j is an index denoting the surface cover; h_{wt} is water-table depth below a reference level placed at the highest water level measured (0.11 m above land surface) at the evapotranspiration station (uplands environment), in meters; and PAR is photosynthetically active radiation, in micromoles per square meter per second. Error statistics: r^2, coefficient of determination of measured and simulated values of latent heat flux, dimensionless; SEE, standard error of estimate (in watts per square meter); CV, coefficient of variation, dimensionless, equal to SEE divided by the mean of the measured values of latent heat flux]

	Unburned areas (j=1)	Three-part model for burned areas		
		Post-fire/pre-logging (j=2)	Post-logging I (j=3)	Post-logging II (j=4)
Time period	January 1, 1998 through December 31, 1999	June 25, 1998 through December 16, 1998	December 17, 1998 through April 22, 1999	April 23, 1999 through December 31, 1999
Parameters				
C_{1j}	-0.175	-0.167	-0.312	-0.508
C_{2j}	-.00102	-.00147	-.00031	.00013
C_{3j}	1.42	1.26	1.03	1.36
Error statistics: r^2 = .90; SEE = 9.67; CV = .11				

Surprisingly, the annual pattern of leaf growth and drop for the deciduous cypress trees within the watershed was not apparent in values of NDVI, perhaps because of the exposure of understory vegetation following leaf drop. Simulations that attempted to use NDVI directly as an explanatory variable for variations in evapotranspiration were unsuccessful. This failure is perhaps related to erratic variations in NDVI (fig. 24), which are a product of sensor and data registration limitations (Kevin Gallo, NOAA, written commun., 2001).

An analysis of error in the preliminary model showed a seasonal pattern in the residuals (difference of measured and simulated latent heat fluxes) within the post-logging period (fig. 25). Measured evapotranspiration generally was overestimated in the early part of this period and underestimated in the late part of the period. The bias was apparently unrelated to changes in green leaf density, based on the relatively constant value of NDVI following logging (fig. 24). Possible explanations for the model bias include factors not clearly identified by NDVI: phenological changes associated with maturation or seasonality of plants that emerged after the fire or successional changes in composition of the plant community within burned areas. To reflect the apparent change in system function during the post-logging period, this period was further subdivided into an early period (December 17, 1998 through April 22, 1999) and a late period (April 23 through December 31, 1999). This subdivision of the post-logging period resulted in an improved model (standard error of estimate = 9.67 watts per square meter), compared to the model with a single post-logging period (standard error of estimate = 10.82 watts per square meter) and reduced the seasonal bias in residuals (fig. 25).

The general form of α was identical for all surface covers (eq. 28), although model parameter values varied with surface cover (table 3):

$$\alpha_j = C_{1j}h_{wt} + C_{2j}PAR + C_{3j}, \qquad (28)$$

where

α_j is the Priestley-Taylor coefficient for the jth surface cover;

j is an index denoting the surface cover; j=1 (unburned areas); j=2 (burned areas during post-fire/pre-logging period; j=3 (burned areas during initial post-logging period); and j=4 (burned areas during final post-logging period);

C_{1j}, C_{2j}, and C_{3j} are empirical parameters that are estimated through regression, within the context of eqs. 22, 23, 24, and 25; and

h_{wt} is water-table depth below a reference level placed at the highest water level measured (0.11 meters above land surface) at the evapotranspiration station (uplands environment) during the study period, in meters; h_{wt} is constrained to be greater than zero.

Regressions to estimate the model parameters within eq. 28 were designed to minimize the sum of squares of error residuals between measured and simulated latent heat fluxes. Measured latent heat flux was used as the dependent variable of the regression; the right side of eq. 22 contained the independent variables, as well as the unknown parameter (C_{1j}, C_{2j}, and C_{3j}; j = 1 to 4). The values of λE_u and λE_b were estimated with eq. 22, using the appropriate values of net radiation (R_{nu} and R_{nb} of eq. 26 for λE_u and λE_b, respectively), and eq. 28. The variable w_b was estimated with eqs. 24 and 25.

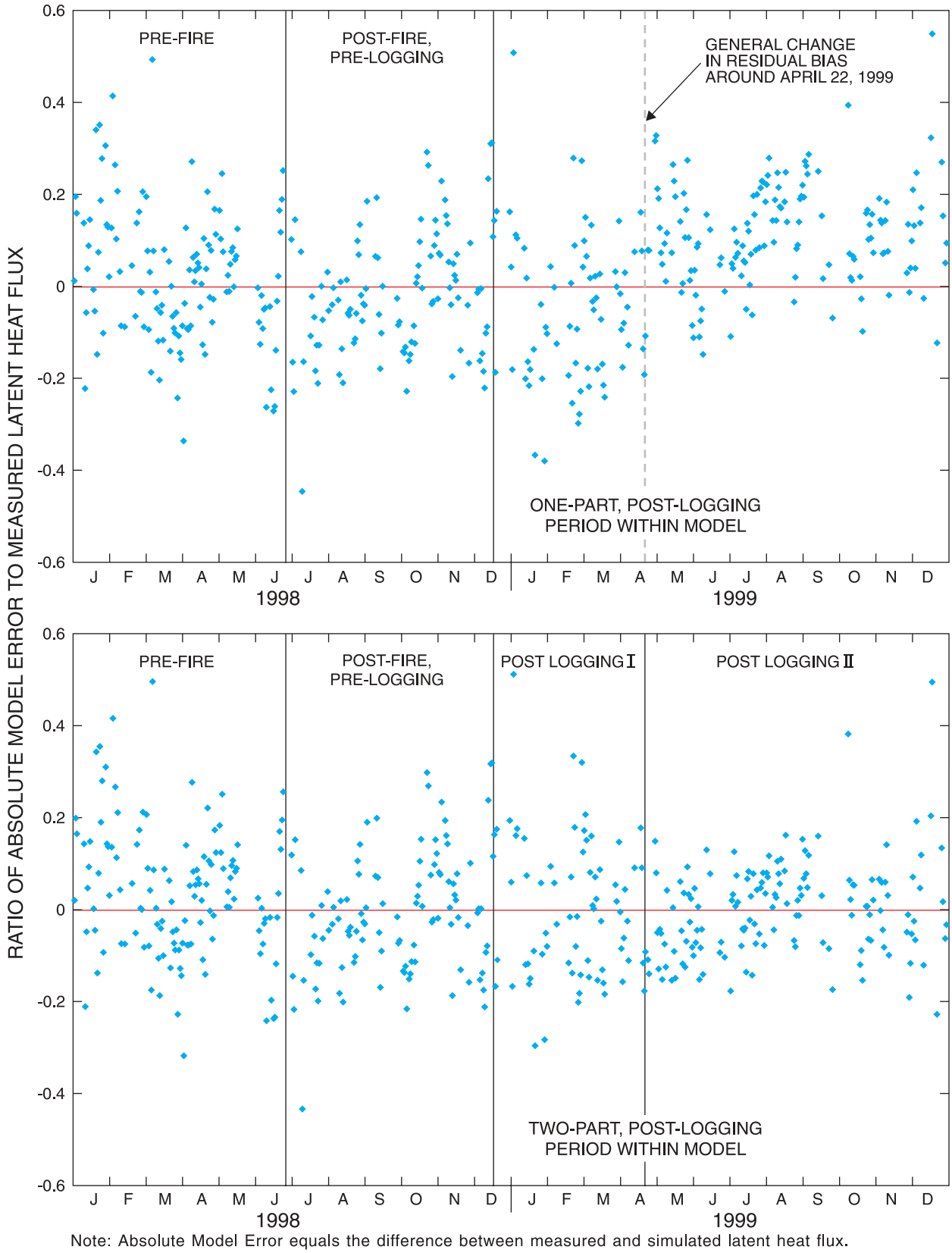

Note: Absolute Model Error equals the difference between measured and simulated latent heat flux.

Figure 25. Temporal variability in relative error of evapotranspiration model.

The form of α used in this study is similar to that used by German (2000) for south Florida wetlands, where water level and incoming solar radiation were the sole determinants of α. In that study, however, the form of α involved both first and second order terms of incoming solar radiation. In the present study, addition of the second-order PAR term added negligible improvement to simulation of evapotranspiration.

A comparison between simulated and measured values of latent heat flux is shown in figure 26 and regression statistics are shown in table 3. The model exhibited little temporal bias (fig. 25), even in the post-fire/pre-logging period when substantial transient changes (re-growth) in vegetative cover occurred in the burned areas. The lack of significant temporal bias supports the utilization of the particular discretization of time used in the model. More than 95 percent of the values of latent heat flux were within 25 percent of the measured values.

Application of Evapotranspiration Model

The calibrated evapotranspiration model (eqs. 22 and 23, with α values given by eq. 28 and regression-derived parameters given in table 3) described in the previous section was used to estimate average, daily values of evapotranspiration for both burned and unburned areas of the watershed during the 2-year study period. The model also provided a quantitative framework to examine the relation between evapotranspiration and the environment. The input variables for the model included daily values of net radiation (fig. 16), PAR (fig. 17), water-table depth at the evapotranspiration station (fig. 27), and air temperature (fig. 28).

Values of latent heat flux and evapotranspiration for January 1998 through December 1999 were estimated using the calibrated model (fig. 29). Despite the relatively high net radiation in burned areas (fig. 16), evapotranspiration from burned areas generally remained lower than that from unburned areas until spring 1999. This effect presumably was a result of destruction of transpiring vegetation by fire and then logging. Beginning in spring 1999 (post-logging II period for burned areas), evapotranspiration from burned areas increased sharply relative to unburned areas, sometimes exceeding evapotranspiration from unburned areas by almost 100 percent. From a simulation perspective, this change in evapotranspiration in spring 1999 was clearly the result of the change in Priestley-Taylor α model parameters between the two post-logging periods. From a physics perspective, the possible explanation(s) for the change in evapotranspiration is identical to those described in the earlier discussion of the differentiation of the early and late post-logging periods within the evapotranspiration model. Evapotranspiration from burned areas for the 10-month period after the fire (July 1998-April 1999) averaged about 17 percent less than that from unburned areas and, for the following 8-month period (May 1999-December 1999), averaged about 31 percent higher than from unburned areas. During the 554-day period after the fire, the average evapotranspiration for burned areas (1,043 mm/yr) averaged 8.6 percent higher than that for unburned areas (960 mm/yr).

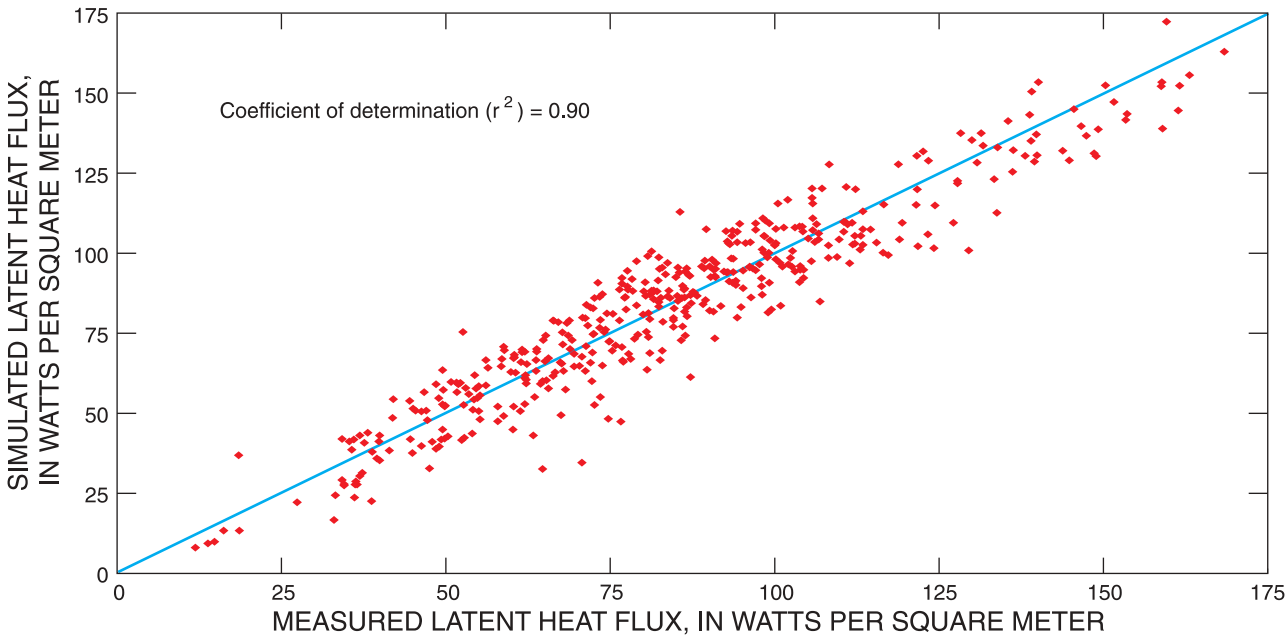

Figure 26. Comparison of simulated and measured values of daily latent heat flux.

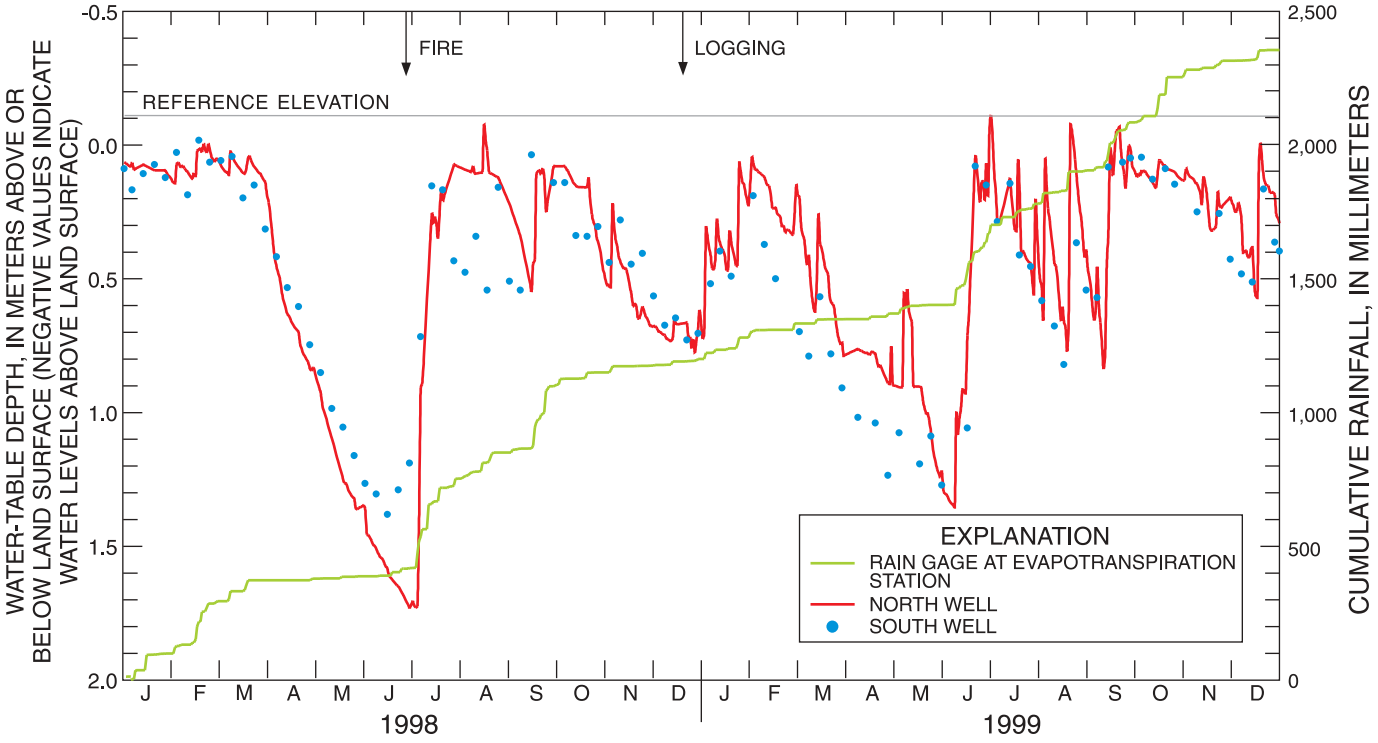

Figure 27. Water-table depth and cumulative rainfall.

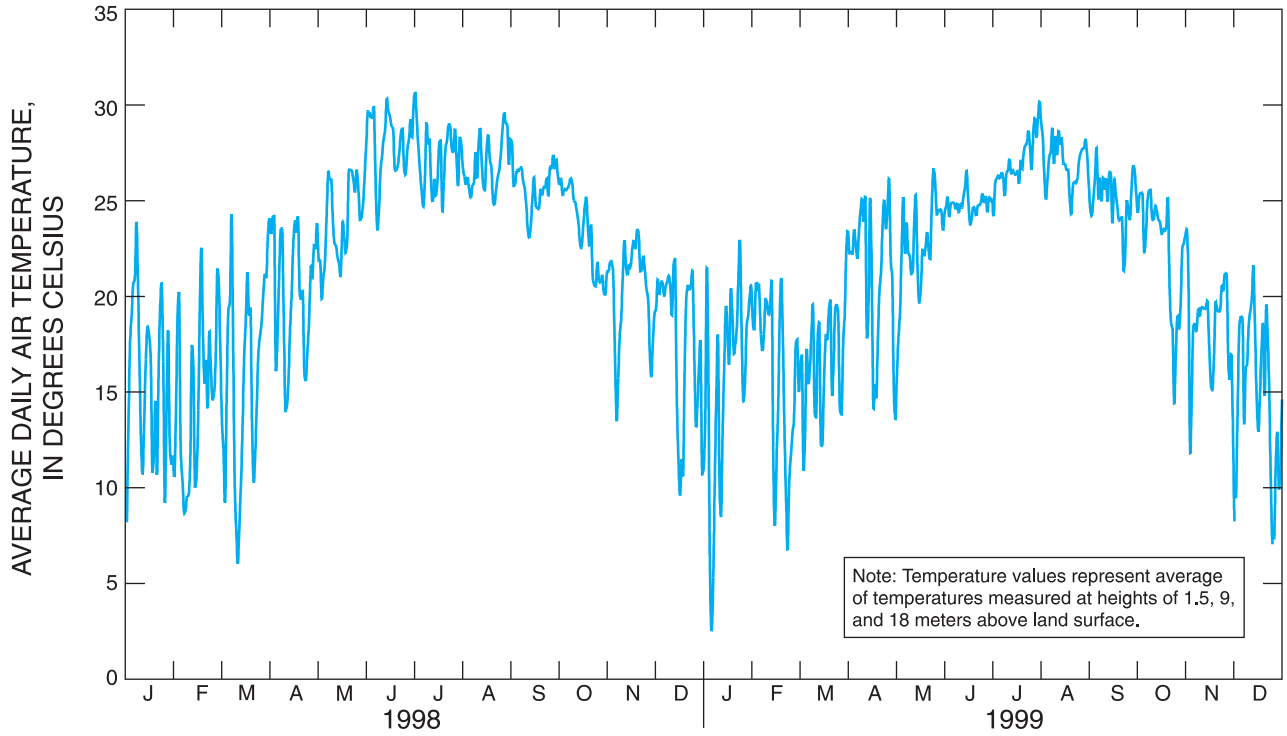

Figure 28. Average daily air temperature.

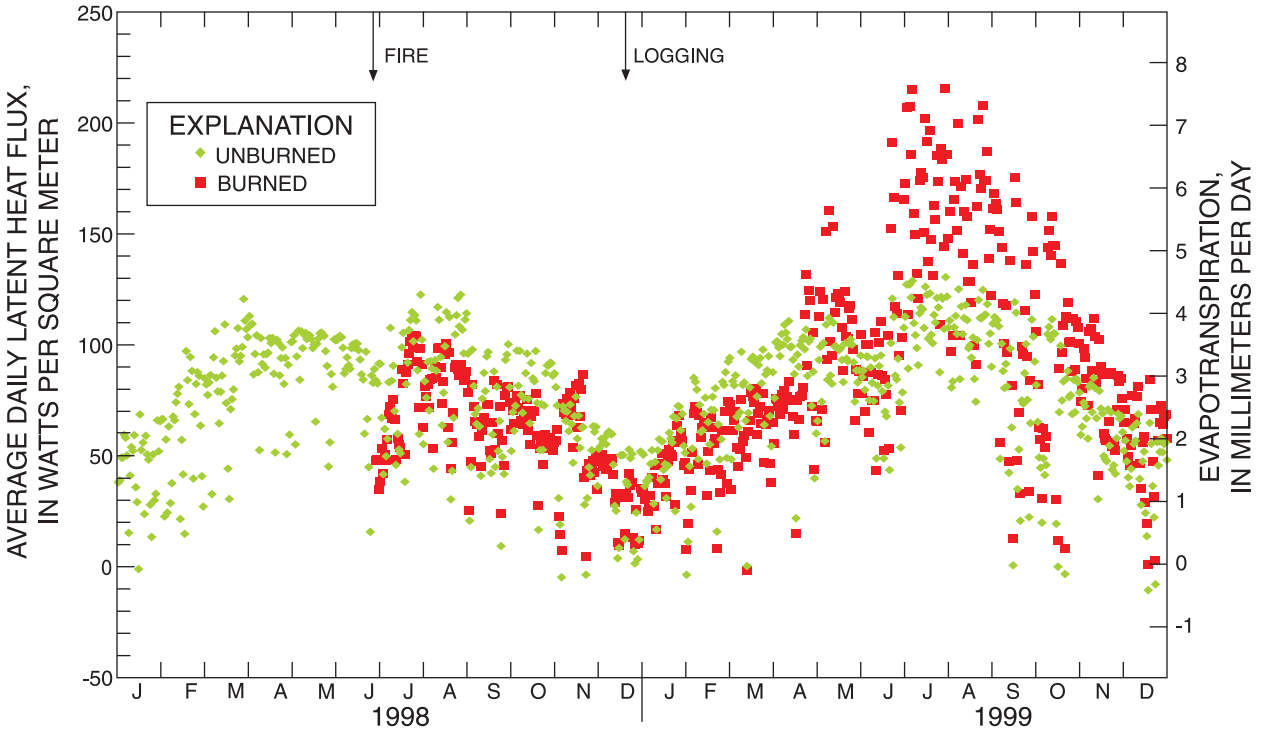

Figure 29. Average daily latent heat flux and evapotranspiration.

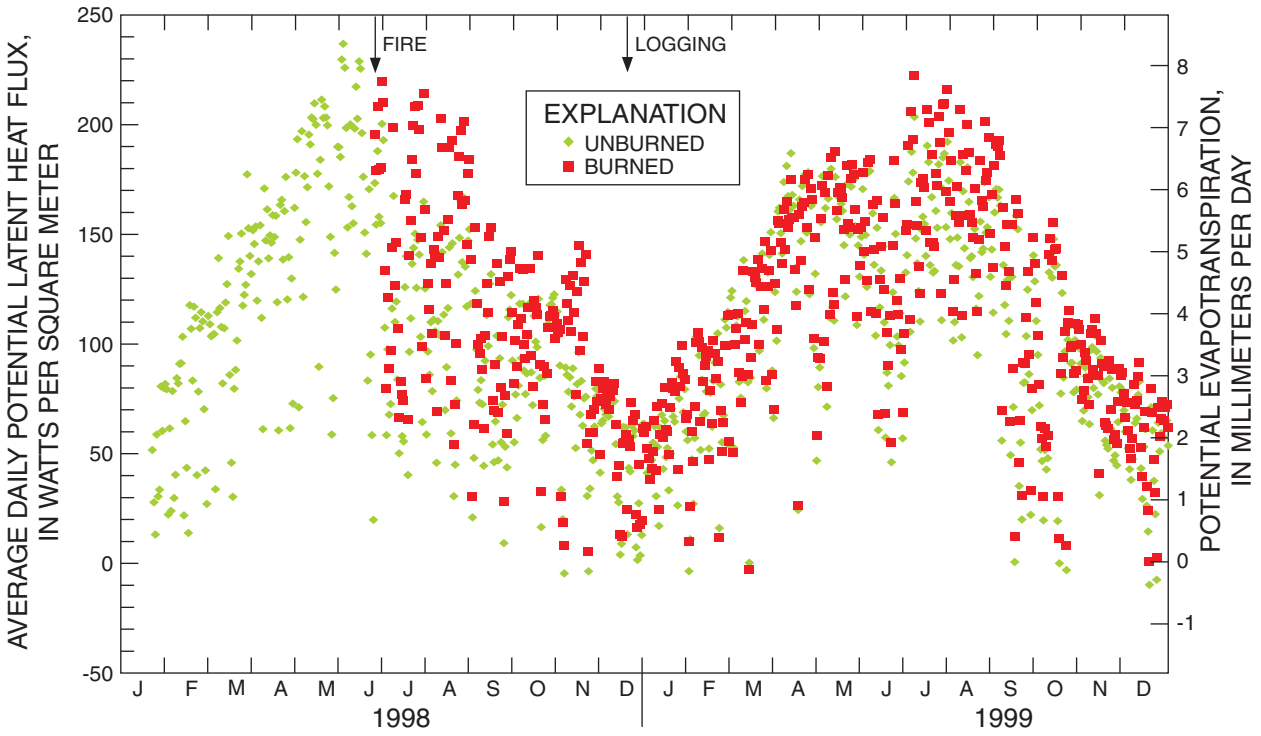

Figure 30. Average daily potential latent heat flux and potential evapotranspiration.

Annual evapotranspiration from the watershed was 916 mm for 1998 and 1,070 mm for 1999, and averaged 993 mm. The extensive burning and logging that occurred during the study produced a landscape that was not typical of forested areas of Florida. The estimated evapotranspiration from unburned areas can be considered representative of more typical forest cover. Annual evapotranspiration from unburned areas was 937 and 999 mm for 1998 and 1999, respectively, and averaged 968 mm. Both actual and potential evapotranspiration showed strong seasonal patterns and day-to-day variability (figs. 29 and 30). Actual evapotranspiration from the watershed averaged only 72 percent of potential evapotranspiration.

The effect of the extreme drought period in spring 1998 (fig. 27) on turbulent fluxes was substantial (figs. 29, 31, and 32). Turbulent fluxes usually emulate the general sinusoidal, seasonal pattern of solar radiation and air temperature (Knowles, 1996; Sumner, 1996; and German, 2000). The usual sinusoidal pattern of latent heat flux was truncated in spring 1998 (fig. 29) because of a lack of available moisture (figs. 27 and 33). The drought-induced reduction in latent heat flux was compensated by an increase in sensible heat flux (fig. 31) with an associated increase in the Bowen ratio. Comparison of the Bowen ratio (fig. 32) with the water-table and soil moisture records (figs. 27 and 33) indicates that the moisture status of the watershed has a major role in the partitioning of the available energy. Relative evapotranspiration (ratio of actual to potential evapotranspiration and computed as $\alpha / 1.26$) decreased from about 1 in the early, wet part of 1998 to less than 0.50 during the drought (fig. 34). After the drought ended in late June and early July 1998 and water levels quickly returned to near land surface, evapotranspiration increased sharply. The evapotranspiration rate, however, averaged only about 60 percent of the potential rate in the burned areas, as compared to about 90 percent in the unburned areas. This discrepancy can be explained as a result of fire damage to vegetation.

Potential evapotranspiration rates for burned and unburned areas were similar (fig. 30), although actual evapotranspiration rates for the two areas were quite distinct from each other (fig. 29). The relation between actual and potential evapotranspiration was not a simple constant multiplier (for example, a crop factor), but rather was time-varying as a function of water-table depth, PAR, and surface cover (fig. 34). Relative evapotranspiration exceeded a value of 1 at times, probably as a result of experimental error, as well as the approximate and empirically derived nature of the assumed potential value of 1.26 for α. The potential evapotranspiration rates (fig. 30) did not strongly reflect either the drought or surface burning and logging, as does the actual evapotranspiration.

Within the framework of the calibrated model, variations in the environmental variables contained in α (water-table depth and PAR) reduce actual evapotranspiration below potential evapotranspiration for a given surface cover. The evapotranspiration model indicated that relative evapotranspiration decreased as the depth to the water table increased (fig. 35). The range of water-table depths prevalent during the study period was slightly above land surface to about 1.75 m below land surface. Presumably, at some water-table depth greater than 1.75 m, relative evapotranspiration would reach an asymptotic constant value as vegetation becomes unable to access moisture below the water table. The rate of decline of relative evapotranspiration with water-table depth was greater for the post-logging period than for the pre-logging period. This result is perhaps a manifestation of the replacement of many deep- rooted trees by shallow-rooted understory vegetation following the fires. Shallow-rooted plants would be less able to tap into deep soil moisture or the water table than would deep-rooted vegetation.

Water-table depth has been considered an important predictor of evapotranspiration in hydrologic analysis (Tibbals, 1990), but little empirical evidence has been available to define the relation between these two environmental variables. The USGS modular finite-difference ground-water flow model (MODFLOW) simulates relative evapotranspiration as a unique, piece-wise, linear function of water-table depth, where evapotranspiration declines from a potential rate when the water table is at or above land surface to zero at the "extinction depth" (McDonald and Harbaugh, 1984). Contrary to the MODFLOW conceptualization of evapotranspiration, this study indicates that the variation in relative evapotranspiration is explained not only by water-table depth, but also by PAR. Relative evapotranspiration decreased with increasing PAR (fig. 36), with the exception of the late post-logging period, which showed a slight increase in relative evapotranspiration with increasing PAR. This observation perhaps can be explained by assumptions within the Priestley-Taylor formulation that the energy and aerodynamic terms of the Penman equation are proportional to each other. Under non-potential conditions, these two terms might deviate from the assumption of proportionality, but in such a manner that can be "corrected" through a functional relation between the multiplier α and a term (PAR) strongly correlated with the energy term.

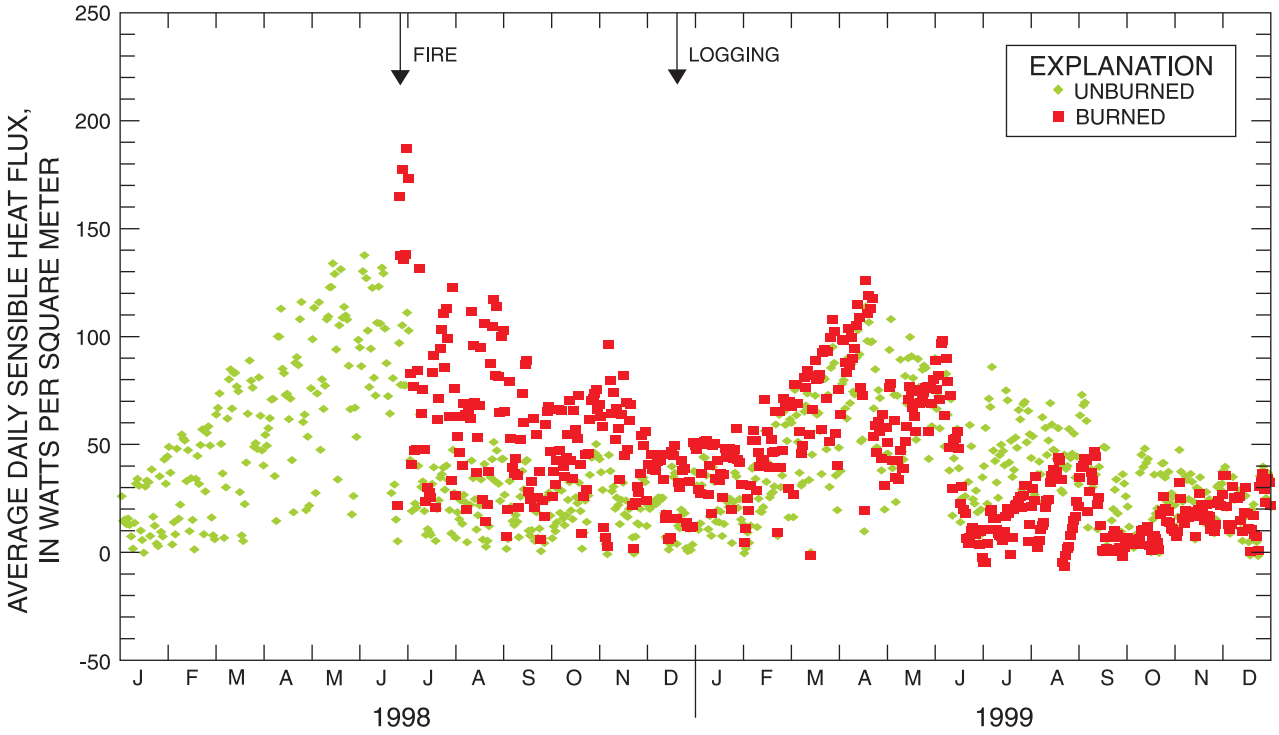

Figure 31. Average daily sensible heat flux.

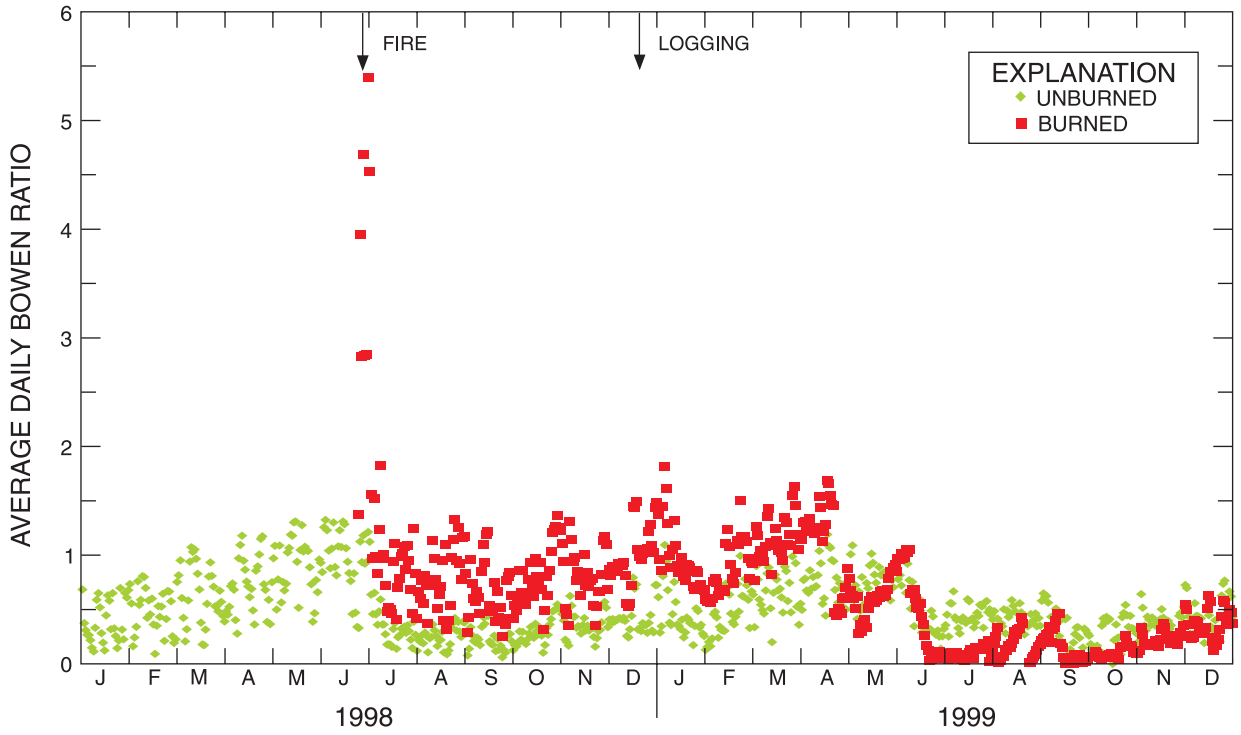

Figure 32. Average daily Bowen ratio.

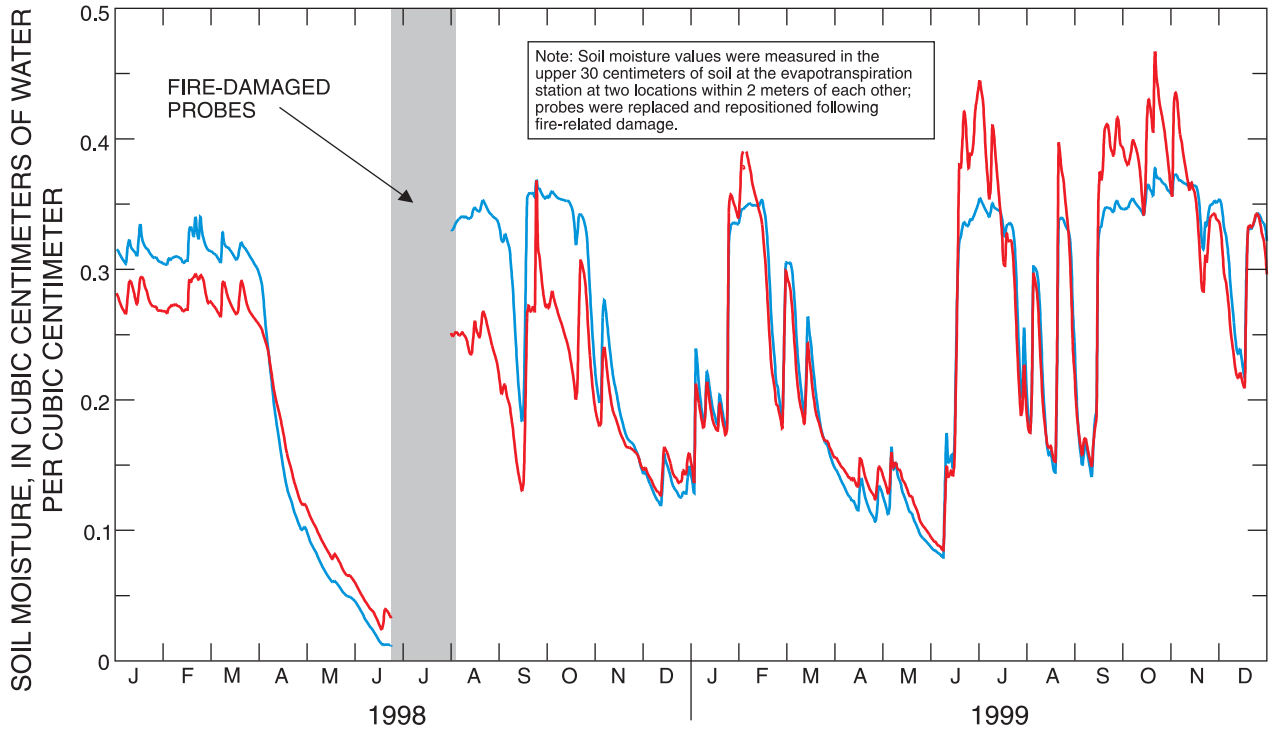

Figure 33. Shallow, volumetric soil moisture at evapotranspiration station.

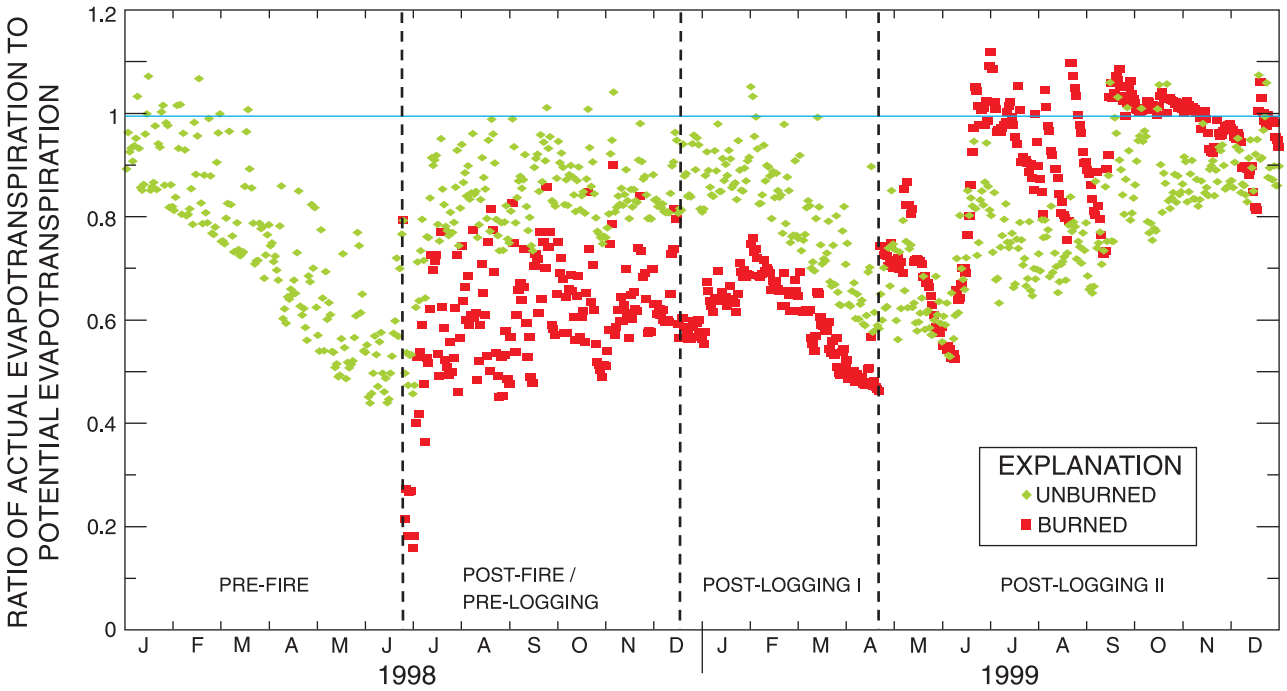

Figure 34. Temporal variability of daily values of relative evapotranspiration.

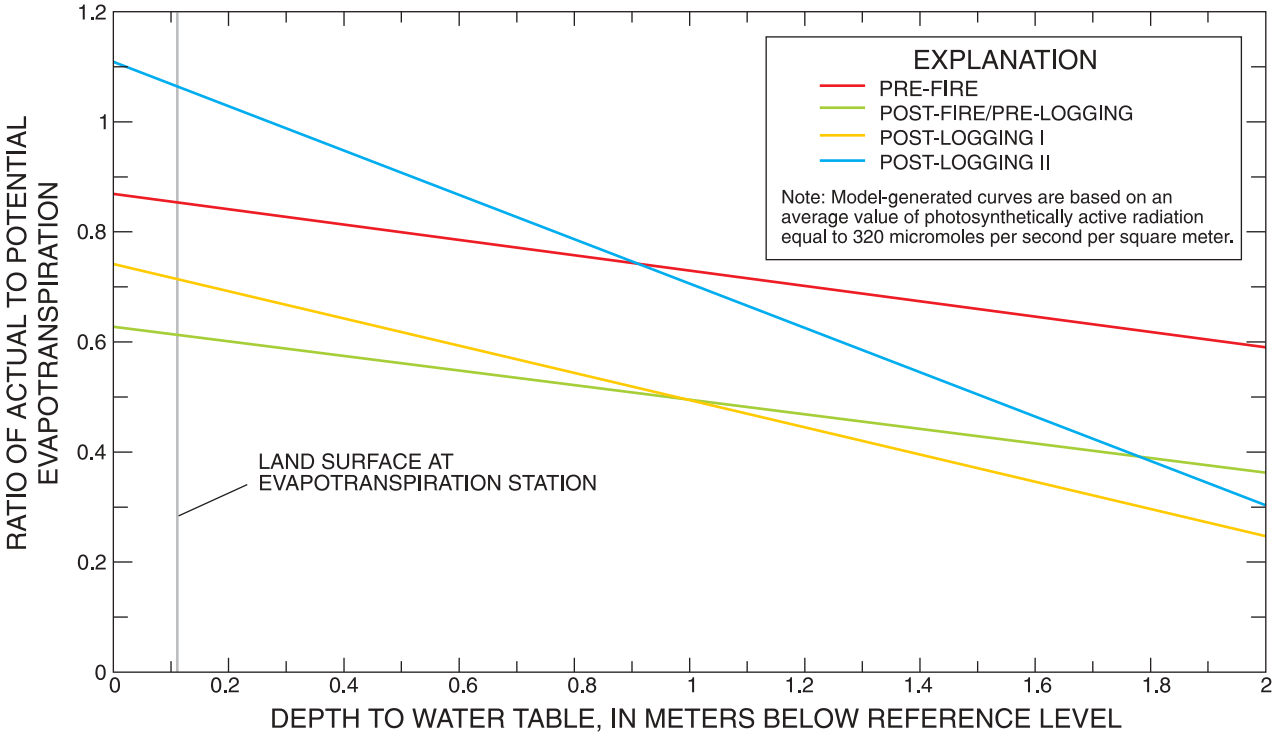

Figure 35. Relation between relative evapotranspiration and depth to water table.

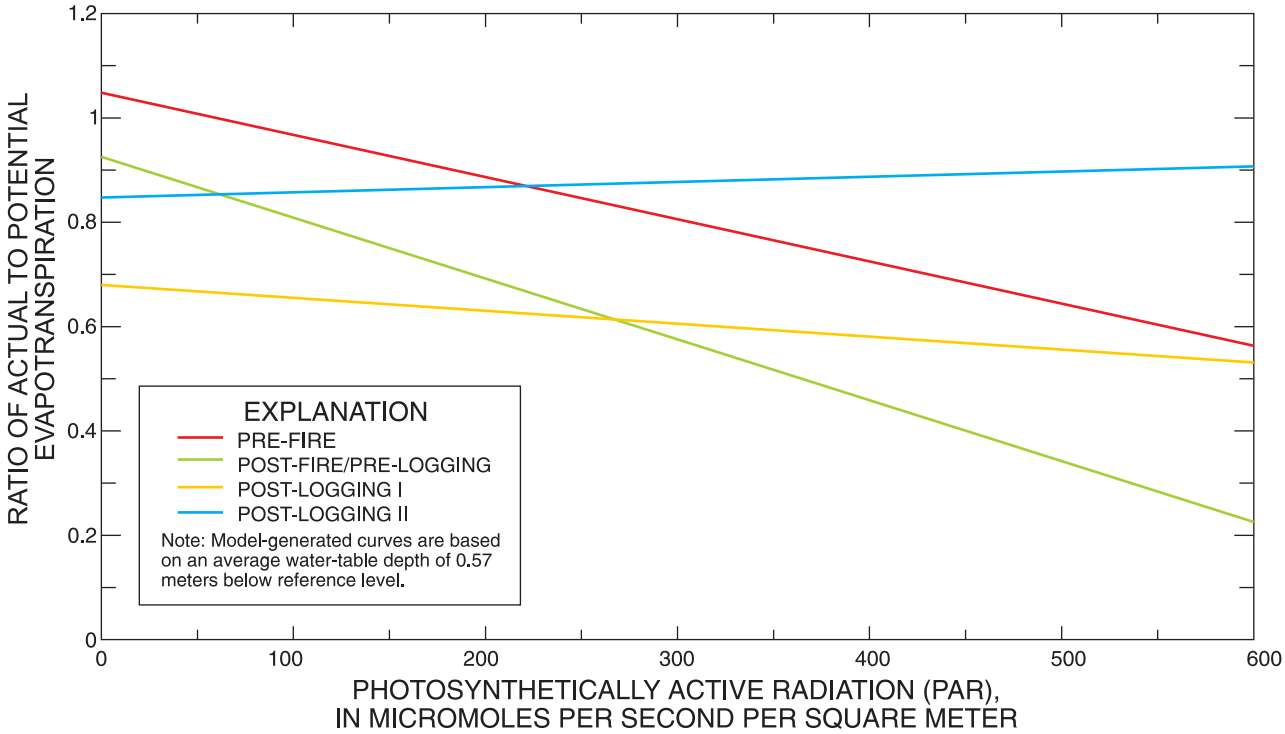

Figure 36. Relation between relative evapotranspiration and photosynthetically active radiation (PAR).

Within the model developed in this study, net radiation and air temperature do not directly affect the Priestley-Taylor α and relative evapotranspiration, although net radiation has an indirect effect through the correlation of this variable with PAR. These variables, however, are important in the determination of evapotranspiration, as can be seen in equation 22. Evapotranspiration is directly proportional to $\Delta / (\Delta + \gamma)$, a term that is a function of temperature (fig. 37). For example, a change in air temperature from 20 to 30 degrees Celsius will produce about a 14-percent increase in evapotranspiration, assuming the environment is otherwise unchanged. The relation of net radiation and evapotranspiration is one of direct proportionality. Net radiation displayed dramatic temporal variations, both day-to-day (as a result of variations in cloud cover) and seasonally (fig. 16), making this variable the most important determinant of evapotranspiration. This conclusion is supported by a sensitivity analysis (table 4) based on perturbing each environmental variable of the evapotranspiration model by an amount equal to the observed standard deviation of the daily values of that variable. All unperturbed variables were assumed equal to mean values. This analysis indicated that variations in net radiation explained the greatest amount of the variation in evapotranspiration. Variations in PAR, closely correlated with net radiation, explained a large amount of the variation in evapotranspiration prior to logging, but explained little of the variation after logging. Evapotranspiration was moderately sensitive to variations in air temperature. Variations in water-table depth explained a moderate amount of the variation in evapotranspiration prior to the fire; however, evapotranspiration became more sensitive to variations in water-table depth after logging.

The model developed in this study is subject to several qualifications. The form of the equation developed for α was empirical, rather than physics-based, and was simply designed to reproduce measured values of evapotranspiration as accurately as possible. The correlation between environmental variables complicates a unique determination of parameters. The model was developed for a limited range of environmental conditions, and therefore, extrapolation of the model to conditions not encountered in this study should be done with caution. The measured (upland) water-table depth at the evapotranspiration station, used as an independent variable in the model, explained some of the variation in evapotranspiration from the mixed upland/wetland watershed. However, water-table depth is not uniform within the watershed and, in particular, water-table depth in wetland areas usually is less than in upland areas. Therefore, caution should be used in applying the model to estimate evapotranspiration based on water-table depth measurements made at other locations in the watershed. For these reasons, the evapotranspiration model described in this report should be viewed as a general guide, rather than as a definitive description of the relation of evapotranspiration to environmental variables. The fact that the model successfully ($r^2 = 0.90$) reproduced 449 daily measurements of site evapotranspiration over a wide range of seasonal and surface-cover values lends credence to the ability of the model to estimate evapotranspiration at the site.

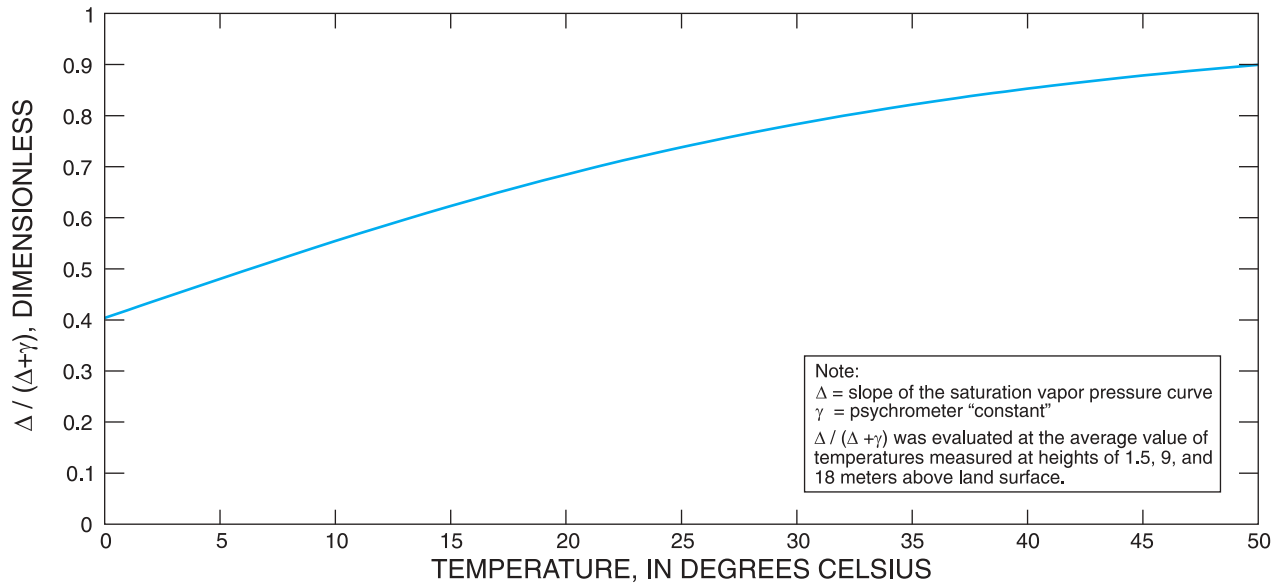

Figure 37. The Priestley-Taylor variable $\Delta/(\Delta + \gamma)$ as a function of temperature.

Table 4. Sensitivity of evapotranspiration models to environmental variables

[Values are computed using each of four evapotranspiration models; mean and standard deviation values are representative of daily values during the 2-year period of record, with the exception of net radiation for which these values are representative of 1999. ET is evapotranspiration rate, in millimeters per day (mm/d); $ET(\bar{x})$ = 2.92, 2.19, 2.38, and 3.49 mm/d for the unburned, post-fire/pre-logging, post-logging I, and post-logging II models, respectively. Percent change (+) is defined as 100 $(ET(\bar{x} + \sigma) - ET(\bar{x})) / ET(\bar{x})$; percent change (-) is defined as 100 $(ET(\bar{x} - \sigma) - ET(\bar{x})) / ET(\bar{x})$. R_n is net radiation, in watts per square meter (W/m^2); PAR is photosynthetically active radiation, in micromoles per square meter per second ($\mu moles/m^2/s$); T_a is air temperature, in degrees Celsius; h_{wt} is water-table depth below reference point, in meters (m)]

Environmental variable (x)	Mean ($\bar{x}$)	Standard deviation (σ)
R_n (unburned)	118.3	50.0
R_n (burned)	127.6	49.6
PAR	320.0	118.3
T_a	21.3	5.4
h_{wt}	.57	.42

Unburned model

Environmental variable (x)	$ET(\bar{x} + \sigma)$	$ET(\bar{x} - \sigma)$	Percent change (+)	Percent change (-)
R_n (unburned)	4.15	1.69	42	-42
PAR	2.58	3.27	-12	12
T_a	3.16	2.64	8	-10
h_{wt}	2.71	3.14	-7	7

Post-fire/pre-logging model

Environmental variable (x)	$ET(\bar{x} + \sigma)$	$ET(\bar{x} - \sigma)$	Percent change (+)	Percent change (-)
R_n (burned)	3.05	1.33	39	-39
PAR	1.64	2.74	-25	25
T_a	2.37	1.98	8	-10
h_{wt}	1.97	2.41	-10	10

Post-logging I model

Environmental variable (x)	$ET(\bar{x} + \sigma)$	$ET(\bar{x} - \sigma)$	Percent change (+)	Percent change (-)
R_n (burned)	3.32	1.45	39	-39
PAR	2.26	2.50	-5	5
T_a	2.58	2.15	8	-10
h_{wt}	1.97	2.80	-17	17

Post-logging II model

Environmental variable (x)	$ET(\bar{x} + \sigma)$	$ET(\bar{x}_i - \sigma)$	Percent change (+)	Percent change (-)
R_n (burned)	4.86	2.12	39	-39
PAR	3.53	3.44	1	-1
T_a	3.78	3.15	8	-10
h_{wt}	2.8	4.16	-19	19

Water Budget

Construction of a water budget for the Tiger Bay watershed serves to provide a tool for watershed management and for assessing the integrity of the eddy correlation evapotranspiration measurements. The water budget for the watershed is given by:

$$P - (ET + R + L - \Delta S) = 0, \qquad (29)$$

where

P is precipitation, in millimeters per year;
ET is evapotranspiration, in millimeters per year;
R is runoff, in millimeters per year;
L is leakage to the Upper Floridan aquifer, in millimeters per year; and
ΔS is rate of change in storage, in millimeters per year.

A water budget for the Tiger Bay watershed during the 1998-1999 study period is shown in table 5 and figure 38. Precipitation (figs. 9 and 27), evapotranspiration (fig. 29), and runoff (fig. 39) were measured or obtained as described previously in this report. The estimated value of deep leakage to the Upper Floridan aquifer (112 mm/yr) during 1995 (Stan Williams, St. Johns River Water Management District, oral commun., 2000) also was assumed to be appropriate for the study period (1998-99). The rate of change in watershed storage over the study period was not directly measured, but was estimated as the water-budget residual.

Table 5. Water budget of Tiger Bay watershed

[P is the precipitation (average of north and south storage rain gages (fig. 1)), in millimeters per year (mm/yr); ET is the evapotranspiration (energy-budget variant of eddy correlation method), in mm/yr; R is the runoff from watershed at Tiger Bay canal, in mm/yr; L is the estimated (1995) leakage to the Upper Floridan aquifer, in mm/yr (Stan Williams, St. Johns River Water Management District, oral commun., 2000); ΔS is the rate of change in watershed storage estimated as a water-budget residual, in mm/yr]

Year	P	ET	R	L	ΔS
1998	1,233	916	357	112	-152
1999	1,396	1,070	114	112	100
1998-99	1,315	993	236	112	-26

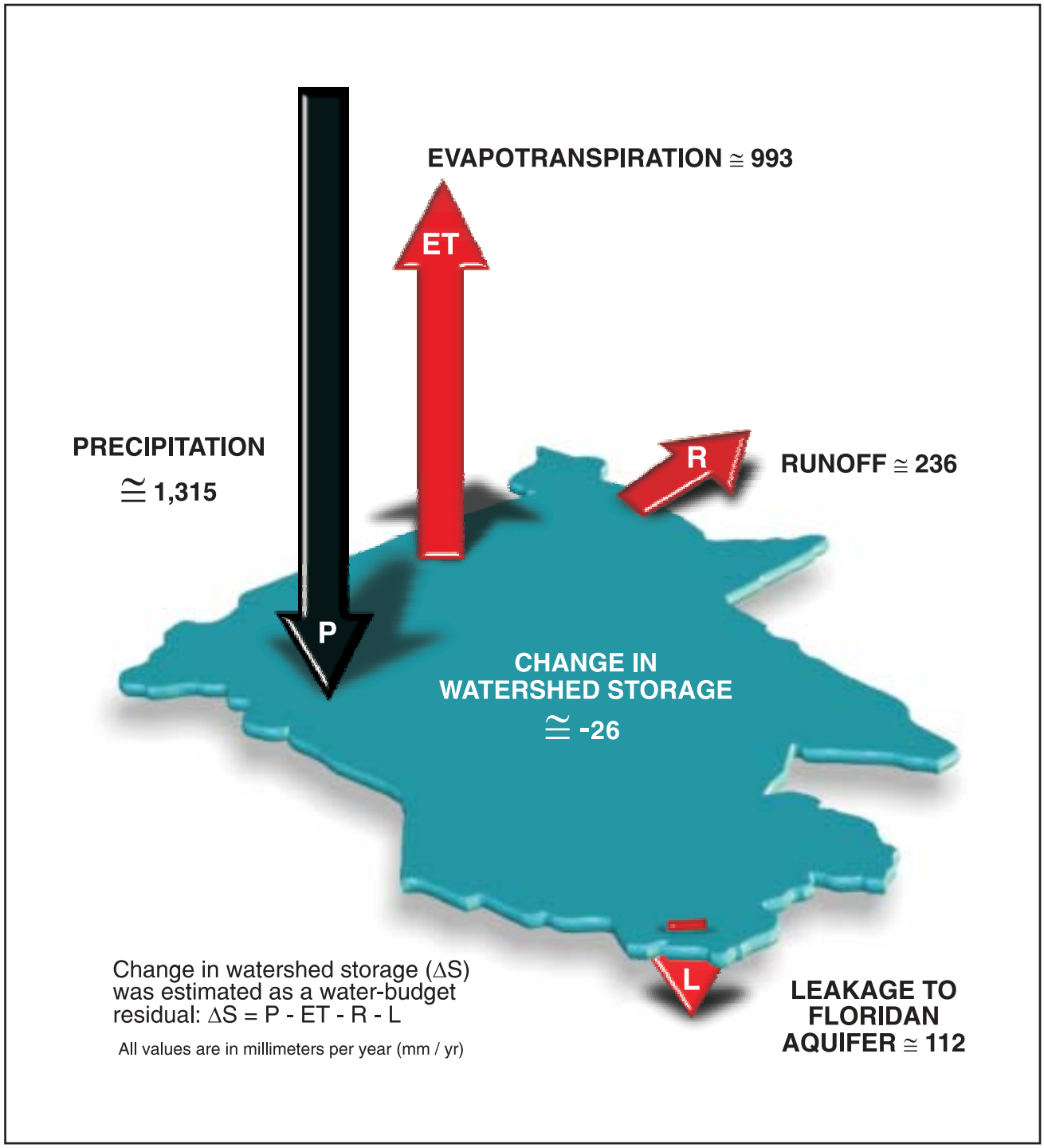

Figure 38. Water budget for Tiger Bay watershed during calendar years 1998 - 99.

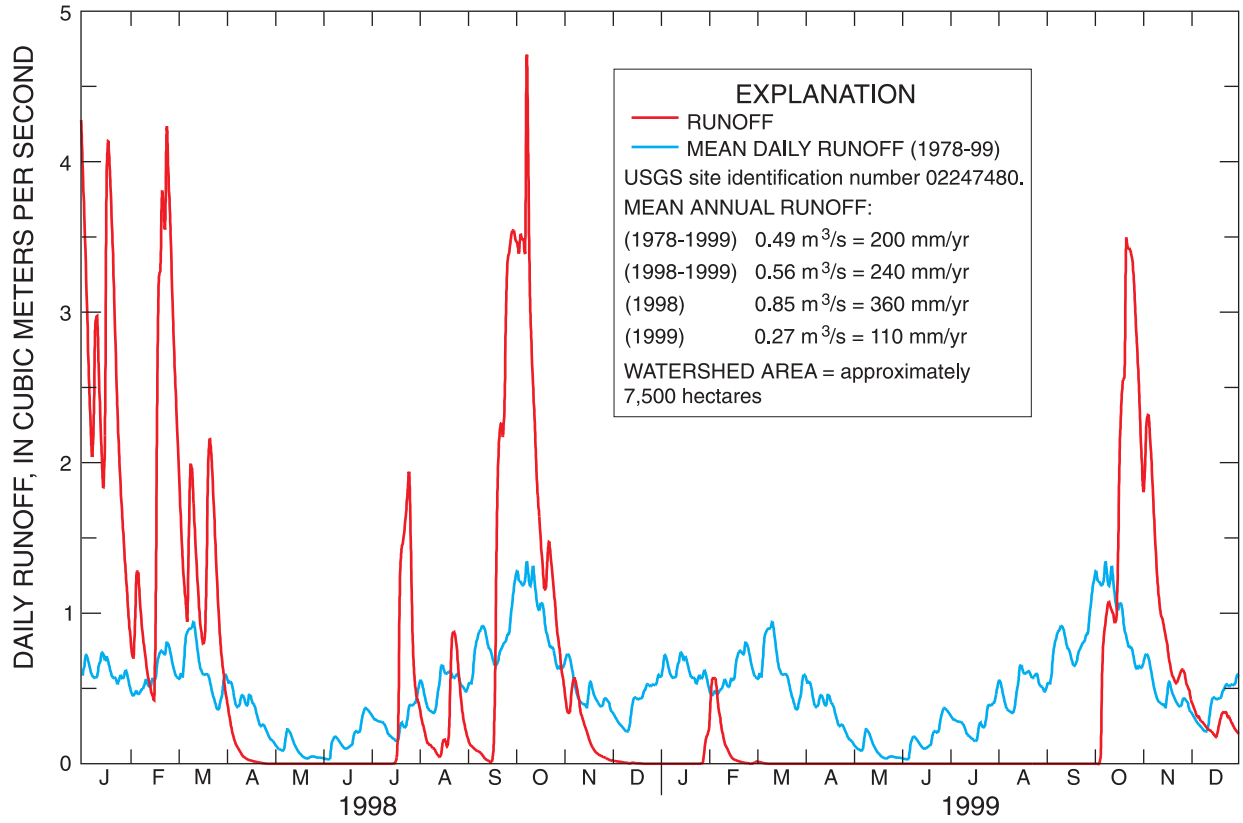

Figure 39. Runoff from Tiger Bay watershed.

The water budget (tables 5 and 6; fig. 38) indicated that about 76 percent of watershed rainfall was lost as evapotranspiration during the 2-year study. The percentage of rainfall evapotranspired was remarkably stable from year-to-year (74 percent in 1998 and 77 percent in 1999). This stability occurred despite the very different environmental conditions prevailing during the study. Rainfall was a more consistent predictor of evapotranspiration than was potential evapotranspiration. The relative evapotranspiration varied rather greatly (67 percent in 1998 to 77 percent in 1999).

Runoff removed about 18 percent of the rainfall during the study period, but this percentage varied widely from year-to-year (29 percent in 1998 and 8 percent in 1999) as shown in figure 39. The runoff for 1998 was over three times that of 1999, despite the greater rainfall in 1999. This disparity can be explained largely by the antecedent water-table conditions for individual rain periods (fig. 27). A relatively large fraction of precipitation in 1998 occurred when the water-table depth was shallow, leading to relatively high rejection of infiltration and subsequent runoff. Additionally, the temporal distribution of precipitation affects the amount of watershed runoff. Runoff is maximized following short, but intense, rainfall during which the infiltration capacity of the soil is exceeded. This phenomenon may explain the disparate runoff responses in July 1998 (very intense rainfall and significant runoff) and June-July 1999 (less intense rainfall and no runoff). This disparity was noted despite similar total amounts of precipitation with similar antecedent water-table conditions for each of the two periods. An alternative explanation may be that the soils became hydrophobic as a result of the fire, contributing to relatively more runoff in July 1998. Also, seasonal or fire-related variations in evapotranspiration can result in variations in the amount of precipitation available as runoff. Deep leakage was a relatively small fraction of the rainfall (about 9 percent), although this water-budget term could increase (at the expense of runoff and evapotranspiration) if continued development of the Upper Floridan aquifer in the area increases the hydraulic gradient between the surficial aquifer system and the underlying Upper Floridan aquifer.

Table 6. Potential evapotranspiration and relative rates of annual water-budget terms for Tiger Bay watershed

[PET is the potential evapotranspiration, in mm/yr; ET is the evapotranspiration (energy-budget variant of eddy correlation method), in millimeters per year (mm/yr); P is the precipitation (average of the north and south storage rain gages), in mm/yr; R is the runoff from watershed at Tiger Bay canal, in mm/yr; and L is the estimated (1995) leakage to the Upper Floridan aquifer, in mm/yr (Stan Williams, St. Johns River Water Management District, oral commun., 2000)]

Year	PET	$\frac{ET}{PET}$	$\frac{ET}{P}$	$\frac{R}{P}$	$\frac{L}{P}$
1998	1,356	0.67	0.74	0.29	0.09
1999	1,391	.77	.77	.08	.08
1998-99	1,374	.72	.76	.18	.09

The consistency of the water-budget terms can be expressed by the absolute and relative water-budget closures:

$$C_a = P - (ET + R + L + \Delta S), \text{ and} \quad (30)$$

$$C_r = \frac{100 C_a}{P}, \quad (31)$$

where

C_a is absolute water-budget closure, in millimeters per year;

C_r is relative water-budget closure, in percent; and

P, ET, R, L, and ΔS are the same as in eq. 29.

Watershed storage (ΔS) was an unmeasured quantity within the water budget. Therefore, evaluation of water-budget closure was facilitated by the judicious choice of a time period when negligible change in storage occurred within the watershed. Based on the measured water levels in the watershed (fig. 27), the time period from March 3, 1998, through September 23, 1999, was selected as an interval when change in watershed storage could be assumed to be zero. The beginning and ending of this interval occurred at times when temporal changes in water level were relatively slight, implying that the water levels measured at the two monitor wells at the beginning and ending dates of the interval were probably representative of the watershed. The absolute value of the measured rate of change in water level was less than 6 mm/yr at both monitor wells over this 570-day interval. Based on measured or estimated values of P (1,245 mm/yr), ET (1,048 mm/yr), R (132 mm/yr), and L (112 mm/yr), the absolute and relative water-budget closures were -47 mm/yr and 3.8 percent, respectively. The consistency of these independently measured water-budget terms provides support for, but not confirmation of, the reliability of the measured evapotranspiration. Compensating errors among water-budget terms or compensating errors within the temporal pattern of estimated evapotranspiration also could produce a consistent water budget.

Evapotranspiration was estimated during the present study using an energy-budget variant (eq. 18) of the eddy correlation method, rather than the standard eddy correlation method (eq. 5). The water-budget analysis provided an independent means to evaluate the relative accuracies of the two eddy correlation methods. The standard method produced turbulent flux estimates that were, on average, about 84.7 percent of those produced by the energy-budget variant. Applying this fraction to the evapotranspiration total for the water budget period from March 3, 1998, to September 23, 1999, the absolute and relative water budget closures corresponding to the standard eddy correlation method are 113 mm/yr and 9.1 percent, respectively. These closure values are greater than the values reported for the energy-budget variant, consistent with the assumption that the energy-budget variant was more accurate than the standard eddy correlation method.

Additional support for the assumption that the energy-budget variant was preferable to the standard eddy correlation method could be discerned from a residual analysis that assumed that precipitation, leakage, runoff, and evapotranspiration were accurately measured and that a lack of water-budget closure can be explained solely by the residual-calculated storage term. The specific yield representative of the watershed was then computed as the rate of change of watershed storage divided by a representative rate of change in water level within the watershed. The specific yield, estimated in this manner, was evaluated for credibility as a means of identifying the preferred variant of the eddy correlation method. Specific yield is defined as the volume of water yielded per unit area per unit change in water level. Specific yield can range from near zero if the capillary fringe intersects land surface (Gillham, 1984) to near unity for standing water. The specific yield of sandy soils (such as those in the uplands) ranges from 0.10 to 0.35 (Johnson, 1967). In this analysis, the representative rate of change in water-table depth for the watershed was assumed equal to the average rate of change in water-table depth at the two upland monitor wells (table 7). As mentioned previously, upland and wetland water levels are expected to change at the same rate in the low relief environment of this watershed.

Table 7. Average rate of change in water-table depth at monitor wells

[Δh_{North} is the rate of change in water-table depth at the evapotranspiration station, in millimeters per year (mm/yr); Δh_{South} is the rate of change in water-table depth at the south storage rain gage, in mm/yr; Δh_{avg} is the average rate of change in water-table depth ($(\Delta h_{North} + \Delta h_{South}) / 2$), in mm/yr]

Year	Δh_{North}	Δh_{South}	Δh_{avg}
1998	-660	-616	-638
1999	+432	+308	+370
1998-99	-114	-154	-134

Results of the residual analysis, using evapotranspiration estimated by both approaches, are shown in table 8. The energy-budget variant of the eddy correlation method produced specific yield estimates (0.24 in 1998, 0.27 in 1999, and 0.19 in 1998-99) that were somewhat consistent between each of the three time periods and were within the range of possible values. The standard eddy correlation method produced estimates of specific yield that were inconsistent between each of the three time periods and were unreasonable (0.02 in 1998, 0.71 in 1999, and -0.94 in 1998-99). The residual analysis of water budgets further supports the assumption that the energy-budget variant of the eddy correlation method is more accurate than the standard method.

Table 8. Comparison of estimates of specific yield based on evapotranspiration estimated with the energy-budget variant and with the standard eddy correlation method

[ΔS is the rate of change in watershed storage computed as a residual of the water budget ($\Delta S = P - (ET + R + L)$), in millimeters per year (mm/yr); P is the average watershed precipitation, in mm/yr; evapotranspiration (ET) estimated by the standard variant of the eddy correlation method is approximated as 84.7 percent of that estimated (table 5) by the energy-budget variant of the eddy correlation method; R is the average watershed runoff, in mm/yr; L is the estimated (1995) leakage to the Upper Floridan aquifer, in mm/yr (Stan Williams, St. Johns River Water Management District, oral commun., 2000). S_y is specific yield ($\Delta S / \Delta h_{avg}$), dimensionless; and Δh_{avg} is the estimated, average rate of change in water-table depth, in mm/yr (table 7)]

Year	Energy-budget variant		Standard method	
	ΔS	S_y	ΔS	S_y
1998	-152	0.24	-12	0.02
1999	100	.27	268	.71
1998-99	-26	.19	126	-.94

SUMMARY AND CONCLUSIONS

A 2-year (1998-99) study was conducted to estimate evapotranspiration from a forested watershed (Tiger Bay, Volusia County, Florida), which was subjected to natural fires, and to evaluate the causal relations between the environment and evapotranspiration. The watershed characteristics are typical of many areas within the lower coastal plain of the southeastern United States - nearly flat, slowly draining land with a vegetative cover consisting primarily of pine flatwood uplands interspersed within cypress wetlands. Drought-induced fires in spring 1998 burned about 40 percent of the watershed and most of the burned area was logged in late-fall 1998.

Evapotranspiration was measured using eddy correlation sensors placed on a tower 36.5-meter (m) high within an 18.3-m-high forest. About 27 percent of the 30-minute eddy correlation data were missing as a result of either inoperation of the sensors related to scaling of the hygrometer windows, collection of rainfall or dew on the sensors, or spurious turbulence created by the sensor mounting arm and the attached tower. These missing data generally occurred during periods (evening to early morning) when evapotranspiration was relatively low. Linear relations between photosynthetically active radiation (PAR) and the fluxes of evapotranspiration and sensible heat were used to estimate missing 30-minute values. Data were composited into daily values if the turbulent fluxes for more than 18 hours of a given day were directly measured, rather than being estimated with the PAR-based relation. Daily values for which more than 6 hours of data were missing were considered non-measured. This procedure resulted in 449 measurements of daily evapotranspiration over the 2-year (730-day) period. An energy-budget variant of the standard eddy correlation method that accounts for the common underestimation of evapotranspiration by the standard method was computed.

Following the fires, the daily measurements of evapotranspiration were a composite of rates representative of burned and unburned areas of the watershed. The fraction of a given daily measurement derived from burned areas was estimated based on the diurnal pattern of wind direction and PAR for that day and on the spatial distribution of burned areas upwind of the evapotranspiration station. The daily values of evapotranspiration were used to calibrate a Priestley-Taylor model. The model was used to estimate evapotranspiration for burned and unburned areas and to identify and quantify the environmental controls on evapotranspiration. The

evapotranspiration model successfully ($r^2 = 0.90$) reproduced daily measurements of site evapotranspiration over a wide range of environmental conditions, giving credence to the ability of the model to estimate evapotranspiration at the site.

Estimation of evapotranspiration from the watershed was based on an area-weighted composite of estimated values for burned and unburned areas. Annual evapotranspiration from the watershed was 916 and 1,070 millimeters (mm) for 1998 and 1999, respectively, and averaged 993 mm. These values are comparable to those reported by previous researchers. Evapotranspiration has been estimated to average about 990 millimeters per year (mm/yr) over Volusia County (Rutledge, 1985) and to average about 890 mm/yr in the Tiger Bay watershed (Camp, Dresser and McKee, Inc., 1996). Bidlake and others (1993) estimated annual cypress evapotranspiration (970 mm) to be only 8.5 percent less than that of pine flatwoods (1,060 mm) based on studies conducted in Sarasota and Pasco Counties, Florida. Liu (1996) estimated average, annual evapotranspiration of both cypress and pine flatwoods to be 1,080 mm based on a study in Alachua County, Florida.

The extensive burning and logging that occurred during the study produced a landscape that was not typical of forested areas of Florida. The estimated evapotranspiration from unburned areas can be considered more representative of typical forest cover. Annual evapotranspiration from unburned areas was 937 and 999 mm for 1998 and 1999, respectively, and averaged 968 mm. Evapotranspiration from burned areas for the 10-month period after the fire (July 1998-April 1999) averaged about 17 percent less than that from unburned areas and, for the following 8-month period (May-December 1999), averaged about 31 percent higher than from unburned areas. During the 554-day period after the fire, the average evapotranspiration for burned areas (1,043 mm/yr) averaged 8.6 percent higher than that for unburned areas (960 mm/yr). Both actual and potential evapotranspiration showed strong seasonal patterns and day-to-day variability. Actual evapotranspiration from the watershed averaged only 72 percent of potential evapotranspiration.

Evapotranspiration declined from near potential rates in the wet conditions of January 1998 to less than 50 percent of potential evapotranspiration after the fire and at the peak of the drought in June 1998. After the drought ended in early July 1998 and water levels returned to near land surface, evapotranspiration increased sharply. The evapotranspiration rate, however, was only about 60 percent of the potential rate in the burned areas, as compared to about 90 percent of the potential rate in the unburned areas. This discrepancy can be explained as a result of fire damage to vegetation. Beginning in spring 1999, evapotranspiration from burned areas increased sharply relative to unburned areas, sometimes exceeding unburned evapotranspiration by almost 100 percent. Possible explanations for the dramatic increase in evapotranspiration from burned areas are not clear at this time, but may include phenological changes associated with maturation or seasonality of plants that emerged after the fire or successional changes in composition of plant community within burned areas.

Within the framework of the Priestley-Taylor model developed during this study, variations in daily evapotranspiration were the result of variations in: surface cover, net radiation, PAR, air temperature, and water-table depth. Potential evapotranspiration depended solely on net radiation and air temperature and increased as each of these variables increased. The extent to which potential evapotranspiration was approached was determined by the Priestley-Taylor coefficient α. In this study, Priestley-Taylor α was a linear function of water-table depth and PAR. Unique parameters within the α function were estimated for each of four surface covers or time periods: unburned; burned, but unlogged; and both burned and logged (early post-logging and late post-logging). The evapotranspiration model indicated that relative evapotranspiration (the ratio of actual to potential evapotranspiration) decreased as the depth to the water table increased. The rate of decline of relative evapotranspiration with water-table depth was greater for the post-logging period than for the pre-logging period, perhaps indicative of the replacement of many deeply rooted trees by shallow-rooted understory vegetation following the fires. Shallow-rooted plants would be less able to tap into deep soil moisture or the water table than deep-rooted trees. Relative evapotranspiration decreased with increasing PAR, with the exception of the late post-logging period, which showed a slight increase in relative evapotranspiration with increasing PAR.

A water budget for the watershed supported the validity of the estimates of evapotranspiration produced with the energy-budget variant of the eddy correlation method. Independent estimates of average rates of rainfall (1,245 mm/yr), runoff (132 mm/yr), deep

leakage (112 mm/yr), as well as evapotranspiration (1,048 mm/yr) were compiled for a 570-day period over which the change in watershed storage was negligible. Water-budget closure was 47 mm/yr or 3.8 percent of rainfall, indicating good consistency between the estimated evapotranspiration and estimates of the other terms of the water budget. Estimates of evapotranspiration produced by the standard eddy correlation method were relatively inconsistent with the water budget (water-budget closure was 113 mm/yr or 9.1 percent of rainfall), indicating that the energy-budget variant is superior to the standard eddy correlation method.

Specific yield was estimated based on estimated changes in watershed storage and water level. The change in watershed storage was estimated as a residual of the water budget. Specific yield values produced using evapotranspiration estimated by the energy-budget variant of the eddy correlation method were reasonable and relatively consistent from year-to-year (0.19 to 0.27). However, specific yield values based on evapotranspiration estimated by the standard eddy correlation method were unreasonable and inconsistent from year-to-year (-0.94 to 0.72). These results further support the premise that the energy-budget variant is more accurate than the standard eddy correlation method.

Evapotranspiration rates were about 74 and 77 percent of rainfall for 1998 and 1999, respectively, relatively constant considering the variability in surface cover and rainfall patterns between the 2 years. Potential evapotranspiration was less consistent as an indicator of actual evapotranspiration; evapotranspiration was 67 and 77 percent of potential evapotranspiration for years 1998 and 1999, respectively.

REFERENCES

Baldocchi, D.D., Hicks, B.B., and Meyers, T.P., 1988, Measuring biosphere-atmosphere exchanges of biologically related gases with micrometeorological methods: Ecology, v. 69, no. 5, p. 1331-1340.

Baldwin, R., Bush, C.L., Hinton, R.B., Huckle, H.F., Nichols, P., Watts, F.C., and Wolfe, J.A., 1980, Soil Survey of Volusia County, Florida: U.S. Soil Conservation Service, 207 p. and 106 pls.

Bidlake, W.R., Woodham, W.M., and Lopez, M.A., 1993, Evapotranspiration from areas of native vegetation in west-central Florida: U.S. Geological Survey Open-File Report 93-415, 35 p.

Bowen, I.S., 1926, The ratio of heat losses by conduction and by evaporation from any water surface: Physical Review, 2nd series, v. 27, no. 6, p. 779-787.

Brutsaert, W., 1982, Evaporation into the atmosphere - Theory, history, and applications: Boston, Kluwer Academic Publishers, 299 p.

Businger, J.A., and Yaglom, A.M., 1971, 'Introduction to Obukhov's paper on "Turbulence in an atmosphere with a non-uniform temperature"', Boundary-Layer Meteorology, v. 2, p. 3-6.

Camp, Dresser and McKee, Inc., 1996, Volusia County, Florida - Tiger Bay water conservation and aquifer recharge evaluation - Phase I: Volusia County, Florida, Technical Report.

Campbell, G.S., and Norman, J.M., 1998, An introduction to environmental biophysics: New York, Springer, 286 p.

Dyer, A. J., 1961, Measurements of evaporation and heat transfer in the lower atmosphere by an automatic eddy-correlation technique: Quarterly Journal of the Royal Meteorological Society, v. 87, p. 401-412.

Eichinger, W.E., Parlange, M.B., and Stricker, H., 1996, On the concept of equilibrium evaporation and the value of the Priestley-Taylor coefficient: Water Resources Research, v. 32, no. 1, p. 161-164.

Eidenshink, J. C., 1992, The 1990 conterminous U.S. AVHRR data set: Journal of Photogrammetry and Remote Sensing, v. 58, p. 809-813.

Fleagle, R.G., and Businger, J.A., 1980, An introduction to atmospheric physics: New York, Academic Press, 432 p.

Flint, A.L., and Childs, S.W., 1991, Use of the Priestley-Taylor evaporation equation for soil water limited conditions in a small forest clearcut: Agricultural and Forest Meteorology, v. 56, p. 247-260.

Garratt, J.R., 1980, Surface influence upon vertical profiles in the atmospheric near-surface layer: Quarterly Journal of the Royal Meteorological Society, v. 106, p. 803-819.

German, E.R., 2000, Regional evaluation of evapotranspiration in the Everglades: U.S. Geological Survey Water-Resources Investigations Report 00-4217, 48 p.

Gillham, R. W., 1984, The capillary fringe and its effect on water-table response: Journal of Hydrology, v. 67, p. 307-324.

Goulden, M.L., Munger, J.W., Fan, S-M, Daube, B.C., and Wofsy, S.C., 1996, Measurements of carbon sequestration by long-term eddy covariance: methods and a critical evaluation of accuracy: Global Change Biology, v. 2, p. 169-182.

Johnson, A.I., 1967, Specific yield - Compilation of specific yields for various materials: U.S. Geological Survey Water-Supply Paper 1662-D, 74 p.

Kaimal, J.C., and Businger, J.A., 1963, A continuous wave sonic anemometer-thermometer: Journal of Applied Meteorology, v. 2, p. 156-164.

Kaimal, J.C., and Gaynor, J.E., 1991, Another look at sonic thermometry: Boundary-layer meteorology, v. 56, p. 401-410.

Kimrey, J.O., 1990, Potential for ground-water development in central Volusia County, Florida: U.S. Geological Survey Water-Resources Investigations Report 90-4010, 31 p.

Knowles, L., Jr., 1996, Estimation of evapotranspiration in the Rainbow Springs and Silver Springs basins in north-central Florida: U.S. Geological Survey Water-Resources Investigations Report 96-4024, 37 p.

Lee, X., and Black, T.A., 1993, Atmospheric turbulence within and above a Douglas-fir stand. Part II: Eddy fluxes of sensible heat and water vapor: Boundary-layer meteorology, v. 64, p. 369-389.

Liu, S., 1996, Evapotranspiration from cypress (*Taxodium ascendens*) wetlands and slash pine (*Pinus elliottii*) uplands in north-central Florida: Ph. D. Dissertation, University of Florida, Gainesville, 258 p.

Lowe, P.R., 1977, An approximating polynomial for the computation of saturation vapor pressure: Journal of Applied Meteorology, v. 16, no. 1, p. 100-103.

McDonald, M.G., and Harbaugh, A.W., 1984, A modular three-dimensional finite-difference ground-water flow model: U.S. Geological Survey Open-File Report 83-875, 528 p.

Monteith, J.L., 1965, Evaporation and environment *in* The state and movement of water in living organisms, Symposium of the Society of Experimental Biology: San Diego, California, (G. E. Fogg, ed.), Academic Press, New York, p. 205-234.

Monteith, J.L., and Unsworth, M.H., 1990, Principles of environmental physics (2d ed.): London, Edward Arnold, 291 p.

Moore, C.J., 1976, Eddy flux measurements above a pine forest: Quarterly Journal of the Royal Meteorological Society, v. 102, p. 913-918.

National Oceanic and Atmospheric Administration, 1998, Climatological data - annual summary - Florida: v. 102, no. 13, 21 p.

———1999, Climatological data - annual summary - Florida: v. 103, no. 13, 21 p.

Penman, H.L., 1948, Natural evaporation from open water, bare soil, and grass: Proceedings of the Royal Society of London, Series A, v. 193, p. 120-146.

Phelps, G.G., 1990, Geology, hydrology, and water quality of the surficial aquifer system in Volusia County, Florida: U.S. Geological Survey Water-Resources Investigations Report 90-4069, 67 p.

Priestley, C.H.B., and Taylor, R.J., 1972, On the assessment of surface heat flux and evaporation using large-scale parameters: Monthly Weather Review, v. 100, p. 81-92.

Reifsnyder, W.E., 1967, Radiation geometry in the measurement and interpretation of radiation balance: Agricultural Meteorology, v. 4, p. 255-265.

Riekerk, H., and Korhnak, L. V., 2000, The hydrology of cypress wetlands in Florida pine flatwoods: Wetlands, v. 20, no. 3, p. 448-460.

Rutledge, A.T., 1985, Ground-water hydrology of Volusia County, Florida with emphasis on occurrence and movement of brackish water: U.S. Geological Survey Water-Resources Investigations Report 84-4206, 84 p.

Schotanus, P., Nieuwstadt, F.T.M., and de Bruin, H.A.R., 1983, Temperature measurement with a sonic anemometer and its application to heat and moisture fluxes: Boundary-Layer Meteorology, v. 50, p. 81-93.

Schuepp, P.H., Leclerc, M.Y., MacPherson, J.I., and Desjardins, R.L., 1990, Footprint prediction of scalar fluxes from analytical solutions of the diffusion equation: Boundary-Layer Meteorology, v. 50, p. 355-373.

Simonds, E.P., McPherson, B.F., and Bush, P., 1980, Shallow ground-water conditions and vegetation classification, central Volusia County, Florida: U.S. Geological Survey Water-Resources Investigations Report 80-752, 1 sheet.

Stannard, D.I., 1993, Comparison of Penman-Monteith, Shuttleworth-Wallace, and modified Priestley-Taylor evapotranspiration models for wildland vegetation in semiarid rangeland: Water Resources Research, v. 29, no. 5, p. 1379-1392.

Stannard, D.I., 1994, Interpretation of surface flux measurements in heterogeneous terrain during the Monsoon ‘90 experiment: Water Resources Research, v. 30, no. 5, p. 1227-1239.

Stull, R.B., 1988, An introduction to boundary layer meteorology: Kluwer Academic Publishers, Boston, 666 p.

Sumner, D.M., 1996, Evapotranspiration from successional vegetation in a deforested area of the Lake Wales Ridge, Florida: U.S. Geological Survey Water-Resources Investigations Report 96-4244, 38 p.

Tanner, B.D., and Greene, J.P., 1989, Measurement of sensible heat and water vapor fluxes using eddy correlation methods: Final report prepared for U.S. Army Dugway Proving Grounds, Dugway, Utah, 17 p.

Tanner, B.D., Swiatek, E., and Greene, J.P., 1993, Density fluctuations and use of the krypton hygrometer in surface flux measurements: Management of irrigation and drainage systems, Irrigation and Drainage Division, American Society of Civil Engineers, July 21-23, 1993, Park City, Utah, p. 945-952.

Tanner, C.B., and Thurtell, G.W., 1969, Anemoclinometer measurements of Reynolds stress and heat transport in the atmospheric boundary layer: United States Army Electronics Command, Atmospheric Sciences Laboratory, Fort Huachuca, Arizona, TR ECOM 66-G22-F, Reports Control Symbol OSD-1366, April 1969, 10 p.

The Orlando Sentinel, 1998, Special report--Florida ablaze: Sunday, July 12, 1998, 12 p.

Tibbals, C.H., 1990, Hydrology of the Floridan aquifer system in east-central Florida: U.S. Geological Survey Professional Paper 1403-E, 98 p.

Twine, T.E., Kustas, W.P., Norman, J.M., Cook, D.R., Houser, P.R., Meyers, T.P., Prueger, J.H., Starks, P.J., and Wesely, M.L., 2000, Correcting eddy-covariance flux underestimates over a grassland: Agricultural and Forest Meteorology, v. 103, p. 279-300.

U.S. Geological Survey, 1998a, Water resources data, Florida, water year 1998, v. 1A, northeast Florida surface water: U.S. Geological Survey Water-Data Report FL-98-1A, 408 p.

——— 1998b, Conterminous U.S. AVHRR: U.S. Geological Survey, National Mapping Division, EROS Data Center, 7 compact disks.

——— 1999a, Water resources data, Florida, water year 1999, v. 1A, northeast Florida surface water: U.S. Geological Survey Water-Data Report FL-99-1A, 374 p.

——— 1999b, Conterminous U.S. AVHRR: U.S. Geological Survey, National Mapping Division, EROS Data Center, 7 compact disks.

——— 2000, Water resources data, Florida, water year 2000, v. 1A, northeast Florida surface water: U.S. Geological Survey Water-Data Report FL-00-1A, 388 p.

Volusia County Department of Geographic Information Services, 1996a, Vegetation, Daytona Beach NW, prepared July 29, 1996, 1 sheet.

——— 1996b, Vegetation - Daytona Beach SW, prepared July 29, 1996, 1 sheet.

Webb, E.K., Pearman, G.I., and Leuning, R., 1980, Correction of flux measurements for density effects due to heat and water vapour transfer: Quarterly Journal of the Royal Meteorological Society, v. 106, p. 85-100.

Weeks, E.P., Weaver, H.L., Campbell, G.S., and Tanner, B.D., 1987, Water use by saltcedar and by replacement vegetation in the Pecos River floodplain between Acme and Artesia, New Mexico: U.S. Geological Survey Professional Paper 491-G, 37 p.

APPENDIX I

APPENDIX I

The assumptions inherent in the weighting scheme used in equations 23 through 25 can be seen through derivation of equation 24 for w_b.

The latent heat flux measured by the eddy correlation sensors and derived from burned surface covers over a given day of 48 measurements is given by:

$$\lambda E_{bm} = \sum_i g_i \frac{1}{48} \sum_k \lambda E_{bk} \delta_i(\psi_k), \quad \text{(A1)}$$

where

λE_{bm} is daily latent heat flux derived from burned surface covers and measured by the flux sensors, in watts per square meter;

g_i is fractional contribution of burned area within burn zone i to the measured latent heat flux when wind direction is from burn zone i;

λE_{bk} is latent heat flux from burned surface covers for time step k, in watts per square meter;

$\delta_i(\Psi_k)$ is a binary function equal to 1 if Ψ_k is within burn zone i and otherwise equals 0; and

the index i is incremented from zone I to IV, and the index k is incremented from 1 to 48.

By definition, the expression in eq. A1 is equal to the second term of the right side of eq. 23. Setting these two expressions equal and assuming that the high-resolution latent heat flux measurements for burned surfaces are directly proportional to photosynthetically active radiation (PAR), and therefore, that the daily resolution latent heat flux for burned surfaces are directly proportional to average daily PAR:

$$w_b(a\overline{PAR}) = \frac{1}{48} \sum_i g_i \sum_k (aPAR_k)\delta_i(\psi_k), \quad \text{(A2)}$$

where

w_b is the fraction of the measured latent heat flux originating from burned areas, dimensionless; and

overbars represent daily average values and the variable *a* is the constant of proportionality between latent heat flux and PAR.

Solving for w_b:

$$w_b = \frac{\frac{1}{48} \sum_i g_i \sum_k (aPAR_k)\delta_i(\psi_k)}{a\overline{PAR}}, \quad \text{(A3)}$$

$$w_b = \frac{\frac{1}{48} \sum_i g_i \sum_k (aPAR_k)\delta_i(\psi_k)}{a\frac{1}{n} \sum_k PAR_k}, \quad \text{(A4)}$$

$$w_b = \frac{\sum_i g_i \sum_k PAR_k \delta_i(\psi_k)}{\sum_k PAR_k} . \quad \text{(A5)}$$

Equation A5 is identical to eq. 24. The constant of proportionality *a* can change from day-to-day as environmental conditions (for example, water level, air temperature, and green leaf density) change and, in fact, as shown in eq. A5, w_b is independent of the particular value of the constant. An equivalent expression, equal to 1 - w_b, can be derived for the weight applied to daily latent heat flux from unburned surfaces. The constant of proportionality between unburned latent heat flux and PAR can be different than that between burned latent heat flux and PAR.

It is interesting to note that the use of measured high-resolution λE, rather than PAR, as a means of adjusting the weights for the combination of changing source area composition and diurnal variations in evapotranspiration (ET) (eq. 25), produces excessive weighting towards zones with high-ET surface covers. This observation can be illustrated best by an example. Suppose, for a given day, the wind direction were from a lake (high ET) before solar noon and from a desert (near-zero ET) after solar noon. In this case, the appropriate weighting for each surface cover, within an equation of the form of eq. 23, would be 0.5 and the average, measured ET for the day would be about one-half that of the lake. However, weighting by the fraction of ET measured from each zone would lead to a weight of near 1.0 for the lake zone and 0.0 for the desert zone, leading to a model for lake evaporation that would produce underestimates of true lake evaporation.